

UCSF

UC San Francisco Electronic Theses and Dissertations

Title

Helios enhances the preferential differentiation of fetal naïve CD4+ T cells into regulatory T cells

Permalink

<https://escholarship.org/uc/item/71t950pt>

Author

Ng, Melissa

Publication Date

2019

Supplemental Material

<https://escholarship.org/uc/item/71t950pt#supplemental>

Peer reviewed|Thesis/dissertation

Helios enhances the preferential differentiation of fetal naïve CD4+ T cells into regulatory T cells

by
Melissa Shu Feng Ng

DISSERTATION

Submitted in partial satisfaction of the requirements for degree of
DOCTOR OF PHILOSOPHY

in

Biomedical Sciences

in the

GRADUATE DIVISION

of the

UNIVERSITY OF CALIFORNIA, SAN FRANCISCO

Approved:

DocuSigned by:

Qizhi Tang

Qizhi Tang

9BFF9AD92ACD4BA...

Chair

DocuSigned by:

Trevor Burt

Trevor Burt

DocuSigned by:

Alexander Marson

Alexander Marson

DocuSigned by:

Susan Fisher

Susan Fisher

3D7FD5EAA89E411...

Committee Members

To all my family, in work and life, for their love and support.

To my husband, Junying, who showed me how to get to the finish line by getting there first. I still
love you anyway.

Acknowledgments

Looking back on the last five and a half years at UCSF, I am tremendously grateful to have landed in a place that has allowed me to grow not just in my science, but also in self-confidence and resilience. This dissertation that I spawned out of naiveté as a rotation student influenced by exciting developments that I had just read in the literature would not have come to pass without the vibrant and highly collaborative community of scientists that have helped, and continue to help me along the way.

To Trevor - thank you for taking that chance on my wild-eyed ideas and coming along for the ride. We both knew nothing about epigenetics when we started this project together, but your undeterred confidence in my ability to pick it up and be good at it was the best encouragement that any young graduate student could have gotten. Thank you for your calm reassurances in the middle of the night after panicked text messages about not being able to find my sequencing raw data files (which I eventually found with the Gladstone Bioinformatics core). Lastly, thank you for giving me the absolute independence to drive this project, to learn from the failures and press on, that has helped me develop my self-confidence as a scientist today.

If I was excitedly charting a course and going headlong with the wind in my sails, my thesis committee was the steadying hand on the ship that made sure that I didn't end up on the rocks. To Tang, my committee chair, thank you for your steady guidance. I will always remember your strong conviction that good science will always speak for itself, and your advice to prioritize the integrity of the science over an exciting, but less accurate story. You have been such a role model to me and other aspiring female immunologists in the program. To Susan, thank you for your encouragement not just in science, but also for all the life advice. To be able to tap on your

wisdom and know that there was someone who carved out the same path before me is highly inspiring. Last of all, Alex was instrumental to the success of this project, which definitely wouldn't have taken off the way it had if we had not crossed paths. To Alex, I am constantly in awe at how you have always managed to take my complicated tangle of thoughts and experiments and distill it down into a clarifying hypothesis. I have always walked away from my meetings with you with a renewed sense of purpose. Thank you for always looking out for this project at all its major crossroads – from suggesting that I pursue ATACseq, to making sure that I was helped with all the CRISPR techniques that I eventually used. Most of all, thank you for always checking in with me, especially during the last stages of this project. Your encouragement and belief in the significance of the science has always helped to bolster me whenever I was feeling overwhelmed and discouraged. I am so fortunate to have had guidance from a wonderful committee throughout all these years.

Science does not operate in a vacuum, and I have never felt it to be truer than in UCSF. To all my collaborators in the Marson lab – Dimitre, Theo, Kathrin, Michelle, Jessica and Jon, thank you for tolerating my endless questions and desperate need to borrow reagents at the very last minute. To all my classmates in the Biomedical Sciences graduate program, who have been amazing to talk to and exchange ideas with, or just commiserating about the misery of the relentless grind that is doing a Ph.D. To all the Biomedical Science administrators, especially Demian, Ned and Monique, thank you for smoothing the way for us as graduate students so that we could concentrate on the science. To everyone in the flow cytometry core, with whom I have probably spent at least a fifth of my lab time with - Ashley, Tomoko, Lana, Claudia, Nofar, and Vinh, thank you for always keeping Booboo/Jabba and Kermit purring along. I will definitely miss coming in on Thursday morning and bantering with you while the sorters get started up, and I am sorry that I will not be able to bribe you all with cookies every Christmas anymore. To

everyone in the Gladstone Bioinformatics Core that I have bugged incessantly for help – Sean Thomas and Reuben Thomas most of all, thank you so much for your patience and help. To all the people in Pod A of the Stemcell Building – it has been great five years of hurtling along the corridors, happy hours with extremely strong margaritas, and uncoordinated, Christmas string light competitions. I have enjoyed working here immensely, and will miss everyone.

Outside of work, there are so many people to thank for preserving my work-life balance. To all the Singaporean UCSF students who have been my family far from home – being able to celebrate with epic Singaporean feasts on Chinese New Year to just spending time together on board games – you all definitely been a bastion of support. To my climbing crew of amazing science ladies – Kelly, Aarati, Natsumi and Kanaga, it has been such a joy getting to know you all during (and outside of!) our weekly climbing sessions. To Kelly, my fellow regulatory T cell nerd, I will definitely miss our weekly drive to yoga sessions ranting about immunology, regulatory T cells and obsessing over what Alex Honnold is currently attempting. Lastly, to my old girlfriends of more than a decade – thank you for your support and always being a constant source of helpful distraction when I needed it. To Liqi, especially, for always being available to listen and grumble about work in a way that only graduate students in the throes of being forced to write can do.

Joining a lab is one of the biggest life decisions a graduate student can make – and the extraordinary amount of time spent with this amazing group of people has been one of the best decisions in my time here. To Norm and Yishi, thank you for being the two rocks that anchored me during my graduate student innocence during the infancy of the lab, and I always remember celebrating the first time my western blot worked! To Joanna, thank you for your enthusiasm through all iterations of my project, and I am so fortunate to have the opportunity to talk about

and absorb your love for science. To Dan and Ventura, thank you for allowing me to boss you both around the lab, and handling my random and crazy rants and complaints while probably rolling your eyes in the background. And finally, to Elze, the Leslie to my Ann, the dendritic cell to my T cell, my companion through the valley of never-ending manuscript drafts, thank you for everything. I will miss being physically able to text you for coffee and pick your brain on everything under the sun, and hearing all about your latest weird theories or go crazy on your future experiments. Here's to many more long years of long conversations and being immunology nerds together.

I am fortunate to have the love and understanding of my family, who let me spread my wings into the world. To my mom, who has always been the strongest woman I have ever known, and who showered us all with love, and always picked me up when I was down. To my papa, who tried unsuccessfully to get me to be interested in chemistry and physics but ended up creating a daughter who went into immunology instead, dashing his hopes. Both my parents instilled in us that trying our best was more important than being the best. Their gentle patience and generosity of spirit has definitely rubbed off my siblings and me. To my little sister and brother, thank you for picking up the slack and letting me be away for so long without worrying about things back home. To my grandma, who practically raised me from a baby, my eternal gratitude and love for molding me into what I am today. If I could get her on the phone with my reviewers, I am sure she would have my manuscript accepted to the journal of my choice tomorrow.

Last of all, to my fellow nerd, my partner-in-crime, and my life-support system, Junying. We have been on this journey across three continents and 10 years, and I definitely could not have done this without you. Thank you for patiently evaluating my convoluted R code, and then giving up and writing me a newer, better one anyway. Thank you for making sure I had a life outside

the lab by forcing me to put down my work once I got home. Thank you for coming in with me to lab on weekends and waiting patiently for hours at a time, so I did not have to be alone by myself. Thank you for opening my eyes to a totally different world of plants and geology and other macroscopic things that I used to ignore. I could continue, but it would require a whole other chapter. I love you, and look forward to when we are old and tenured and pulling out our respective dissertations out to reminiscence about the good old days. I can't wait to see what we do next.

Contributions to the presented work

The work presented in this dissertation was performed under the direct supervision and guidance of Dr Trevor D. Burt, M.D. Additional guidance and insight were provided by thesis committee members Dr Qizhi Tang, Ph.D., Dr Alexander Marson, M.D., Ph.D., Dr Susan J. Fisher, Ph.D.

Chapters 2 and 3 of this work are largely adopted from a manuscript in revision:

Ng MSF, Roth TL, Mendoza VF, Marson A, Burt TD. Helios predisposes human fetal CD4⁺ naïve T cells towards regulatory T cell differentiation. 2019 (in revision)

Helios enhances the preferential differentiation of fetal naïve CD4⁺ T cells into regulatory T cells

Melissa Ng

Abstract

T cell receptor (TCR) stimulation and cytokine cues drive the differentiation of CD4⁺ naïve T cells into effector T cell populations with distinct pro-inflammatory or regulatory functions. Unlike adult naïve T cells, human fetal naïve CD4⁺ T cells preferentially differentiate into FOXP3⁺ regulatory T (T_{reg}) cells upon TCR activation independent of exogenous cytokine signalling. This cell-intrinsic predisposition for T_{reg} differentiation is implicated in generating tolerance *in utero*; however, the underlying mechanisms remain largely unknown. Here, we reveal FOXP3-independent transcriptional and epigenetic programs shared between fetal naïve T cells and committed adult T_{reg} cells that are inactive in adult naïve T cells. We further demonstrate that these transcriptional programs are retained upon T_{reg} cell differentiation only in fetal-derived, but not adult-derived induced T_{reg} (iT_{reg}) cells. We identify a subset of T_{reg}-specific enhancers that are already active in fetal naïve T cells, including two active super-enhancers at *Helios*, a signature thymic T_{reg} gene. Helios is expressed in fetal naïve T cells, but not in adult naïve T cells, and only fetal iT_{reg} cells maintain Helios expression. Fetal, but not adult iT_{reg} cells, have suppressed IL-2 production, which is regulated by Helios in committed T_{reg} cells. CRISPR-Cas9 ablation of Helios in fetal naïve T cells thus resulted in increased IL-2 production by fetal iT_{reg} cells. Critically, *Helios* knockout in fetal naïve T cells impaired their subsequent differentiation into T_{reg} cells upon TCR stimulation, reduced the upregulation of immunosuppressive genes such as *IL10* in fetal iT_{reg} cells, and resulted in the increased upregulation of pro-inflammatory genes including *IFNG*. Subsequently, Helios knockout fetal iT_{reg} cells produced less IL-10 and

more IFN γ cytokines. Taken together, our results indicate a dual role for Helios in enhancing the cell-intrinsic predisposition of fetal naïve T cells for T_{reg} differentiation and fine-tuning eventual fetal T_{reg} function through transcriptional modulation. The T_{reg}-biased transcriptional and epigenetic programs within fetal naive T cells identified here could thus be utilized to engineer enhanced iT_{reg} populations from adult naïve T cells for adoptive cellular therapies.

Table of Contents

CHAPTER 1: INTRODUCTION.....	1
1.1 The generation of immune tolerance in early life.....	2
1.2 Regulatory T cells – differentiation and function.....	4
1.3 Aims of this study.....	7
CHAPTER 2: Helios enhances the preferential differentiation of fetal naïve CD4⁺ T cells into regulatory T cells.....	9
2.1. ABSTRACT.....	10
2.2. INTRODUCTION.....	11
2.3. RESULTS.....	15
2.3.1. <i>Human fetal naïve T cells express a partial T_{reg} transcriptome.....</i>	<i>15</i>
2.3.2. <i>Fetal-derived induced T_{reg} (iT_{reg}) cells maintain differential expression of the partial T_{reg}-specific transcriptome present in fetal naïve T cells at the steady state.....</i>	<i>16</i>
2.3.3. <i>Fetal iT_{reg} cells have increased sensitivity to TGFβ signaling.....</i>	<i>18</i>
2.3.4. <i>Fetal naïve T cells share a partial epigenetic landscape with adult T_{reg} cells.....</i>	<i>19</i>
2.3.5. <i>Fetal naïve T cells have increased open and active chromatin at two T_{reg}⁻ accessible superenhancers associated with Helios.....</i>	<i>22</i>
2.3.6. <i>Fetal naïve T cells have increased Helios protein expression at baseline.....</i>	<i>24</i>
2.3.7. <i>The predisposition of fetal naïve T cells towards T_{reg} differentiation is not explained by recent thymic emigrant (RTE) abundance or increased proliferative ability.....</i>	<i>24</i>
2.3.8. <i>Fetal naïve T cells do not have increased demethylation at the FOXP3 T_{reg}⁻ specific demethylated region (TSDR).....</i>	<i>26</i>

2.3.9.	<i>Fetal naïve T cells upregulate and maintain Helios expression during iTreg differentiation.....</i>	<i>26</i>
2.3.10.	<i>Helios knockout in fetal naïve T cells impairs their ability to preferentially differentiate into T_{reg} cells.....</i>	<i>28</i>
2.3.11.	<i>Helios suppresses IL-2 secretion in fetal iT_{reg} cells.....</i>	<i>29</i>
2.3.12.	<i>Helios knockout results in the downregulation of genes associated with T_{reg} differentiation and function and the concurrent upregulation of pro-inflammatory genes.....</i>	<i>30</i>
2.3.13.	<i>Helios knockout fetal iT_{reg} cells have decreased IL-10 and increased IFNγ production.....</i>	<i>33</i>
2.4.	DISCUSSION AND CONCLUSIONS.....	35
2.5.	ACKNOWLEDGEMENTS.....	40
2.6.	FIGURES.....	41
2.7.	TABLES.....	92
	CHAPTER 3: MATERIALS AND METHODS.....	99
3.1.	Study design.....	100
3.2.	Cell isolation and purification.....	100
3.3.	Magnetic isolation of CD4 ⁺ T cells and fluorescence activated cell sorting (FACS) for sequencing and cell culture.....	101
3.4.	RNA sequencing for <i>ex vivo</i> sorted cells.....	102
3.5.	RNA sequencing for adult and fetal induced T _{reg} populations.....	102
3.6.	Gene set enrichment analysis (GSEA) for pairwise fetal versus adult iT _{reg} comparisons.....	104
3.7.	Assay for transposase-accessible chromatin (ATACseq)	104
3.8.	H3K27ac chromatin immunoprecipitation sequencing (ChIPseq)	101

3.9.	Identification of superenhancers (SEs) and transcriptional enhancers (TE) and comparison of enhancers with DESeq2.....	107
3.10.	Motif analysis for differentially expressed ATAC and H3K27ac peaks.....	109
3.11.	Flow cytometry staining for Helios and activation markers in sorted naïve and T _{reg} cells.....	110
3.12.	T _{reg} induction assays.....	111
3.13.	Methylation analysis of Treg-specific demethylated region (TSDR) in <i>FOXP3</i> conserved non-coding sequence 2 (CNS2).....	111
3.14.	CRISPR-Cas9 editing reagents.....	112
3.15.	CRISPR-Cas9 editing of the <i>Helios</i> locus.....	113
3.16.	RNA sequencing for Helios ^{KO} and Helios ^{WT} T _{reg} populations.....	114
3.17.	T cell restimulation and intracellular cytokine staining.....	115
3.18.	Cytokine bead assays.....	116
3.19.	Statistical analyses.....	116
3.20.	Sequencing data availability.....	117
	CHAPTER 4: FUTURE DIRECTIONS.....	118
4.1.	Evaluating the transition from a pro-tolerance fetal immune system towards sterilizing immunity in adulthood.....	119
4.2.	Identifying upstream environmental stimuli that “imprint” the fetal Treg-biased epigenome/transcriptome.....	120
4.3.	Generating functional and stable T _{reg} cell populations from naïve T cells <i>in vitro</i>	123
	REFERENCES.....	126

LIST OF FIGURES

Figure 2.6.1 Gating strategy and purity assessment for sorted naïve and T _{reg} cells.....	42
Figure 2.6.2 Definition of the T _{reg} transcriptional signature.....	44
Figure 2.6.3 Fetal naïve T cells have expression of a partial T _{reg} transcriptome.....	46
Figure 2.6.4 Fetal induced T _{reg} cells retain expression of the partial T _{reg} -specific transcriptome detected in fetal naïve T cells in steady state.....	48
Figure 2.6.5 Assessing the enrichment of T _{reg} upregulated or downregulated genes in fetal and adult induced T _{reg} (iT _{reg}) populations.....	50
Figure 2.6.6 Fetal induced Treg cells have increased sensitivity to TGFβ signaling.....	52
Figure 2.6.7 Identification of T _{reg} -accessible and inaccessible enhancers.....	54
Figure 2.6.8 Fetal naïve T cells have increased ATAC and H3K27ac enrichment at two T _{reg} -accessible superenhancers associated with Helios.....	56
Figure 2.6.9 Binding motifs for downstream effectors of T _{reg} differentiation are enriched within shared T _{reg} -accessible peaks in fetal naïve T cells.....	59
Figure 2.6.10 The highest ranked super-enhancers shared across all cell populations are associated with T cell development and function.....	61
Figure 2.6.11 Helios expression is increased in fetal naïve T cells.....	63
Figure 2.6.12 Chromatin accessibility and H3K27ac enrichment at the Helios locus in fetal naïve T cells correlate with increased RNA and protein expression.....	65
Figure 2.6.13 Fetal naïve T cells do not have an increased proportion of CD31 ⁺ recent thymic emigrants (RTE) relative to adult naïve T cells.....	67

Figure 2.6.14 A fraction of fetal naïve T cells are highly proliferative.....	69
Figure 2.6.15 Fetal naïve T cells do not have demethylation at the <i>FOXP3</i> CNS2 (conserved non-coding sequence 2) Treg-specific demethylated region (TSDR).....	71
Figure 2.6.16 Helios ⁺ fetal induced T _{reg} cells have increased FOXP3 expression.....	73
Figure 2.6.17 Fetal naïve T cells upregulate Helios during T _{reg} induction.....	75
Figure 2.6.18 Validation of CRISPR-Cas9 editing at the Helios locus.....	77
Figure 2.6.19 CRISPR-Cas9 mediated knockout of Helios in fetal naïve T cells reduces their preferential differentiation into T _{reg} cells.....	79
Figure 2.6.20 The effect of CRISPR-Cas9 knockout of Helios on protein expression of T _{reg} functional markers is variable.....	81
Figure 2.6.21 Fetal, but not adult, induced T _{reg} cells have suppressed IL-2 production after restimulation.....	83
Figure 2.6.22 Helios knockout in fetal iT _{reg} cells result in a subtle shift in the underlying transcriptome.....	86
Figure 2.6.23 Ablation of Helios in fetal iT _{reg} results in downregulation of T _{reg} -specific genes, and the concurrent upregulation of pro-inflammatory genes	88
Figure 2.6.24 Fetal Helios knockout iT _{reg} cells have decreased IL-10 and increased IFN γ cytokine production.....	90

LIST OF TABLES

<u>Table 2.7.1</u> T _{reg} -specific upregulated and downregulated signature in <i>ex vivo</i> T _{reg} cells with cluster assignment	
<u>Table 2.7.2</u> Upregulated/downregulated differentially expressed genes between fetal and adult iT _{reg} cells differentiated in IL-2 alone or with added exogenous TGFβ with cluster assignment	
<u>Table 2.7.3</u> Pre-ranked gene set enrichment analysis results for fetal versus adult iT _{reg} comparisons.....	93
<u>Table 2.7.4</u> T _{reg} -accessible enhancers	
<u>Table 2.7.5</u> T _{reg} -inaccessible enhancers	
<u>Table 2.7.6</u> De novo motifs enriched in ATAC T _{reg} -accessible peaks shared between fetal naïve and adult T _{reg} cells	
<u>Table 2.7.7</u> Shared superenhancers between adult naïve, adult T _{reg} and fetal naïve T cells.....	95
<u>Table 2.7.8</u> Experimental setup for experiments investigating Helios upregulation in fetal iT _{reg} cells over days 1,3 and 5.....	97
<u>Table 2.7.9</u> Experimental setup for experiments investigating the impact of Helios knockout on T _{reg} differentiation.....	98
<u>Table 2.7.10</u> Upregulated/downregulated differentially expressed genes in Helios knockout versus wild type fetal iT _{reg} cells	

Underlined tables can be found as supplemental files in the online version of this dissertation.

CHAPTER 1 - INTRODUCTION

1.1 The generation of immune tolerance in early life

The immune system must constantly maintain balance between two contradictory functions – it must achieve a sterilizing, pro-inflammatory response against pathogens defined as non-self, while minimizing collateral, non-specific damage towards the host organism. This ability to recognize the enormous variety of pathogens that come into contact with the host necessitates the generation of a large repertoire of receptors recognizing these non-self entities; however, since the receptor generation process is largely governed by probability and is thus non-specific, the immune system must find a way to prune cells bearing receptors that end up recognizing self antigens. Within the T cell arm of the immune system, this is enforced during T cell development in the thymus by a mechanism termed “central tolerance”. Presentation of tissue-specific antigens driven by the Aire transcription factor (1, 2), and as well as other self antigens presented by thymic dendritic cells (3) and migrating antigen-presenting cells (4), weeds out reactive T cells by apoptosis in the process of negative selection.

Notably, the concept of tolerance first arose by experiments on neonatal animals – first through studies in 1945 by Ray Owen on dizygotic male-female twin cattle which showed that both twins had an equal mix of autologous (self) and allogenic (non-self) erythrocytes that persisted throughout life, indicating the generation of tolerance towards the foreign antigens derived from the genetically distinct twin (5). Additional studies also emerged supporting the concept of tolerance generated in early life by skin graft transplant studies between fraternal cattle twins, which again showed the absence of rejection between two genetically dissimilar animals (6). Further dissection in mice and chickens revealed that this phenomenon could also be recreated in strains that were of completely different genetic backgrounds, but only if antigenic stimulation was provided during fetal life (7). These findings actively kick-started the discoveries leading to the formulation of the theory of central tolerance – that tolerance was actively

generated in response to antigen exposure by the elimination of cell “clones” carrying a receptor that recognized the particular antigen.

Interestingly, it has been perhaps overlooked that the tolerance obtained in Billingham’s and Medawar’s skin graft experiments is not fully penetrant, since the only three out of the five transplant grafts on fetal mice were actually tolerated. Furthermore, tolerance to the graft in mice could be revoked easily if they were re-implanted with lymph nodes from the same strain of mice that were actively immunized against the donor mice (i.e. a crude transfer of antigen-experienced memory and effector cells!) (7). On hindsight, it seems that these experiments were maybe more suggestive of a second mechanism of tolerance – that of dominant tolerance being enforced by a cell population that is actively suppressing effector cell responses, which could be overturned by overwhelming the population with antigen-experienced cells. Within the T cell compartment, the best-studied population is CD4⁺CD25^{hi}FOXP3^{hi} regulatory T (T_{reg}) cells, which were first described as CD25^{hi} suppressor cells in 1995 by Sakaguchi (8), and were jointly described as FOXP3⁺ in 2003 by three independent groups (9-11). In another nod to the importance of dominant tolerance in early life, inklings that such a cell population was present within the T cell compartment was borne from observations in thymectomy of 3 day old mice that resulted in autoimmune disease (12). Full ablation of the T_{reg} population in mice by genetic knockout of FOXP3, the master transcription factor regulating T_{reg} development and function or by transfer of only CD25^{lo} T cells into an athymic nude mouse, then resulted in early-onset fatal autoimmunity within a month (summarized in (13)).

Similarly, the loss of FOXP3 manifests within human as the disease IPEX (Immune dysregulation, polyendocrinopathy, enteropathy, X-linked), where mutations at the *FOXP3* locus lead to an absent or non-functional T_{reg} population, leading to death of the neonate without

hematopoietic stem cell transplant (11, 14, 15). There has been growing recognition that IPEX can initiate *in utero*, and the onset of autoimmunity coincides with the emergence of T cells in the peripheral lymphoid organs in the second trimester. This suggests that active T_{reg} cell mediated tolerance is required as early as the second trimester in humans, and the loss of tolerance leads to pro-inflammatory responses that trigger adverse outcomes such as miscarriage and preterm birth (16-20).

1.2 Regulatory T cells – differentiation and function

T_{reg} cells have been delineated into two distinct populations based on their differentiation origin – thymic or peripheral. Thymic T_{reg} (tT_{reg}) cells have been proposed to be derived in the thymus from CD4 single positive (SP) thymocytes bearing T cell receptors that have a strong affinity for self-antigens that straddle a middle ground for TCR signaling strength between negative and positive selection thresholds. By directing self-reactive thymocytes away from deletion towards a T_{reg} cell fate, this allows the immune system to generate dominant tolerance towards self-antigens (summarized in (21)). In contrast, peripheral T_{reg} (pT_{reg}) cells are generally assumed to have differentiated from CD4⁺ naïve T cells after antigen stimulation that is received simultaneously with specific signaling cues from cytokines such as TGFβ, and small molecules such as retinoic acid (RA) that are produced locally in peripheral organs such as the gut (22-24). Signaling by TGFβ is especially crucial for pT_{reg} over tT_{reg} generation, since T cell specific ablation of TGFβ1 (25) and TGFβRII (26, 27) results in the paucity of the former and not the latter. Given that activation usually occurs to non-self antigen, this is thought to be a mechanism by which dominant tolerance to harmless non-self antigens derived from environmental, food or commensal microbial origins is generated. Regardless of their developmental origins, both T_{reg} subsets are characterized by constitutive expression of FOXP3, which is maintained by epigenetic and transcriptional mechanisms at the *FOXP3* gene locus. One such epigenetic

mechanism is DNA demethylation at T_{reg}-specific demethylated region (TSDR) the within conserved non-coding sequence (CNS) 2 region in the *FOXP3* gene, which is required for continued stability of the T_{reg} phenotype. Acquisition of TSDR demethylation occurs concurrently, but independently of FOXP3 expression (28). Deletion of the CNS2 in the T_{reg} population led to the gradual loss of FOXP3 expression over time, as seen in the reduced percentages of T_{reg} cells in the peripheral lymphoid organs in old but not young mice (29). This was linked to proliferation-induced instability as FOXP3^{ΔCNS2-gfp} T_{reg} cells lost FOXP3 progressively over rounds of division induced by TCR signaling *in vitro* (29).

Additional changes in the enhancer landscape also precede the upregulation of FOXP3 and commitment to the T_{reg} phenotype, and this has been elucidated most clearly in thymic T_{reg} precursors (30). These changes are governed by the acquisition of permissive histone modifications such as acetylation at lysine 27 at histone 3 (H3K27ac), which increase the accessibility of the underlying histone-wrapped DNA to allow the recruitment of transcriptional machinery to the associated gene to initiate gene transcription. By collapsing individual enhancer regions into large stitched super-enhancer (SE) regions, SEs identified to be specific to T_{reg} and not conventional T cells were found to be associated with genes regulating T_{reg} function and commitment such as *FOXP3*, *IL2RA* and *CTLA4* (30). These T_{reg} SE regions gained permissive histone marks progressively throughout thymic T_{reg} differentiation before FOXP3 upregulation and final commitment into tT_{reg} cells (30). The genome organizer SATB1 (Special AT-rich sequence binding protein 1) plays a key role in facilitating enhancer activation at closed T_{reg} SE. Deletion of SATB1 within CD4 SP thymocytes resulted in the depletion of thymic T_{reg} populations and this was specifically attributed to the inability of thymic T_{reg} progenitors to acquire permissive histone marks at T_{reg} SE that impaired their subsequent differentiation into T_{reg} cells (30). Given that the pT_{reg} population also show a similar enhancer

landscape and demethylation patterns (28, 30, 31), it seems likely that similar mechanisms also govern their differentiation from naïve T cells; however the upstream mediators and molecular pathways that regulate this have yet to be elucidated.

Although that T_{reg} cells comprise such a small fraction of the total population in mice and humans (naturally about 5% in human adult peripheral blood), they exert outsized effects on dominant immune tolerance given the fatal immunopathology that results when the entire population is ablated. T_{reg} cells have been proposed to mediate suppression of a large variety of cell types (summarized in (32)), and this is likely due to their ability to mediate “bystander” suppression even after antigen-specific activation through the use of non-specific suppressive mechanisms. Mechanisms utilized include (1) the secretion of immunosuppressive cytokines such as IL-10, TGFβ and IL-35, (2) preferential consumption, and thus deprivation of survival factors such as IL-2 to conventional T cells, (3) cell-contact dependent suppression via cell surface molecules such as CTLA-4 and (4) the functional modulation of antigen presentation capability of antigen presenting cells (APCs) to suppress their subsequent activation of antigen-specific conventional T cells. (summarized in reviews (33, 34)). Given the potent and multifactorial effects of immunosuppression mediated by T_{reg} cells, there has been great interest in their generation *in vitro* for use in clinical settings of autoimmunity and inflammation. Early studies found that a FOXP3^{hi}CD25^{hi} induced T_{reg} (iT_{reg}) population can be generated *in vitro* from naïve T cells in both mice and humans through the use of TCR stimulation together with TGFβ (35, 36). However this conversion is only observed for a subset of human naïve T cells and not the full population, which presents a problem of obtaining a phenotypically pure population of FOXP3^{hi}CD25^{hi} iT_{reg} (37). Additionally, human iT_{reg} cells generated from adult naïve T cells fail to repress the *IL2* and *IFNG* locus, leading to re-stimulation induced production of IL-2 and IFNγ (37). Lastly, iT_{reg} cells fail to acquire T_{reg}-specific demethylation patterns at *FOXP3* and other

well-defined T_{reg} gene regions such as *GITR* and *CTLA4* (28), which resulted in the failure of iT_{reg} cells to retain the T_{reg} phenotype upon transfer *in vivo*, and reversion into an effector phenotype (38). As such, it is clear that TGFβ driven *in vitro* T_{reg} differentiation does not fully recapitulate T_{reg} differentiation *in vivo*, and further characterization of upstream factors that drive T_{reg} commitment and stability *in vivo* is greatly needed.

1.3 Aims of this study

Consistent with the need for T_{reg} mediated tolerance in fetal development, we observe that T_{reg} cells comprise a larger percentage of the CD4⁺ T cell population in secondary lymphoid tissues compared to adults, ranging from 10% up to 20% (39-41). However, thymic T_{reg} percentages within the fetal and postnatal thymus were not found to be different (40), excluding the possibility that increased tT_{reg} output could account for the increased T_{reg} cell frequency in the periphery.

We have also shown that a larger proportion of fetal naïve T cells differentiate *in vitro* into T_{reg} cells upon antigenic stimulation with APCs (41), or TCR stimulation with TGFβ (42).

Interestingly, an average of about 20-40% of fetal naïve T cells can differentiate into T_{reg} cells *in vitro* with TCR stimulation in the absence of TGFβ supplementation (42), which is unusual given that TGFβ is thought to be necessary for inducing FOXP3 expression and T_{reg} differentiation *in vitro*. This unique ability for increased T_{reg} differentiation in the absence of TGFβ suggests that cell-intrinsic mechanisms predispose fetal naïve T cells towards the T_{reg} cell fate, and implies that conversion from naïve T cells in the periphery might be responsible for the increased T_{reg} proportions observed.

The aims of this work were to identify the molecular mechanisms underpinning preferential T_{reg} differentiation; specifically, whether the transcriptional and epigenetic landscape in fetal naïve T cells were analogous to that of thymic T_{reg} progenitors, thus poising the fetal naïve T cell for T_{reg}

differentiation. We predicted that this approach would result in the identification of candidate genes that would allow us to more carefully dissect the pathways leading to fetal T_{reg} differentiation. Lastly, this approach would provide a valuable resource to the community by identifying cell-intrinsic factors that could contribute to strategies to induce T_{reg} populations *in vitro* that more closely resemble T_{reg} populations *in vivo* in terms of stability and function.

CHAPTER 2 - Helios predisposes fetal naïve CD4⁺ T cells towards regulatory T cell differentiation

Material for this chapter was modified from a manuscript currently in revision:

Ng MSF, Roth TL, Mendoza VF, Marson A, Burt TD. Helios predisposes human fetal CD4⁺ naïve T cells towards regulatory T cell differentiation. 2019 (in revision)

2.1 ABSTRACT

T cell receptor (TCR) stimulation and cytokine cues drive differentiation of CD4⁺ naïve T cells into effector T cell populations with distinct pro-inflammatory or regulatory functions. Unlike adult naïve T cells, human fetal naïve CD4⁺ T cells preferentially differentiate into FOXP3⁺ regulatory T (T_{reg}) cells upon TCR activation independent of exogenous cytokine signalling. This cell-intrinsic predisposition for T_{reg} differentiation is crucial for generating tolerance *in utero*; however, the underlying mechanisms remain largely unknown. Here, we identify epigenetic and transcriptional programs shared between fetal naïve T and committed T_{reg} cells that are inactive in adult naïve T cells, and that only fetal-derived induced T_{reg} (iT_{reg}) cells retain these transcriptional programs. We show that a subset of T_{reg}-specific enhancers are accessible in fetal naïve T cells, including two active super-enhancers at *Helios*. *Helios* is expressed in fetal naïve T cells, but not in adult naïve T cells, and only fetal iT_{reg} cells maintain *Helios* expression. CRISPR-Cas9 ablation of *Helios* in fetal naïve T cells impaired their differentiation into T_{reg} cells upon TCR stimulation, reduced expression of genes in fetal iT_{reg} cells associated with immunosuppressive function such as *IL10*, and increased expression of pro-inflammatory genes including *IFNG*. Subsequently, *Helios* knockout fetal iT_{reg} cells had reduced IL-10 and increased IFN γ cytokine production. Together, our results reveal an important role for *Helios* in enhancing preferential fetal T_{reg} differentiation and fine-tuning eventual T_{reg} function. The T_{reg}-biased programs identified within fetal naïve T cells could potentially be utilized to engineer enhanced iT_{reg} populations for adoptive cellular therapies.

2.2 INTRODUCTION

The adaptive immune system must generate immunotolerance in order to prevent or resolve pro-inflammatory responses that can cause host damage (24, 43, 44), while still permitting functional effector responses for host defense against pathogens (45, 46). A primary mechanism by which this flexibility is achieved is via the capacity of CD4⁺ naive T cells to differentiate into multiple distinct specialized T helper subsets with either pro-inflammatory or immunosuppressive functions. The presence of polarizing cytokines within their immediate environment determine the eventual helper T (Th) cell fate by triggering the expression and/or activation of master transcription factors that enact lineage specific transcriptional programs (47). Signaling by transforming growth factor β (TGF β) promotes the induction of FOXP3 (35, 36, 48), which is the master transcription factor required for the differentiation of naïve T cells into immunosuppressive regulatory T (T_{reg}) cells.

Mutations of the *FOXP3* gene leading to the complete absence or dysfunction of T_{reg} cells results in the loss of T_{reg}-mediated immunotolerance, and triggers fatal, early onset multi-organ autoimmunity in both mice and humans (9, 11, 14, 15, 49, 50). Autoimmunity resulting from the loss of FOXP3⁺ T_{reg} cell-mediated tolerance in humans, defined as the disease IPEX (Immune dysregulation, polyendocrinopathy, enteropathy, X-linked), can manifest within the fetus *in utero* and result in miscarriage, preterm birth, and ultimately neonatal death without hematopoietic stem cell transplant (16-20). The initiation of autoimmunity in IPEX coincides with the emergence of T cells in the second trimester of human development, suggesting that T_{reg} cell-mediated peripheral tolerance is required during fetal development (51, 52). This is supported by the presence of an abundant population of fetal T_{reg} cells in the secondary lymphoid tissues, which comprise a larger percentage of the total CD4⁺ T cell population compared to adults (39-41). However, thymic T_{reg} cell frequencies in fetal and infant thymus are not significantly different

(40), indicating that increased thymic output is not responsible for the increased frequency of fetal T_{reg} cells. Fetal naïve T cells, unlike their adult counterparts, preferentially differentiate into functional T_{reg} cells upon antigenic encounter, which include non-inherited maternal allo-antigens (i.e. NIMAs) on maternal antigen presenting cells (40). These findings suggest that the abundance of fetal T_{reg} cells observed in fetal lymphoid tissues is due to peripheral conversion from naïve T cells. This propensity for T_{reg} differentiation is retained *in vitro*, as a high frequency of fetal naïve T cells differentiate into FOXP3⁺ T_{reg} cells upon TCR activation even in the absence of exogenous TGFβ (42). The unique capability of fetal naïve T cells initiate T_{reg} differentiation in the absence of exogenous TGFβ suggests that this ability is cell-intrinsic; however, the molecular mechanisms that underlie this predisposition are largely unknown.

Chromatin changes are also implicated in driving the final effector phenotype and function of differentiated T cells, defined by increases in chromatin accessibility of active lineage-specific genes, and the silencing of genes associated with other effector lineages (53, 54). In thymic and peripheral T_{reg} cells, the accumulation of permissive/active histone marks and DNA demethylation at T_{reg} associated genes such as *IL2RA* (i.e., CD25), *CTLA4*, *IKZF2* (i.e., Helios), and *IKZF4* (i.e., Eos) (28, 30) must be acquired for commitment to and maintenance of the T_{reg} phenotype (28-30, 55). This T_{reg}-chromatin landscape is acquired within developing thymic T_{reg}-cell precursors before FOXP3 protein expression (30), suggesting that a T_{reg}-specific epigenome may be responsible for initiating and promoting the expression of *FOXP3*. Additionally, other key genes associated with the T_{reg} epigenome, such as Helios, are expressed independently of FOXP3 expression (28, 30, 56), and can direct the partial acquisition of the T_{reg}-specific transcriptional signature when over-expressed in FOXP3⁻CD4⁺ T cells (57). We therefore hypothesized that fetal naïve T cells might already possess a partial T_{reg}-specific

epigenetic and transcriptional signature that predisposes them for differentiation towards the T_{reg} cell fate even without exogenous TGFβ signaling.

Here, we interrogated the transcriptional and chromatin landscape of fetal and adult naïve and T_{reg} cells, and indeed discovered that components of the T_{reg} gene regulatory program are already activated in fetal naïve T cells, but not in adult naïve T cells. We show the partial T_{reg}-specific gene signature detected at steady state in fetal naïve T cells is retained only fetal-derived, but not adult induced T_{reg} cells. We further identify two T_{reg}-specific super-enhancers (SEs) associated with the *Helios* locus that are active in fetal naïve, but not adult naïve T cells. Correspondingly, protein expression of Helios was increased in fetal naïve T cells over adult naïve T cells. Only induced T_{reg} (iT_{reg}) cells generated from fetal naïve T cells *in vitro* retained Helios expression and were characterized by repression of IL-2 production; both of which were not observed in adult iT_{reg} cells. CRISPR-mediated ablation of Helios in fetal naïve T cells impaired their cell-intrinsic ability to differentiate into T_{reg} cells in the absence of exogenous TGFβ. Analysis of the transcriptome in *Helios* knockout iT_{reg} cells revealed that Helios enhanced the upregulation of T_{reg}-specific genes (e.g., *IL10*) and mediated the repression of pro-inflammatory genes involved in Th effector differentiation and function (e.g., *IFNG*). Helios ablation in fetal iT_{reg} cells subsequently resulted in decreased IL-10 cytokine production concurrent with increased IFNγ and IL-2. Given that Helios has been previously characterized to be a gene specific to thymic T_{reg} cells, our data reveal a new role for Helios as part of a pre-existing epigenetic and transcriptional program within human fetal naïve T cells that lowers the threshold for T_{reg} differentiation and functional commitment. Taken together, we thus identify a TGFβ-independent mechanism unique to fetal naïve T cells that favors their differentiation into

T_{reg} cells, and may contribute insights into better engineering T_{reg} cells *in vitro* from naïve T cells for use in immunotherapy.

2.3 RESULTS

2.3.1 Human fetal naïve T cells express a partial T_{reg} transcriptome.

Given that fetal naïve T cells preferentially differentiate into T_{reg} cells upon TCR stimulation alone (42), we first asked if fetal naïve T cells shared elements of their transcriptome with T_{reg} cells that could predispose them towards the T_{reg} lineage. We performed RNA sequencing (RNAseq) on sorted fetal and adult $CD4^+$ naïve and T_{reg} cells (for sort gating strategy and purity confirmation, see Fig. 1). Principal component analysis (PCA) revealed that fetal and adult populations first segregated by cell origin (PC1, fetal or adult) before cell phenotype (PC2, naïve versus T_{reg} , Fig. 3A). PC2 scores for fetal naïve samples were intermediate to adult naïve and T_{reg} samples (Fig. 3A), suggestive of intermediate expression of T_{reg} -specific genes in fetal naïve T cells. In order to test this hypothesis, we first defined a T_{reg} -specific transcriptional signature by identifying genes differentially expressed in both fetal and adult T_{reg} cells relative to adult naïve T cells based on a false discovery rate cut-off of $FDR < 0.05$ and log 2 fold change (\log_2FC) increase in expression of 1.5 (Fig. 2, Table 1). Fetal naïve T cells possessed intermediate upregulation/downregulation (Fig. 3B) across genes upregulated/downregulated in our T_{reg} -specific transcriptional signature. More specifically, relative to adult naïve T cells, fetal naïve T cells had 88 T_{reg} -upregulated and 42 T_{reg} -downregulated genes within the T_{reg} -specific transcriptome (Fig. 1C). Using k-means clustering, we defined four different clusters within the full T_{reg} -specific transcriptome (Fig. 3B, Table 1) – two of which corresponded to all T_{reg} -upregulated genes (Cluster 1.1, 1.2), while the other two clusters contained all T_{reg} -downregulated genes (Cluster 1.3, 1.4). Within T_{reg} -upregulated genes, fetal naïve T cells did not share expression of canonical T_{reg} genes such as *FOXP3*, *IL2RA* and *CTLA-4* with adult and fetal T_{reg} cells (Cluster 1.1, Fig. 3B). Instead, fetal naïve T cells had increased expression of T_{reg} -upregulated genes associated with Cluster 1.2 (Fig. 3B), which contained genes previously

associated with T_{reg} function such as *CCR4* (58, 59) and *KLF10* (60-62), as well as the transcription factors *IKZF2* (Helios) (63-65) and *IKZF4* (Eos) (57, 66) (Cluster 2, Fig. 3B,1C) which are transcribed independently of FOXP3 expression in mice (28, 56, 67). Similarly, fetal naïve T cells and both the T_{reg} cell populations shared similar downregulation of a subset of genes such as *TSHZ2* and *SERPINB6* (68-70) (Cluster 1.3, Fig. 3B) previously characterized as being downregulated in T_{reg} cells. Taken together, our data suggest that although both fetal and adult naïve T cells share expression of genes corresponding to their naïve T cell phenotype such as *TCF7* and *IL7R* (Cluster 1.4, Fig. 3B), fetal naïve T cells are already transcriptionally primed at steady state to differentiate into T_{reg} cells. The presence of a partial T_{reg} -specific signature in fetal naïve T cells could then help potentiate T_{reg} differentiation upon the receipt of TCR signaling, consistent with the lowered threshold and greater propensity for these cells towards T_{reg} differentiation (40, 42).

2.3.2 Fetal-derived induced T_{reg} (iT_{reg}) cells maintain differential expression of the partial T_{reg} -specific transcriptome present in fetal naïve T cells at the steady state.

We next asked if the partial T_{reg} -specific transcriptome detected in fetal naïve T cells would remain differentially expressed in fetal iT_{reg} cells, or whether adult iT_{reg} cells eventually acquire the T_{reg} -specific transcriptome after *in vitro* differentiation. To assess this, we performed RNAseq on fetal and adult iT_{reg} cells that underwent differentiation with TCR stimulation in media supplemented with interleukin 2 (IL-2- iT_{reg}) alone or additionally supplemented with TGF β (TGF β - iT_{reg}). PCA revealed that PC1 still segregated iT_{reg} populations by cell origin (fetal or adult), after which populations separated by the stimulus received during differentiation (absence/presence of TGF β , PC2, Figure 2A). This indicated that fetal-derived iT_{reg} cells were

still transcriptionally different from adult-derived iT_{reg} cells, although the addition of TGFβ was sufficient to drive differential expression of a shared set of genes. We then evaluated all differentially expressed genes (FDR<0.05 and log₂FC>1.5) across all iT_{reg} populations (Fig. 4B), and defined six clusters using k-means clustering (Table 2). Both populations of fetal and adult TGFβ-iT_{reg} cells upregulated expression of two gene clusters (Cluster 2.1& 2.2, Fig. 4B, Fig. 5A), and downregulated expression of one gene cluster (Cluster 2.6, Fig.4B, Fig. 5A). This included T_{reg}-specific genes known to be upregulated with TGFβ signaling such as *FOXP3* and *IKZF4* (71), as well genes potentially implicated in T_{reg} differentiation and function such as *SEMA4A* (72), *LTBP1*, *LTBP4* (73) and *LGALS3* (74, 75). However, although adult TGFβ-iT_{reg} cells acquire expression of several T_{reg}-specific genes, only fetal iT_{reg} cells had increased expression of T_{reg}-specific genes associated with Cluster 2.3 (Fig. 4B, Fig. 5A) regardless of stimulation condition, including genes such as *IKZF2*, *DUSP4*, *TOX* and *RGS1* that already had increased expression in *ex vivo* fetal naïve T cells (Fig. 1C). Decreased transcription of pro-inflammatory transcripts such as *IFNG*, *IL2*, *GZMB* and *IRF7* (Cluster 2.5, Fig. 4B, Fig. 5A), and increased expression of genes involved in T_{reg} cell suppressive function such as *IL10* (Cluster 2.3, Fig. 4B) were only observed in fetal, but not adult, iT_{reg} cells. This suggested that qualitatively, fetal iT_{reg} cells, especially TGFβ-iT_{reg} cells, have a transcriptome more reflective of *ex vivo* T_{reg} populations relative to adult iT_{reg} cells. We thus utilized Gene Set Enrichment Analysis (GSEA) to independently compare the transcriptomes of fetal or adult-derived iT_{reg} populations against published gene sets comparing T_{reg} and conventional T cell populations that also underwent TCR and cytokine stimulated activation *in vitro* (56, 76) (Fig. 5B, Table 3). In comparison to adult iT_{reg} cells, fetal iT_{reg} cells differentiated in both stimulation conditions had enrichment in genes upregulated in activated T_{reg} populations (Fig. 4B), as well as continued enrichment of the partial T_{reg}-specific signature as defined by Cluster 1.2 and 1.3 (Fig. 3B, 2C,

left, Fig. 5C). Exogenous TGF β signaling during T_{reg} differentiation then resulted in the enrichment of Cluster 1.1 and depletion of Cluster 1.4 genes within fetal TGF β -iT_{reg} but not adult TGF β -iT_{reg} cells (Fig. 4C, right, Fig. 5D). Our data thus show that differentiating fetal naïve T cells, independently of exogenous TGF β , retain increased expression of the partial T_{reg}-specific transcriptional signature detected in *ex vivo* naïve T cells. Furthermore, the expression of these genes do not reach the same levels in adult iT_{reg} cells, suggesting that upstream mechanisms might be responsible for driving the transcriptional differences that favor T_{reg} differentiation in fetal naïve T cells.

2.3.3 Fetal iT_{reg} cells have increased sensitivity to TGF β signaling

In addition to increased expression of genes associated with T_{reg} function, fetal IL-2-iT_{reg} cells strongly upregulated a gene cluster which included key genes associated with TGF β sequestration and downstream signaling – including *SMAD1*, *TGFBR3*, *LRRC32* (37, 77) and *LIN28B* (42) (Cluster 2.4, Fig. 4B, Fig. 6A). Additionally, increased expression of Lin28b protein exclusively in fetal naïve T cells results in increased expression of TGFBR1, TGFBR3, SMAD2, as well as increased phosphorylation of SMAD2/3 (42). GARP (*LRRC32*) is expressed highly on the cell surface of activated T_{reg} cells and captures the inactive TGF β bound to the latency-associated peptide (LAP) (37, 78). This reservoir of cell-surface associated TGF β is further implicated in the maintenance of oral tolerance in mice (77), as well as in the induction of FOXP3 in naïve T cells co-cultured with GARP⁺T_{reg} cells (37). Here we demonstrate that fetal but not adult iT_{reg} cells highly expressed GARP (Fig. 6B) and LAP in a linear fashion (Fig. 6C). Furthermore, fetal iT_{reg}, but not adult iT_{reg} cells have increased transcription of *ITGB8* (Cluster 3, Fig. 4B), the beta chain for the integrin $\alpha\beta$ 8 that processes and releases bioactive TGF β 1 from

LAP (77). Since fetal iTreg cells have increased cell surface-associated TGF β and the machinery to mediate its potential release, we tested whether blockade of TGF β 1 with TGF β -neutralizing antibodies resulted in decreased fetal T_{reg} differentiation in response to TCR stimulation alone. As hypothesized, fetal Treg induction was blunted in the setting of TGF β blockade (Fig. 6D, E). However, fetal naïve T cells still retained an increased ability for T_{reg} differentiation over adult naïve T cells at both blocking antibody concentrations, as well as when exogenous bioactive TGF β was added (Fig. 6D,E). Hence, although active TGF β 1 biogenesis may contribute to fetal iT_{reg} differentiation in the absence of exogenous TGF β , additional upstream mechanisms are responsible for driving enhanced fetal T_{reg} differentiation *in vitro*.

2.3.4 Fetal naïve T cells share a partial epigenetic landscape with adult T_{reg} cells

Given that fetal naïve T cells already express a partial T_{reg}-specific signature, we next assessed if we could also detect the presence of permissive epigenetic marks in fetal naïve T cells that could further drive the predisposition towards more robust T_{reg} cell differentiation. In order to identify these chromatin features, we used Assay for Transposase-Accessible Chromatin followed by sequencing (ATACseq) and H3K27ac chromatin immunoprecipitation sequencing (ChIPseq) to compare regions of open and active chromatin in adult T_{reg} cells relative to fetal and adult naïve T cells. Super-enhancers (SEs) and typical transcriptional enhancers (TEs) were classified using the ROSE algorithm (79, 80), and PCA was performed across enhancers identified in all samples. Cell origin (fetal versus adult) was the primary source of variance (PC1) in both ATACseq (Fig. 8A) and H3K27ac ChIPseq (Fig. 8B), and together with cell phenotype (naïve or T_{reg}), largely accounted for differences in the epigenome across all three populations. However, fetal naïve and adult T_{reg} cell samples clustered together across the second source of variance (PC2) in both datasets (Fig. 8A,B). This suggested that, in addition to

expression of a partial T_{reg}-specific transcriptome, fetal naïve T cells share a small subset of open and active T_{reg}-specific enhancers with adult T_{reg} cells.

We first independently defined enhancers differentially enriched for ATAC (Fig. 7A) or H3K27ac (Fig. 7B) signal in adult T_{reg} cells relative to adult naïve T cells (FDR<0.05; expression fold change>1.5). Enhancers classified as having both increased H3K27ac and ATAC signals in adult T_{reg} cells relative to adult naïve T cells were termed T_{reg}-accessible enhancers (Fig. 7C, Table 4), while common enhancers were defined as having no difference in enrichment of both signals (Fig. 7C). T_{reg}-inaccessible enhancers with decreased signals were similarly defined (Table 5). We then assessed if any T_{reg}-accessible enhancers that were enriched in fetal naïve T cells relative to adult naïve T cells. We found that fetal naïve T cells had increased ATAC signal at 38.8% (933/2405, Fig. 7D) and increased H3K27ac signal at 4.6% (110/2405, Fig. 7E) of enhancers within the T_{reg}-accessible enhancer signature (Fig. 8C). T_{reg}-accessible enhancers preferentially enriched in fetal naïve T cells (Table 4) were annotated to genes previously described to be part of the T_{reg}-specific epigenome, such as *IKZF2* (i.e., Helios), *IKZF4* (i.e., Eos) and *RXRA* (i.e., retinoic receptor RXR-alpha) (28, 30, 55). Similarly, 23.1% (426/1837, Fig. D) and 14% (258/1837, Fig. 7E) of T_{reg}-inaccessible enhancers also had decreased ATAC and H3K27ac signal, respectively, in fetal naïve T cells (Fig. 8C).

Since fetal naïve T cells demonstrated intermediate expression across the full T_{reg}-specific transcriptional signature, we assessed if fetal naïve T cells also had intermediate enrichment of open and active chromatin across the full T_{reg}-accessible/inaccessible enhancer signature. Fetal naïve T cells had increased enrichment of open chromatin across all T_{reg}-accessible enhancers relative to adult naïve T cells (left, Fig. 7F), and decreased enrichment of open chromatin across all T_{reg}-inaccessible enhancers (right, Fig. 7F). However, we did not detect similar

enrichment/depletion for H3K27ac across the T_{reg} -accessible or T_{reg} -inaccessible enhancer signature (Fig. 7G), consistent with the lower number of T_{reg} -accessible/inaccessible enhancers identified with increased/decreased H3K27ac signal in fetal naïve T cells (Fig. 8C). Taken together, our data suggests that fetal naïve T cells at steady state are poised for T_{reg} differentiation by the partial acquisition of a T_{reg} epigenomic landscape characterized by increased chromatin accessibility at more than a third of total T_{reg} -accessible enhancers relative to adult naïve T cells. Given that chromatin accessibility may precede H3K27ac deposition (81), acquisition of the T_{reg} epigenetic signature within fetal naïve T cells could occur in a stepwise fashion where full enhancer activation via H3K27ac deposition is acquired with the triggering of T_{reg} cell differentiation.

In support of this hypothesis, we evaluated transcription factor motif enrichment within all T_{reg} -accessible peaks shared between fetal naïve and committed adult T_{reg} cells (defined in a similar manner as TEs/SEs). Peak calls were utilized to minimize false positives stemming from the broadness of SE regions. Fetal naïve T cells had minimal enrichment of T_{reg} -accessible H3K27ac peaks, but had increased chromatin accessibility at a third of all T_{reg} -accessible ATAC peaks (Fig. 9A). These shared T_{reg} -accessible peaks had a large enrichment of binding motifs for the AP-1 complex (Fig. 9B) and RUNX1 (Fig. 9C, Table 6), which are downstream of TCR signaling and play critical roles as transcriptional regulators of the FOXP3 locus and as co-factors for FOXP3 (82). We also detected a smaller subset of peaks that had enrichment of binding motifs for STAT5 (Fig. 9D) and SMAD2/3 (Fig. 9E). This suggests that increased chromatin accessibility could potentially synergize with enhancer activation and faster transcription of genes underlying STAT5 and SMAD2/3 binding sites with IL-2 and TGF β signaling during fetal T_{reg} differentiation. Lastly, we examined differentially enriched T_{reg} -

accessible peaks in fetal naïve T cells for the presence of FOXP3 binding sites previously identified in human T_{reg} cells (82). We show that only 5% (116/2213) of shared T_{reg}-accessible peaks with increased chromatin accessibility have FOXP3 binding sites (Fig. 9F). Taken together, we further illustrate that increased chromatin accessibility within fetal naïve T cells is largely poised to synergize with TCR and cytokine signaling cues, and to a smaller extent, FOXP3 upregulation, to drive their preferential differentiation into T_{reg} cells.

2.3.5 Fetal naïve T cells have increased open and active chromatin at two T_{reg}-accessible superenhancers associated with Helios

SE regions nucleate the assembly of transcription factors to drive gene expression associated with cell lineage commitment (79, 80, 83). Highly ranked SEs shared across fetal naïve, adult naïve, and adult T_{reg} samples thus corresponded to genes commonly associated with global T cell development and function such as *BCL11B* (84) and *ETS1* (85) (Fig. 10A, Table 7).

Because increased accessibility at T_{reg} SE regions in murine thymic T_{reg} progenitors precedes FOXP3 upregulation and commitment to the T_{reg} lineage (30), we asked if increased accessibility at T_{reg}-accessible SEs in fetal naïve T cells could contribute to the priming of fetal naïve T cells for T_{reg} differentiation. Out of the 121 T_{reg}-accessible SEs identified, many were proximal to canonical T_{reg} genes including *FOXP3*, *IL2RA*, *CTLA4*, *TNFRSF4* (i.e., TNF receptor superfamily member 4) and *IKZF2* (Fig. 8D) as previously described in mice (30). Globally, fetal naïve T cells did not have greater accessible chromatin or H3K27ac enrichment at all T_{reg}-accessible SEs compared to adult naïve T cells (Fig. 10B). This suggested that unlike thymic T_{reg} progenitors, fetal naïve T cells might acquire active enhancer marks at the full T_{reg}-accessible SE signature only after T_{reg} differentiation. Since we did not observe enrichment of

open or active chromatin across the full T_{reg} -accessible SE signature, we wondered if any SEs independently classified by ROSE, and preferentially enriched within fetal naïve T cells relative to adult naïve T cells, were proximal to genes associated with T_{reg} accessible-SEs, since their presence would have been masked by the global analysis. Most genes associated with T_{reg} accessible-SEs did not have enrichment of H3K27ac signal that met the SE cut-off in both fetal and adult naïve T cells (Fig. 8E). One exception was the transcription factor *IKZF2* (i.e., Helios), which was unique to fetal naïve T cells (left, Fig. 8E), and previously identified to be one of the first T_{reg} -SEs to acquire permissive epigenetic marks in murine thymic T_{reg} progenitors (30). Adult naïve T cells had independent SE classification for one gene, *ZC3H12D* (right, Fig. 8E); however, its association with T_{reg} cell function is yet unknown.

Cell-specific SE regions are typically found proximal to genes encoding transcription factors that play key roles in cell identity by controlling the transcription of lineage-specific transcriptional programs (30, 79). We next expanded our analysis to evaluate if any T_{reg} -accessible SEs defined within adult T_{reg} cells had increased enrichment of either ATAC or H3K27ac signal in fetal naïve T cells relative to adult naïve T cells (Fig. 8C), and were also associated with known transcription factors. We identified five T_{reg} -accessible SEs associated with four different transcription factors with increased ATAC signal (Fig. 8F), of which only two T_{reg} -accessible SEs were also differentially enriched for H3K27ac (Figure 3G). Both of these active, H3K27ac-marked T_{reg} -accessible SEs were located in the intragenic and upstream regions within the *Helios* locus (Figure 4A), indicating that active expression of Helios might already be present in fetal naïve T cells. Helios was identified as a major contributor to PC2 (Fig. 11B) by RNAseq, which segregated cells by naïve or T_{reg} phenotypes, and was among the significant T_{reg} -upregulated genes with increased RNA transcription in fetal naïve T cells relative to adult naïve

T cells (Fig. 1C, Fig. 11C). Since a SE was also independently identified at the Helios locus in fetal naïve T cells (Fig. 8E), and enriched permissive epigenetic marks and transcription at the Helios gene locus regulate T_{reg} phenotype and function independent of FOXP3 expression in mice (28, 56, 86, 87), we further investigated Helios as a candidate contributing to the program of fetal T_{reg} differentiation.

2.3.6 Fetal naïve T cells have increased Helios protein expression at baseline.

Using flow cytometry staining, we show that fetal naïve T cells had higher Helios protein expression compared to adult naïve T cells (Fig. 11D,E). In comparison, we also examined the protein expression of two other T_{reg}-specific genes with increased transcription in fetal naïve T cells that had differentially enriched ATAC signal, (*CCR4*; Fig. 12C) or H3K27ac signal (*Eos*; Fig. 12D). Using FOXP3 expression as a reference, *CCR4* and *Eos* expression did not demonstrate a similar shift in expression within fetal naïve T cells from adult naïve T cells when compared to Helios expression (Fig. 12E), which led us to focus on investigating Helios expression in fetal naïve T cell differentiation. As previously described (63, 88), we identified Helios⁻ and Helios⁺ FOXP3⁺ populations in adult T_{reg} cells (Fig. 11F). Fetal T_{reg} cells were all uniformly Helios⁺, which could be indicative that retention of permissive epigenetic marks at *Helios* T_{reg}-accessible SEs may drive high Helios expression (Fig. 11F). An average of 60% of fetal naïve T cells were Helios⁺, while adult naïve T cells did not express Helios (Fig. 11F&G).

2.3.7 The predisposition of fetal naïve T cells towards T_{reg} differentiation is not explained by recent thymic emigrant (RTE) abundance or increased proliferative ability.

Previous studies have demonstrated that CD31⁺ RTEs within the human naïve T cell population (89) have increased T_{reg} differentiation potential, making them potential precursors of T_{reg} cells in the periphery. We sought to evaluate if increased RTE proportions was a contributor to increased T_{reg} differentiation in fetal naïve T cells, since the fraction of CD31⁺ RTEs are highest at birth and decline with age (90). Using flow cytometry, we assessed CD31 staining in sorted fetal and adult naïve T cells (sort strategy in Fig. 1), setting the negative gates based on memory populations in CD4 T cell controls as well as isotype controls (Fig. 13A). Unexpectedly, CD31⁺ RTE proportions were not different between adult and fetal naïve T cell populations (Fig. 13B). Because CD31⁺ RTEs did not demonstrate increased differentiation in the absence of exogenous TGFβ (67), we concluded that the predisposition towards T_{reg} differentiation that we observed within fetal naïve T cells was not attributed to differences in RTE proportions. We further observed that mean CD31 expression levels were reduced within fetal RTEs (Fig. 13C). CD31 is downregulated with TCR signaling (90), and a subset of fetal CD4⁺ T cells are CD69⁺ and actively cycling (39). We therefore assessed the expression of CD69 and Ki-67, a marker of active proliferation, in fetal naïve T cells relative to Helios expression. Neither fetal nor adult naïve T cells express CD69 (Fig. 14A), regardless of Helios expression. However, as previously characterized (39), a small subset of fetal naïve T cells are actively proliferating, while adult naïve T cells are mainly Ki-67⁻ (Fig. 14B), thus possibly accounting for the reduced CD31 expression in fetal naïve T cells. The majority of the Ki-67⁺ population in fetal naïve T cells was also Helios⁺ (Fig. 14C), suggesting that Helios might regulate proliferation. However, with TCR stimulation, both adult and fetal naïve T cells upregulated Ki-67 to a similar extent after 5 days, indicating that Helios expression does not confer any selective proliferation advantage on fetal

naïve T cells during T_{reg} differentiation that may account for their increased T_{reg} differentiation potential.

2.3.8 Fetal naïve T cells do not have increased demethylation at the FOXP3 T_{reg}-specific demethylated region (TSDR)

As Helios was first identified as a marker of thymic T_{reg} cells (63), we sought to rule out possible contamination of thymic T_{reg} cells by assessing demethylation of the TSDR at the conserved non-coding sequence 2 (CNS2) region within the *FOXP3* gene in our sorted naïve T cell populations (Fig. 1). We saw that as expected, only fetal and adult T_{reg} populations had complete TSDR demethylation, while both fetal and adult naïve T cells had a fully methylated TSDR (Fig. 15A). This indicated that Helios expression within fetal naïve T cells was cell-intrinsic and not due to contamination with thymic T_{reg} cells.

2.3.9 Fetal naïve T cells upregulate and maintain Helios expression during iT_{reg} differentiation

Helios is expressed independently of FOXP3 expression (28, 56, 67) and can enhance the acquisition of a T_{reg}-transcriptional signature with the co-expression of FOXP3 (57). As such, Helios expression in fetal naïve T cells, but not in adult naïve T cells, might allow them to bypass the need for TGFβ to initiate FOXP3 upregulation and underlie their preferential differentiation into T_{reg} cells. To assess this, we tracked Helios expression within fetal and adult naïve T cells during T_{reg} differentiation with IL-2 alone or with TGFβ added at 1, 3, or 5 days. As previously observed, a higher frequency of fetal naïve T cells differentiated into CD25^{hi}FOXP3^{hi} iT_{reg} cells relative to adult naïve T cells either in the presence or absence of exogenous TGFβ (40, 41) (Fig. 17A,B). Fetal naïve T cells highly upregulated and maintained Helios protein

expression during the process of iT_{reg} differentiation, whereas adult naïve T cells did not (Fig. 17C,D). Concurrent upregulation of both FOXP3 and Helios was observed only in fetal iT_{reg} cells differentiated in both stimulation conditions; even as FOXP3 expression increased with TGFβ stimulation, Helios expression was not upregulated in adult iT_{reg} cells at any time point (Fig. 16A, B). Although Helios has been implicated as a marker of activation in proliferating cells (91), we show that both fetal and adult iT_{reg} cells upregulated Ki-67 expression to the same extent, but only fetal iT_{reg} maintained upregulation of Helios (Fig. 17E), thus excluding the probability that Helios upregulation in fetal iT_{reg} cells is a result of increased cell proliferation. We also excluded the possibility of thymic T_{reg} outgrowth leading to Helios expression within fetal naïve T cells by sorting (Fig. 15B) and assessing TSDR demethylation in adult FOXP3⁻ and FOXP3⁺Helios⁻ iT_{reg} populations (Fig. 15C). As previously shown (38, 92, 93), we did not detect any TSDR demethylation for adult iT_{reg} cells differentiated *in vitro* (Fig. 15A). Assessment of sorted fetal FOXP3⁻, FOXP3⁺Helios⁻ and FOXP3⁺Helios⁺ IL-2- or TGFβ-iT_{reg} populations (Fig. 15D,E) did not reveal TSDR demethylation in any fetal iT_{reg} populations (Fig. 15A), thus suggesting that the increase in Helios expression happens *de novo* in fetal iT_{reg} cells and not from the outgrowth of thymic T_{reg} cells.

The proportions of fetal IL-2-iT_{reg} cells generated across time tracked closely with proportions of adult TGFβ-iT_{reg} cells (Fig. 17B), suggesting that Helios expression within fetal naïve T cells could enhance their preferential differentiation into T_{reg} cells independently of exogenous TGFβ. We further examined fetal Helios⁺ and Helios⁻ populations after T_{reg} differentiation and found that the majority of fetal iT_{reg} cells were within the Helios⁺ population 24 hours after the initiation of T_{reg} induction (Fig. 16C). The increased frequency of iT_{reg} cells present within the Helios⁺ over the Helios⁻ population was maintained over time and in both stimulation conditions (Fig. 16D).

The Helios⁺ population also consistently had higher FOXP3 expression (Fig. 16E) relative to Helios⁻ cells, suggesting that Helios expression could potentially drive increased FOXP3 expression in differentiating fetal naïve T cells.

2.3.10 Helios knockout in fetal naïve T cells impairs their ability to preferentially differentiate into T_{reg} cells

Given our hypothesized role of Helios in enhancing FOXP3 upregulation during fetal T_{reg} cell differentiation, we predicted that reduced Helios expression in fetal naïve T cells would subsequently inhibit their cell-intrinsic propensity for T_{reg} differentiation. Using CRISPR (clustered regular interspaced short palindromic repeats)-Cas9 (CRISPR-associated protein 9) mediated editing, we knocked out *Helios* with two independent guide RNAs (gRNAs) targeting different exons of the gene. Fetal naïve T cells were then assessed for T_{reg} induction post editing after differentiation in the presence or absence of exogenous TGFβ (Fig. 19A). We first confirmed that both gRNAs were able to successfully disrupt the *Helios* locus (Fig. 18A-C), and observed specific reduction of Helios protein in fetal naïve T cells (Fig. 19B) in comparison to a non-targeting (NT) guide. Both gRNAs resulted in an average of 70% of fetal naïve T cells losing Helios expression (Fig. 18D), and the reduction was maintained after 6 days of T_{reg} induction in both stimulation conditions (Fig. 19B). *Helios* knockout in stimulated fetal naïve T cells reduced subsequent T_{reg} differentiation in the absence of exogenous TGFβ compared to cells that received the NT guide (Fig. 19C,D), and the reduction in T_{reg} percentage correlated with the extent of knockout generated (Fig. 20A). Adult naïve T cells nucleofected with the same guides were used as T_{reg} gating controls (Fig. 18E). In contrast, *Helios* knockout had no effect on fetal iT_{reg} differentiation with addition of exogenous TGFβ (Fig. 19C,D, Fig. 20B). This indicated that signaling via TGFβ compensated for the loss of Helios-driven T_{reg} differentiation, and that Helios

and TGF β may participate in shared signaling pathways. Our data show that Helios expression within fetal naive T cells plays a role in enhancing preferential T_{reg} differentiation specifically in the absence of exogenous TGF β . This mechanism present within fetal naïve T cells could lower the threshold required for T_{reg} cell differentiation, thus potentially allowing for the default generation of peripheral T_{reg}-mediated tolerance upon antigen encounter during fetal development.

2.3.11 Helios suppresses IL-2 secretion in fetal iT_{reg} cells.

Helios maintains an anergic and non-proliferative state characteristic of the T_{reg} phenotype (94) by mediating the epigenetic silencing of the *IL2* locus in T_{reg} cells (95). In contrast to conventional T cells, T_{reg} cells have reduced IL-2 production upon TCR stimulation and depend heavily on paracrine IL-2 for their maintenance (96). Since Helios is highly expressed and maintained in only fetal iT_{reg}, we investigated whether this led to a corresponding suppression of IL-2 secretion. As hypothesized, fetal iT_{reg} cells demonstrated less IL-2 production upon restimulation compared to adult iT_{reg} cells (Fig. 21A), and suppression of IL-2 production was observed regardless of iT_{reg} differentiation conditions (Fig. 21B). When delineated on the basis of Helios^{hi} and Helios^{lo} expression (Fig. 21C), Helios^{hi} fetal iT_{reg} cells consistently had lower IL-2 production across both stimulation conditions (Fig. 21D), suggesting that high Helios expression may be associated with greater repression of the *IL2* locus. *Helios* knockout in fetal iT_{reg} cells then resulted in increased IL-2 production in IL-2-iT_{reg} cells (Fig. 21E,F). Furthermore, even though the addition of exogenous TGF β compensated for loss of Helios during T_{reg} differentiation, *Helios* knockout TGF β -iT_{reg} cells produced more IL-2 upon restimulation when compared to the NT control (Fig. 21E,F). This demonstrates that continued Helios expression in

fetal naïve T cells not only enhances preferential T_{reg} differentiation, but also represses IL-2 production in fetal iT_{reg} cells.

2.3.12 Helios knockout results in the downregulation of genes associated with T_{reg} differentiation and function and the concurrent upregulation of pro-inflammatory genes

Helios also controls the expression of several key genes involved T_{reg} suppressive function (97) including *LRRC32* (GARP). *Helios* knockout in fetal naïve T cells did not impact FOXP3 or CD25 expression (Fig. 20C, D), but resulted in decreased CTLA-4 expression in fetal iT_{reg} cells (Fig. 20E). *Helios* knockout also resulted in a trend towards downregulation of GARP and LAP on fetal iT_{reg} cells (Fig. 20F), reaching significance in fetal IL-2-iT_{reg} cells (Fig. 20G). Since the impact of *Helios* knockout was variable across the T_{reg} markers surveyed, and only fetal iT_{reg} cells retain expression of a partial T_{reg}-specific transcriptional signature, we further assessed the impact of Helios ablation on the fetal iT_{reg} transcriptome by RNA sequencing. CRISPR-Cas9 editing was carried out in fetal naïve T cells with Helios gRNA1 (*Helios*^{KO}) or the non-targeting control guide (*Helios*^{WT}) before T_{reg} differentiation was induced in the absence or presence of TGFβ (Fig. 22A).

PCA revealed that *Helios*^{KO} and *Helios*^{WT} iT_{reg} cells segregated largely according to whether differentiation occurred in the presence or absence of TGFβ (PC1, Fig. 22B). This was not unexpected, since TGFβ signaling is responsible for the upregulation and repression of a significant subset of T_{reg}-specific genes (Fig. 4B-D). We also detected a small but distinct segregation of *Helios*^{KO} from *Helios*^{WT} cells, with PC2 mainly segregating *Helios*^{KO} and *Helios*^{WT} IL-2-iT_{reg} cells (Fig. 22C), while PC3 mainly distinguished *Helios*^{KO} and *Helios*^{WT} TGFβ-iT_{reg} cells

(Fig. 22D). As full knockout of Helios expression is not achieved within the total iT_{reg} population with an average of 30% of all cells still retaining Helios expression (Fig. 22A), we expected that this would result in a lowered signal-to-noise ratio. We thus utilized a more generous cutoff, where genes with at least a 10% change in expression (FC>1.1, FDR<0.05) were defined to be differentially expressed (Fig. 22E,F).

Given that TGFβ signaling is able to compensate for the defect in T_{reg} induction in Helios^{KO} iT_{reg} cells (Fig. 19D,E), we decided to evaluate potential pathways by which Helios might play parallel or additive roles relative to TGFβ signaling. We first looked for genes upregulated (FDR<0.05, FC>1.1) with TGFβ signaling within Helios^{WT} iTreg cells that were subsequently downregulated in Helios^{KO} cells within both stimulation conditions. Genes with expression enhanced by Helios in parallel would be downregulated in Helios^{KO} IL-2-iT_{reg} cells, but due to compensation with TGFβ signaling, would show no change in expression in Helios^{KO} TGFβ-iT_{reg} cells. In contrast, genes with expression enhanced by Helios and TGFβ in an additive manner would have decreased expression in Helios^{KO} TGFβ-iT_{reg} cells. Similar cutoffs were used to define upregulated genes in Helios^{KO} iT_{reg} cells. We identified 199 downregulated and 161 upregulated genes within Helios^{KO} IL-2-iT_{reg} cells that were not differentially expressed in TGFβ-iT_{reg} cells (Fig. 23A, left). Helios^{KO} IL-2-iT_{reg} cells had reduced expression of T_{reg}-specific genes previously identified to be exclusively upregulated in fetal iT_{reg} cells such as *DUSP4*, *IL10* and *ITGAE* (CD103) (Fig. 23A, left, Table 10). Concurrently, Helios^{KO} IL-2-iT_{reg} cells upregulated several chemokine and tumor necrosis factor (TNF) superfamily genes (Fig. 23A, left), indicating that Helios may enhance the expression of a subset of T_{reg} genes while simultaneously reducing expression of pro-inflammatory genes associated with effector function in the absence of TGFβ signaling.

We next found that Helios expression contributed to the upregulation of an additional 351 genes in TGFβ-iT_{reg} cells (Fig. 23A, right), including *SEMA4*, *PTGS1* and *RTKN*, previously identified in the TGFβ induced T_{reg} gene signature (Cluster 2.2, Fig. 4B, Table 10), as well as *TOX2* and *RGS1*, which are upregulated in fetal but not adult iT_{reg} cells (Cluster 2.3, Fig. 4B, Table 10). Additionally, Helios^{KO} TGFβ-iT_{reg} cells had upregulation of 251 genes relative to Helios^{WT}; genes upregulated included chemokine receptor genes, as well as transcription factors involved with Th1, Th2 and Th17 cell differentiation and function such as *PRDM1* (Blimp1)(98), *GATA3* (99), *IKZF1* (Ikaros) (100, 101), and *MAF* (c-MAF) (102)(Fig. 23A, right). These data suggest that Helios performs both parallel and additive roles in enhancing the upregulation of genes associated with the T_{reg} transcriptional signature and repressing genes that might drive differentiation towards other effector T cell pathways during T_{reg} differentiation.

Lastly, we identified genes that were either upregulated or downregulated in Helios^{KO} iT_{reg} cells across both induction conditions, implicating possible transcriptional control by Helios independent of TGFβ signaling during differentiation. 200 genes were downregulated in Helios^{KO} iT_{reg} cells generated in both stimulation conditions, including genes related to T_{reg} phenotype and function such as *CTLA4* and *LTBP4* (Fig. 23B). Although we did not observe reduced protein expression of FOXP3 in Helios^{KO} iT_{reg} cells at Day 6 (Fig. 20C), we observed decreased *FOXP3* transcription across both iT_{reg} populations, suggesting that additional post-transcriptional mechanisms probably regulate FOXP3 expression downstream of Helios. Additionally, Helios^{KO} iT_{reg} cells across both conditions have reduced expression of the *NFATC4* (NFAT3) and *PPARA* (PPARα) transcription factors which regulate the repression of pro-inflammatory cytokines such as IL-2, IFNγ and TNFα (103, 104), as well as the histone H3K27 demethylase *KDM6B* (JMJD3), which suppresses Th2 and Th17 programs (105) (Fig. 23B). Loss of Helios expression

also led to the upregulation of 88 genes, including genes attributed to pro-inflammatory effector T cell function such as *IFNG* (Fig. 23B). Taken together, we show that Helios plays a role in enhancing fetal T_{reg} differentiation through the transcriptional regulation of a key subset of genes that restrict differentiation towards effector T cell helper phenotypes while favoring differentiation towards the T_{reg} cell fate.

2.3.13 Helios knockout fetal iT_{reg} cells have decreased IL-10 and increased IFN γ production

The regulation of cytokine production in T_{reg} cells is important for their suppressive ability; T_{reg} cells must repress secretion of pro-inflammatory cytokines such as IFN γ while maintaining production of immunosuppressive cytokines such as IL-10 (33). The loss of Helios expression in committed T_{reg} populations in mice result in subsequent IFN γ production (64, 65), and we show that fetal Helios^{KO} iT_{reg} cells have increased IFN γ transcription relative to Helios^{WT} iT_{reg} cells (Fig. 23B). Furthermore, fetal, but not adult, iT_{reg} populations have increased *IL10* transcription (Fig. 4B). We next assessed IL-10 and IFN γ concentrations in culture supernatant during iT_{reg} differentiation. We first confirmed that only fetal, but not adult, iT_{reg} cells, produced IL-10 during iT_{reg} differentiation in the absence of TGF β , and this is further augmented by exogenous TGF β (Fig. 24A), which may be related to an increased frequency in T_{reg} cell differentiation (Fig. 7B). Fetal iT_{reg} cells also produced less IFN γ than adult iT_{reg} generated in both stimulation conditions (Fig. 24B). Lastly, fetal IL-2-iT_{reg} cells had a greater ratio of IL-10 produced over IFN γ compared to their adult counterparts, and this effect was greatly enhanced in TGF β -iT_{reg} cells (Figure 24C). Ablation of Helios in fetal iT_{reg} cells then resulted in a reduction of IL-10 produced in Helios^{KO} IL-2-iT_{reg} cells with both gRNA1 and 2 (Fig. 24D). We observed a small but sustained decrease in IL-10 across all Helios^{KO} TGF β -iT_{reg} cells that received gRNA1 but did not detect this decrease in gRNA2 (Fig. 24D), which reflected our RNA sequencing results showing a minimal decrease

in IL-10 in Helios^{KO} TGFβ-iT_{reg} that did not meet fold change cutoffs (Fig. 22G). This consistent with our prediction from our RNAseq sequencing results that TGFβ signaling can compensate Helios knockout to upregulate *IL10* transcription within Helios^{KO} TGFβ-iT_{reg} (Figure 23A). *Helios* knockout within fetal iT_{reg} cells resulted in increased IFNγ production in Helios^{KO} TGFβ-iT_{reg} cells, but the effect was less obvious in IL-2-iT_{reg} cells (Fig. 24E). However, across all differentiation conditions and both gRNA, Helios^{KO} iT_{reg} cells had a striking decrease in their IL-10 to IFNγ ratio (Fig. 24F), especially in Helios^{KO} fetal TGFβ-iT_{reg}, where the majority of samples tipped from a pro-tolerance (ratio>1) to pro-inflammatory cytokine (ratio<1) profile. Overall, this suggests an important role for Helios in regulating the cytokine output of fetal iT_{reg} cells, which could help prevent pro-inflammatory responses which can be detrimental *in utero*.

2.4 DISCUSSION

The predisposition of human fetal naïve T cells towards T_{reg} cell differentiation presents a opportunity to identify potential underlying cell-intrinsic factors that can be utilized to improve *in vitro* iT_{reg} cell generation for cell-based immunotherapies. We show here that fetal naïve T cells already have the partial expression of a T_{reg}-specific transcriptome and epigenome, and that only fetal-derived iT_{reg} cells retain expression of this transcriptome upon differentiation *in vitro*. Furthermore, we observed that fetal naïve T cells had increased chromatin accessibility at approximately a third of all defined T_{reg}-accessible enhancers, but only a small percentage of these were marked by H3K27ac. This suggests that many T_{reg}-specific enhancers are held in a poised (i.e., accessible), but not active state in quiescent fetal naïve T cells. As such, the full acquisition of the T_{reg}-specific epigenetic, and subsequently, transcriptional signature might only occur upon TCR activation and/or cytokine signaling which triggers the final commitment to the T_{reg} cell fate. Furthermore, we discover two active SEs associated with *Helios* that also showed increased transcription and protein expression in fetal naïve T cells. These data thus implicate a broad landscape of T_{reg}-poised chromatin in fetal naïve T cells that contribute to their propensity for T_{reg} differentiation, and identified *Helios* as an important transcription factor whose expression distinguishes fetal and adult naïve T cells. However, it is plausible that there is also a contribution of additional histone marks to the overall chromatin landscape in addition to the two permissive epigenetic characteristics we profiled. For example, since *Helios* has been shown to interact with other histone modifying proteins such as the NuRD co-repressor complex (106, 107), sequencing of additional histone marks such as the repressive H3K27me3 mark would allow us to assess possible repression of genes associated with other effector lineages. Additionally, future experiments that identify *Helios* binding sites by *Helios* ChIPseq within fetal naïve or iT_{reg} populations would be critical to determine if *Helios* is a driving factor behind the acquisition of active or suppressive epigenetic marks at key T_{reg}-specific genes. These further

analyses would reveal a more complete picture of the fetal epigenome and how it contributes to the overall T_{reg} cell differentiation phenotype.

Our group and others have shown that the human fetal immune system is skewed towards tolerance by the presence of a large T_{reg} cell population (40, 41) which is likely derived from preferential conversion of fetal naïve T cells into T_{reg} cells upon antigen encounter (42). Here, we show that Helios enhances the preferential differentiation and phenotypic commitment of fetal naïve T cells towards the T_{reg} cell fate. Ablation of Helios expression in fetal naïve T cells specifically impaired their cell-intrinsic predisposition for iT_{reg} differentiation, and reduction in T_{reg} proportions were correlated with the extent of Helios knockout. Although the addition of exogenous TGFβ compensates for loss of Helios during T_{reg} generation, *Helios* knockout still resulted in the subsequent downregulation of T_{reg}-specific genes and upregulation of pro-inflammatory genes involved in effector T cell differentiation and function in fetal iT_{reg} cells. This is consistent with the known role of Helios in restraining effector Th1 and Th17 cell programs within committed T_{reg} cells in mice (64, 65). Our results suggest that transcriptional regulation by Helios may play a dual role in fetal T_{reg} differentiation – first, by enhancing T_{reg} differentiation through upregulation of a set of T_{reg}-specific genes even in the absence of TGFβ, and second, by repressing pro-inflammatory genes and genes that mediate differentiation towards other effector T cell subsets. This fine-tuning of the fetal iT_{reg} transcriptome subsequently impacts T_{reg} function, as the loss of Helios uniformly results in the upregulation of IFNγ over IL-10 in both fetal IL-2- and TGFβ- iT_{reg} cells. Helios deficiency in mouse T_{reg} cells *in vivo* does not result in overt distortions in FOXP3 expression or T_{reg} proportions at steady state (108), but rather in the loss of immunosuppressive ability and the manifestation of autoimmunity in later life or in response to inflammatory insults (64, 65). Regulation of cytokine and other pro-inflammatory

genes by Helios could then potentially play a role in maintaining the phenotypic stability of fetal iT_{reg} cells *in utero* to prevent unwanted pro-inflammatory responses.

Given the nature of this study, and the exclusive use of primary human cells, there are important limitations to acknowledge in its interpretation. We primarily compared T cells isolated from fetal spleen and adult peripheral blood for our studies, due to the difficulty of obtaining adult splenic tissue and fetal peripheral blood. While we cannot fully rule out immunological differences associated with ontogeny and environmental polarization, we have attempted to reduce confounders resulting from this factor by only deriving the epigenetic T_{reg} signature by comparing adult naïve and adult T_{reg} cell populations, to ensure that only the T_{reg} signature was the main point of comparison between adult and fetal populations. We were able to additionally rule out contributions from age specific differences by selecting genes shared between adult and fetal T_{reg} cells in our RNAseq experiments to ensure that only genes truly contributing to the T_{reg} cell phenotype were included. Gestational age, and on some occasions when it could be determined, sex, were the only demographics collected for our fetal samples. Hence, we were unable to fully rule out any other potential confounders or stratify our samples accordingly. Furthermore, technical variation due to the kinetics of CRISPR-Cas9 editing, together with the inherent biological variability in primary human samples manifested in the high donor variability that we observed within our editing experiments. Lastly, we also observed heterogeneity in Helios expression at steady state in fetal naïve T cells, as well as the extent of Helios upregulation from sample to sample, which could contribute to differences in T_{reg} differentiation. We envision that future work will aim to utilize single cell sequencing techniques to separate and identify populations that will explain the observed biological heterogeneity, and possibly identify subsets that have greater predisposition towards T_{reg} differentiation.

Our work here suggests a key role for Helios in establishing early life peripheral tolerance in humans, and there are some indications to support this hypothesis from studies in neonatal mice. Notably, when Helios^{-/-} mice were first generated, the authors reported the presence of significant fatality in the first two weeks of neonatal life, and a 100% fatality was observed with subsequent crosses to achieve a full B6 background (108). This timing coincides with the emergence and migration of functional T cells into the secondary lymphoid organs within the neonatal mouse, and is developmentally equivalent to when T cells emerge in the second trimester in humans (51). Furthermore in mice, thymic T_{reg} cell populations generated in an early window from birth to 10 days later have been shown to be qualitatively different from those generated later in life (109), indicating that T_{reg} cell populations generated in early life are indispensable to the maintenance of lifelong tolerance. However, these studies did not examine the potential contributions of peripheral T_{reg} differentiation from naïve T cells, which may account for a large percentage of the tolerogenic phenotype observed in the human fetus. This is particularly significant since there is an increased frequency of rapidly proliferating CD4⁺ and CD8⁺CD25⁻ human fetal T cell populations (39) that could potentially bear auto-reactive TCRs that have escaped thymic deletion as observed in neonatal mice (110). In light of our data presented here, we thus speculate that Helios plays a previously unappreciated role in the generation of peripheral T_{reg} cells in this critical period in early human fetal development where the need for peripheral tolerance is perhaps the most acute.

In vitro human T_{reg} cell differentiation from naïve T cells for therapeutic purposes has encountered significant roadblocks due to difficulties in obtaining pure populations of T_{reg} cells that maintain a stable phenotype over time (38, 92, 93). Although Helios⁺ fetal iT_{reg} cells did not show demethylation at the *FOXP3* TSDR, Helios⁺, but not Helios⁻ *ex vivo* T_{reg} cells retain a more highly demethylated TSDR when expanded *in vitro* (111, 112). It is thus highly likely that this

reflects the inability of *in vitro* differentiation to capture the conditions or environmental factors that trigger TSDR demethylation. Regardless, we show that fetal, but not adult iT_{reg} cells are phenotypically more similar to *ex vivo* T_{reg} cells, since they retain expression of Helios, demonstrate suppression of IL-2 production upon restimulation, and produce IL-10 in with T_{reg} differentiation. These attributes are commonly associated with the T_{reg} cell phenotype, but are not acquired in adult human iT_{reg} cell populations. Lastly, given that our data shows that Helios enhances the expression of genes that favor T_{reg} over helper T effector commitment, this may represent a mechanism by which Helios maintains stable T_{reg} function and identity *in vivo* (64, 65, 88, 95, 97). Future studies are thus required to assess this possibility, particularly in pro-inflammatory environments, and whether manipulation of Helios expression within adult naïve T cells can recapture this effect. Additionally, given the importance of the T_{reg}-specific epigenome to function and stability (28, 30), further identification of upstream factors that drive the acquisition of the permissive enhancer landscape in fetal naïve T cells will likely provide important insights for generating stable iT_{reg} cells from adult naïve T cells. This work will be relevant for improving strategies to generate iT_{reg} cells for use in for immunotherapy to establish tolerance in autoimmunity and transplantation.

2.5 ACKNOWLEDGEMENTS

We would like to thank S. Fisher, P. Odorizzi, E. Rackaityte, J. Halkias, D. Bunis, J. Mold and J.Y. Lim for helpful discussion. We thank D. Simeonov and K. Schumann for helpful discussion on CRISPR-Cas9 editing. We thank M. Nguyen for advice and help with cell fixation and DNA extraction for TSDR analysis. We thank R. Krishnakumar, A. Chen, S. Thomas and R. Thomas for their technical help with ChIPseq and advice on bioinformatics analyses. Bioinformatics analyses for genome mapping and bigwig file generation for ATACseq was carried out by the Gladstone Bioinformatics Core at the Gladstone Institutes. Bioinformatic analyses for RNAseq in *ex vivo* naïve and T_{reg} cells were carried out by the Technology Center for Genomics and Bioinformatics (TCGB) at University of California, Los Angeles. Sequencing for ChIPseq and RNAseq in induced T_{reg} cells were carried out at the Center for Advanced Technologies (CAT) Core at UCSF.

2.6 FIGURES

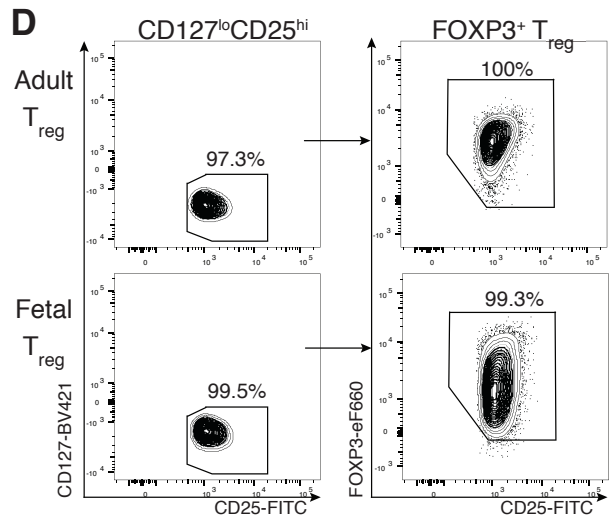
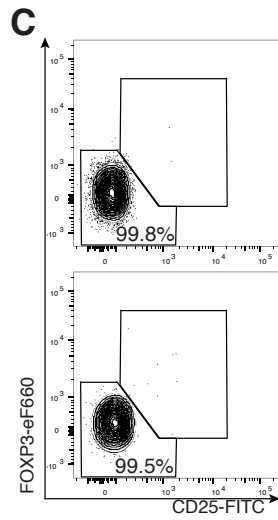
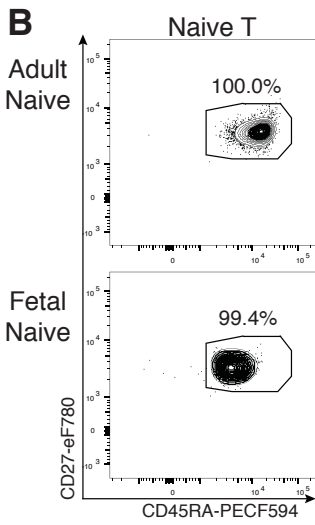
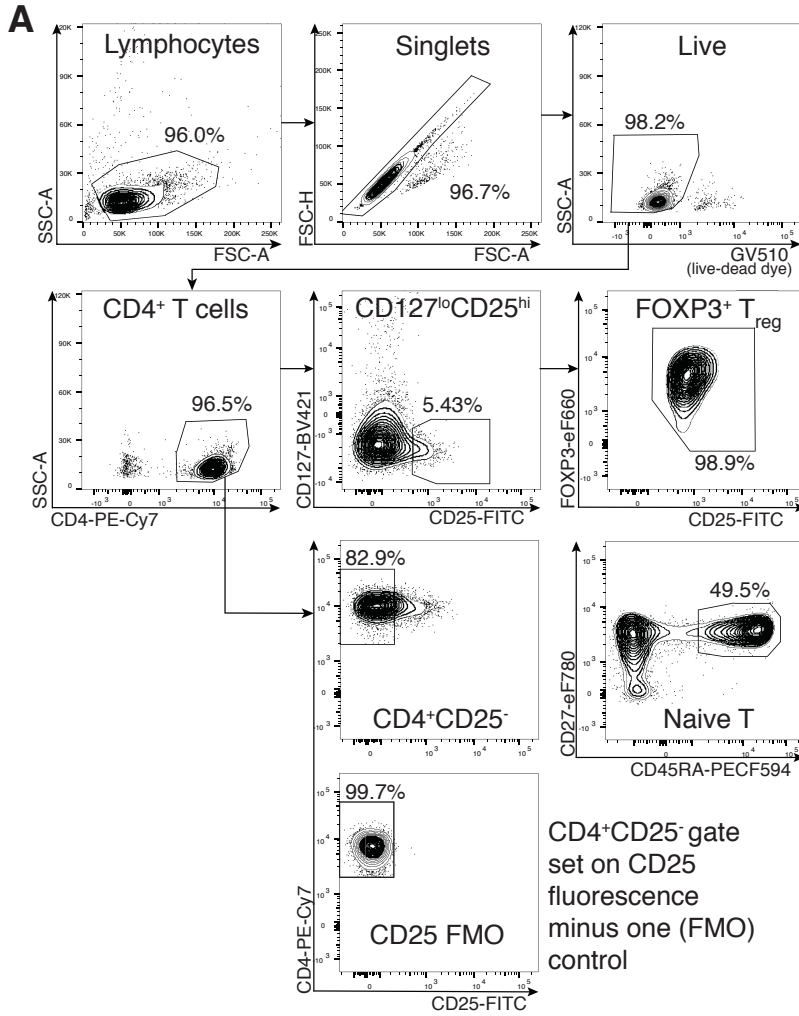


Figure 1. Gating strategy and purity assessment for sorted naïve and T_{reg} cells.

(A) Gating strategy for FACS sorting of CD4⁺ naïve and T_{reg} cells based on adult peripheral mononuclear cells after magnetic pre-enrichment for CD4⁺ T cells.

(B) Flow cytometry analysis post-sorting to assess sort purity for CD27⁺CD45RA⁺ fetal and adult naïve T cells. Percentages indicate proportion of naïve T cells gated in **(A)**.

(C) Flow cytometry analysis post-sorting to verify the lack of CD25^{hi}FOXP3⁺ T_{reg} cells present in sorted naïve fetal and adult T cell populations.

(D) Flow cytometry analysis post-sorting to assess sort purity for CD25^{hi}CD127^{lo} adult and fetal T_{reg} cells (left) gated in **(A)**, and to confirm expression of FOXP3 (right).

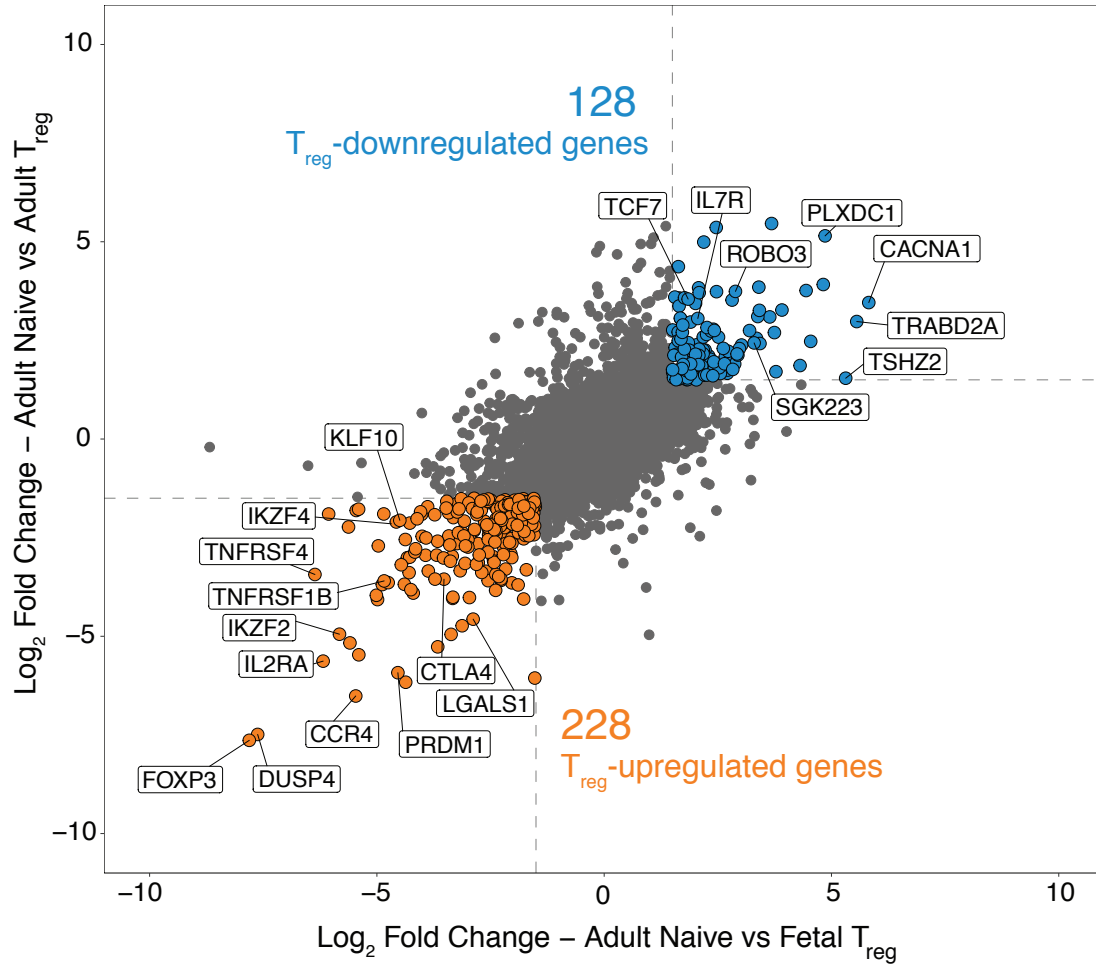


Figure 2. Definition of the T_{reg} transcriptional signature

The T_{reg} transcriptional signature is defined from genes with increased/decreased transcription in adult and fetal T_{reg} populations relative to adult naïve T cells. Cut-offs were set at false discovery rate <0.05 (FDR), and log₂ fold change >1.5 (log₂FC). Scatterplot plots log₂FC values for comparisons of adult naïve against adult T_{reg} (y axis) and adult naïve against fetal T_{reg} (x axis). Dotted lines in grey denote log₂FC cut-offs. T_{reg} upregulated (orange) and downregulated genes (blue) are shown. Genes previously associated with T_{reg} and naïve T cell function are labeled.

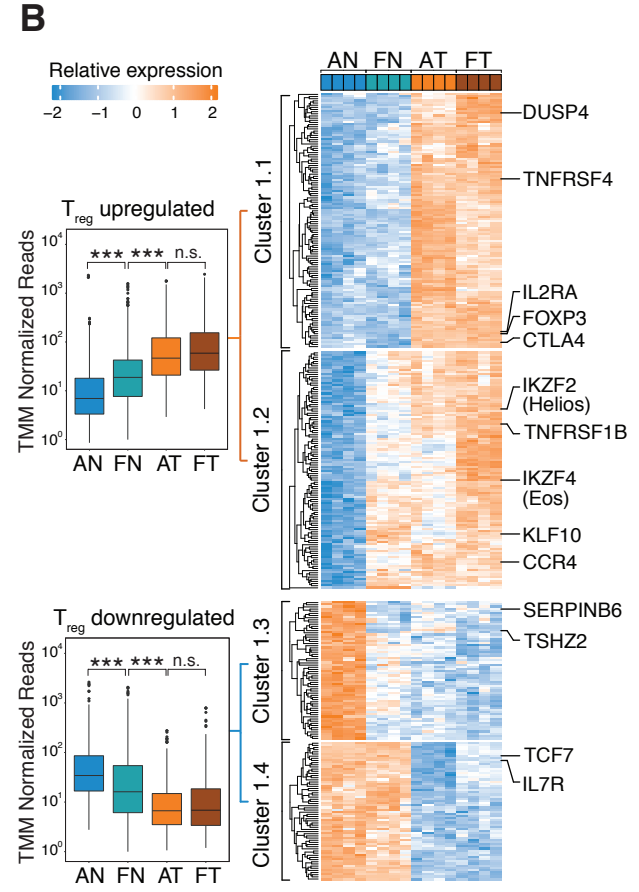
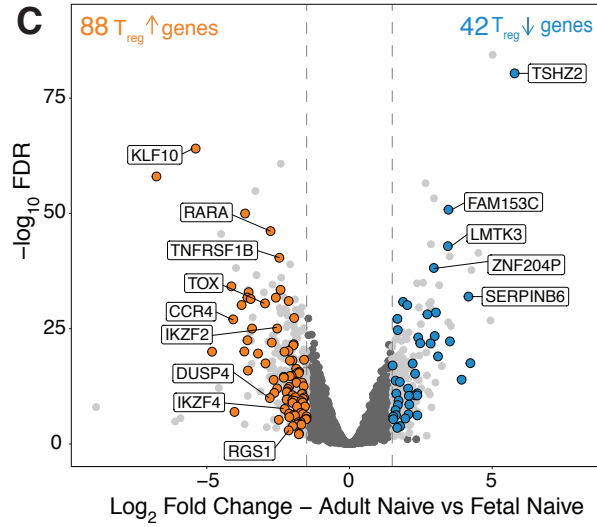
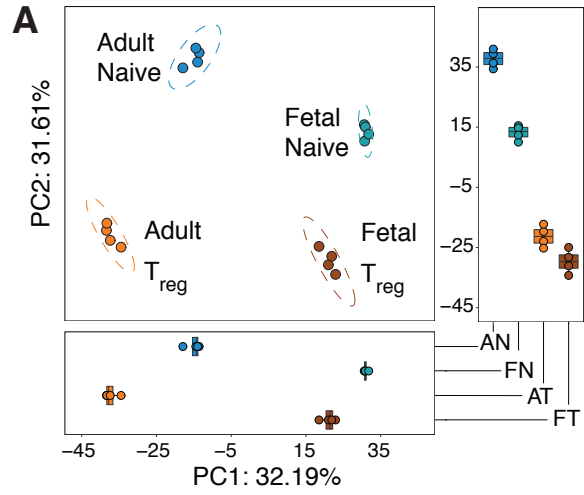


Figure 3. Fetal naïve T cells have expression of a partial T_{reg} transcriptome

(A) Cells segregate first by cell origin (Principal Component, PC1, adult versus fetal), then by functional subtype (PC2, naïve versus T_{reg}). Boxplots show scores for PC1 and 2 (bottom and right respectively).

(B) Fetal naïve T cells have a partial T_{reg} transcriptional signature. Heatmap shows relative expression levels of T_{reg}-specific differentially expressed (DE) genes in adult naïve (AN), fetal naïve (FN), adult T_{reg} (AT) and fetal T_{reg} (FT). Clusters are labeled and defined by k-means clustering. Genes associated with T_{reg} and naïve T cell function are labeled. Boxplots (left) show the averaged trimmed mean of M values (TMM) normalized reads across all upregulated (top, Cluster 1&2) and downregulated (bottom, Cluster 3&4) genes. Kruskal-Wallis test and Dunn's multiple comparison test with Bonferroni correction for multiple testing, *** p<0.001, n.s., p>0.05 (n = 4 biological replicates per group).

(C) 88 and 42 T_{reg}-specific genes are upregulated (orange) and downregulated (blue) in fetal naïve T cells. Volcano plot of DE (log₂ fold change >1.5, p.adj<0.05) genes in fetal and adult naïve T cells, all DE genes in light grey. Dotted lines (grey) denote fold change cut-offs. Among T_{reg}-upregulated genes, genes previously associated with T_{reg} function are labeled. Among T_{reg}-downregulated genes, the top five genes with the lowest p.adj values are labeled.

All boxplots in this figure show median (centre line), interquartile range (box) and tenth and ninetieth percentiles (whiskers).

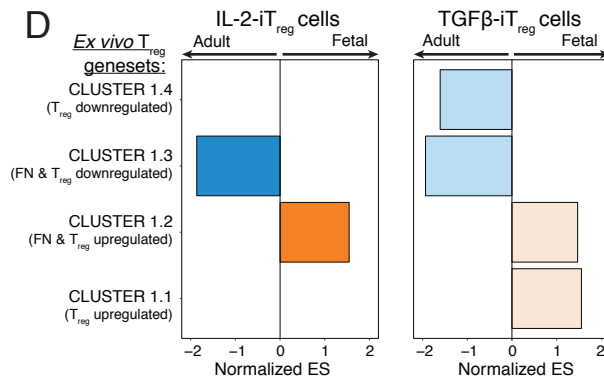
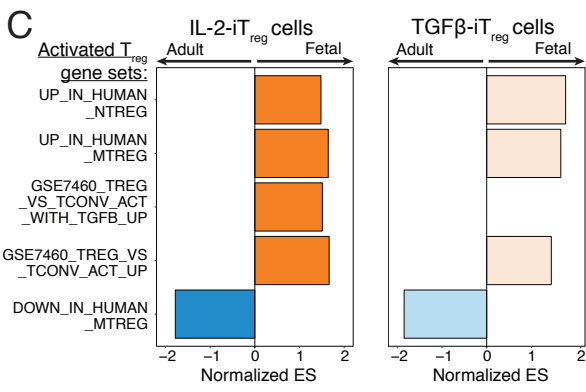
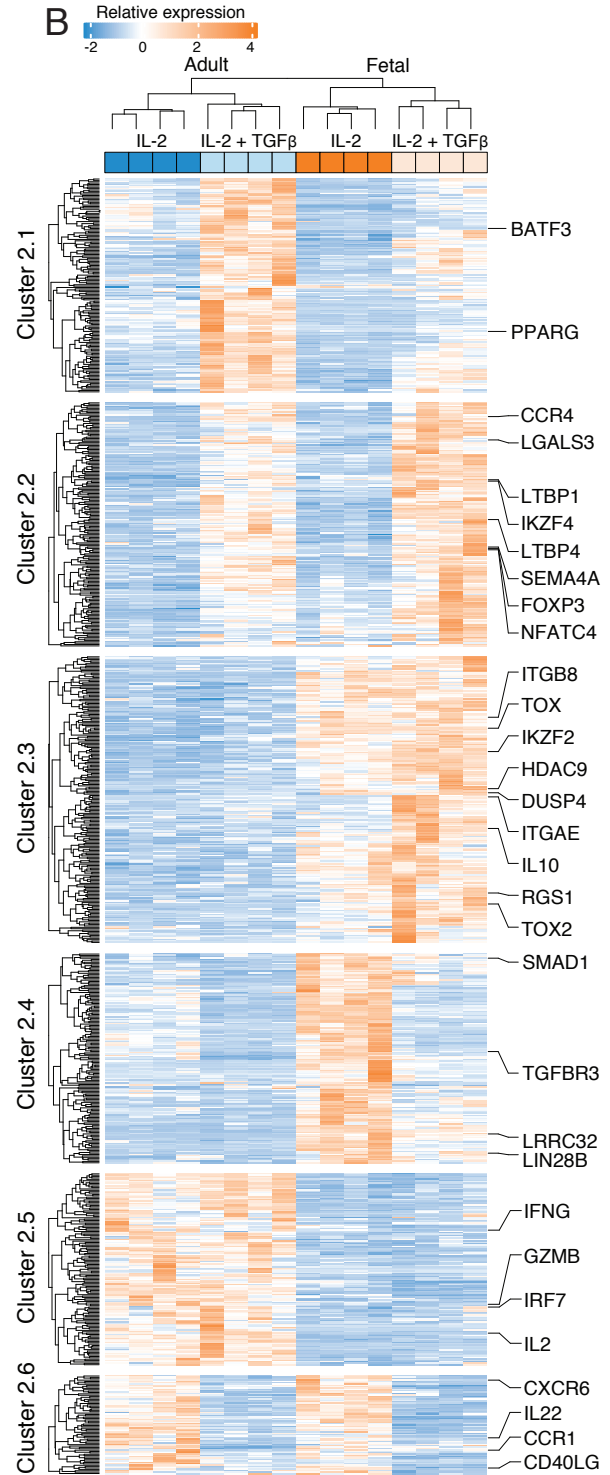
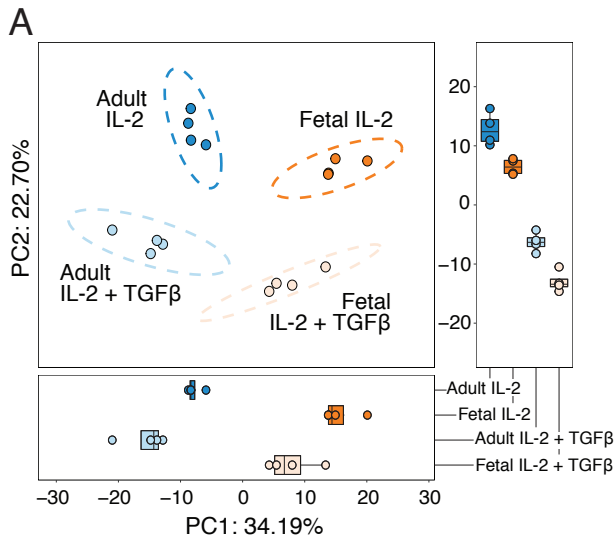


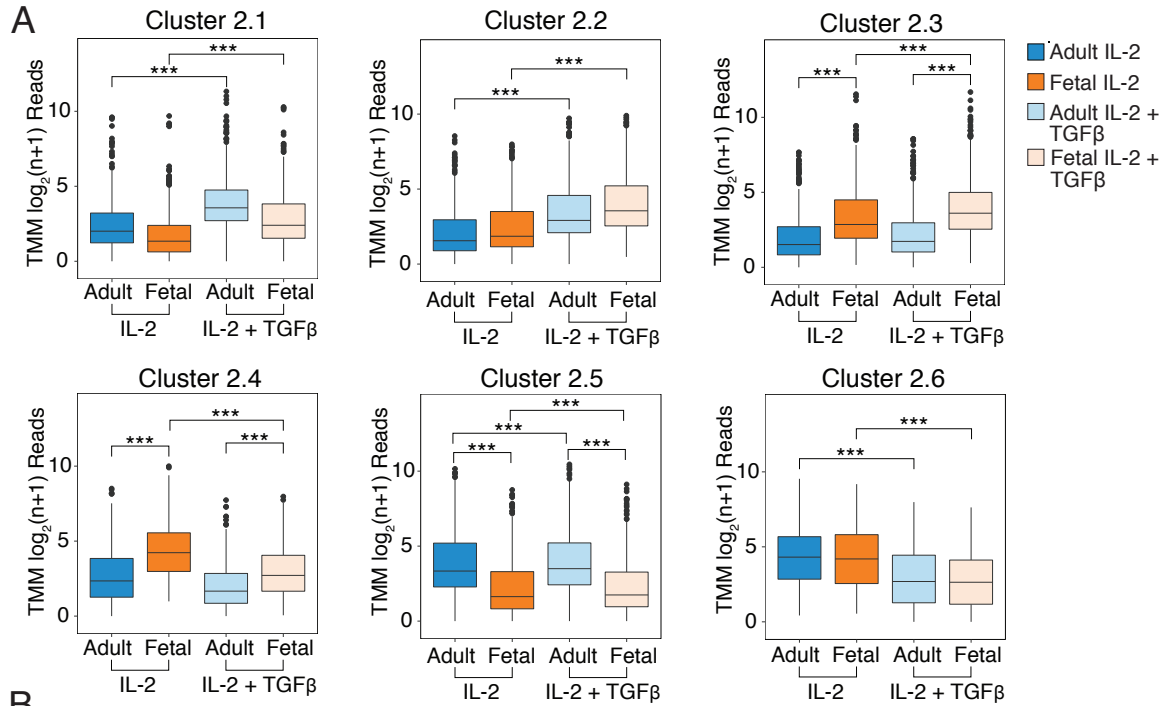
Figure 4. Fetal induced T_{reg} cells retain expression of the partial T_{reg}-specific transcriptome detected in fetal naïve T cells in steady state.

(A) Fetal and adult iT_{reg} cells segregate first by cell origin (Principal Component, PC1, adult versus fetal), then by stimulation received during differentiation (PC2, IL-2 versus IL-2 and TGFβ). Boxplots show scores for PC1 and 2 (bottom and right respectively).

(B) Fetal, but not adult, iT_{reg} cells upregulate a subset of T_{reg}-associated genes independently of exogenous TGFβ. Heatmap shows relative expression levels of differentially expressed genes (log₂ fold change >1.5, false discovery rate, FDR<0.05) in adult and fetal iT_{reg} differentiated with IL-2 (IL-2-iT_{reg}) or IL-2 and TGFβ (TGFβ-iT_{reg}). Clusters are labeled and defined by k-means clustering. Genes associated with T_{reg} or pro-inflammatory/effector T cell function are labeled.

(C) Fetal iT_{reg} populations have enrichment of genes upregulated in *ex vivo* activated T_{reg} cells. Pre-ranked Gene Set Enrichment Analysis (GSEA) was used to assess overrepresentation of pre-defined activated T_{reg}-associated gene sets (see figure S3B for details of all gene sets) in fetal (orange) or adult iT_{reg} cells (blue) differentiated with IL-2 (left) or IL-2 and TGFβ (right), n=4 for all conditions. Barplot shows normalized Enrichment Scores (ES) for gene sets with FDR<0.05, arrows denote direction of enrichment in adult or fetal iT_{reg} cells.

(D) Fetal iT_{reg} populations have differential expression of the partial T_{reg}-specific signature detected in primary fetal naïve T cells. Pre-ranked GSEA was used to assess overrepresentation of each of the gene clusters identified in Figure 1B. Barplot shows normalized Enrichment Scores (ES) for all clusters with FDR <0.05 for fetal (orange) or adult (blue) iT_{reg} cells differentiated with IL-2 (left) or IL-2 and TGFβ (right).



B

Gene set name	Description	Organism
UP_IN_HUMAN_MTREG	Up in human memory T _{reg} vs conventional T _{MEM} cells, FDR<0.05, LFC>1.5	Human
DOWN_IN_HUMAN_MTREG	Down in human memory T _{reg} vs conventional T _{MEM} cells, FDR<0.05, LFC>1.5	Human
UP_IN_HUMAN_NTREG	Up in human naive T _{reg} vs conventional T _N cells, FDR<0.05, LFC>1.5	Human
DOWN_IN_HUMAN_NTREG	Down in human naive T _{reg} vs conventional T _N cells, FDR<0.05, LFC>1.5	Human
GSE7460_TREG_VS_TCONV_ACT_DN	GSE7460_TREG_VS_TCONV_ACT_DN	Mouse
GSE7460_TREG_VS_TCONV_ACT_UP	GSE7460_TREG_VS_TCONV_ACT_UP	Mouse
GSE7460_TREG_VS_TCONV_ACT_WITH_TGFB_DN	GSE7460_TREG_VS_TCONV_ACT_WITH_TGFB_DN	Mouse
GSE7460_TREG_VS_TCONV_ACT_WITH_TGFB_UP	GSE7460_TREG_VS_TCONV_ACT_WITH_TGFB_UP	Mouse
CLUSTER 1.1	T _{reg} -specific upregulated signature in <i>ex vivo</i> T _{reg}	Human
CLUSTER 1.2	T _{reg} -specific upregulated signature shared by <i>ex vivo</i> fetal naive and T _{reg}	Human
CLUSTER 1.3	T _{reg} -specific downregulated signature shared by <i>ex vivo</i> fetal naive and T _{reg}	Human
CLUSTER 1.4	T _{reg} -specific downregulated signature in <i>ex vivo</i> T _{reg}	Human

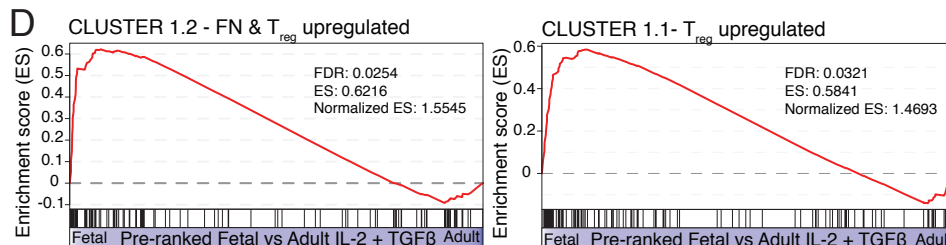
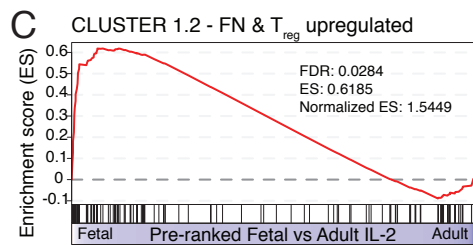


Figure 5. Assessing the enrichment of T_{reg} upregulated or downregulated genes in fetal and adult induced T_{reg} (iT_{reg}) populations

(A) Boxplots show averaged $\log_2(n+1)$ trimmed mean of M values (TMM) normalized reads across each cluster identified in Figure 2D. Statistics were calculated with Kruskal-Wallis test and Dunn's multiple comparison test with Bonferroni correction for multiple testing, *** $p < 0.001$ ($n = 4$ biological replicates per group).

(B) Pre-defined gene sets used for Gene Set Enrichment Analysis (GSEA). See Supplementary Methods and Materials for details on gene set definition.

(C) Fetal iT_{reg} cells differentiated in IL-2 alone (IL-2-iT_{reg}) have increased enrichment of genes previously defined to be upregulated in *ex vivo* fetal naïve, adult, and fetal T_{reg} cells. Lineplot shows the running enrichment score (ES) as the analysis goes through the pre-ranked gene list comparing fetal against adult IL-2-iT_{reg} cells. Genes from Cluster 1.2 appearing within the pre-ranked list are highlighted below the lineplot.

(D) Fetal iT_{reg} cells differentiated in IL-2 and TGF β (TGF β -iT_{reg}) additionally have enrichment of genes previously defined to be upregulated only in *ex vivo* adult and fetal T_{reg} cells. Lineplots show running ES through the pre-ranked gene list comparing fetal against adult TGF β -iT_{reg} cells for Cluster 1.2 (left) and Cluster 1.1 (right) genes. Genes from each cluster appearing within the pre-ranked list are highlighted below the respective lineplots.

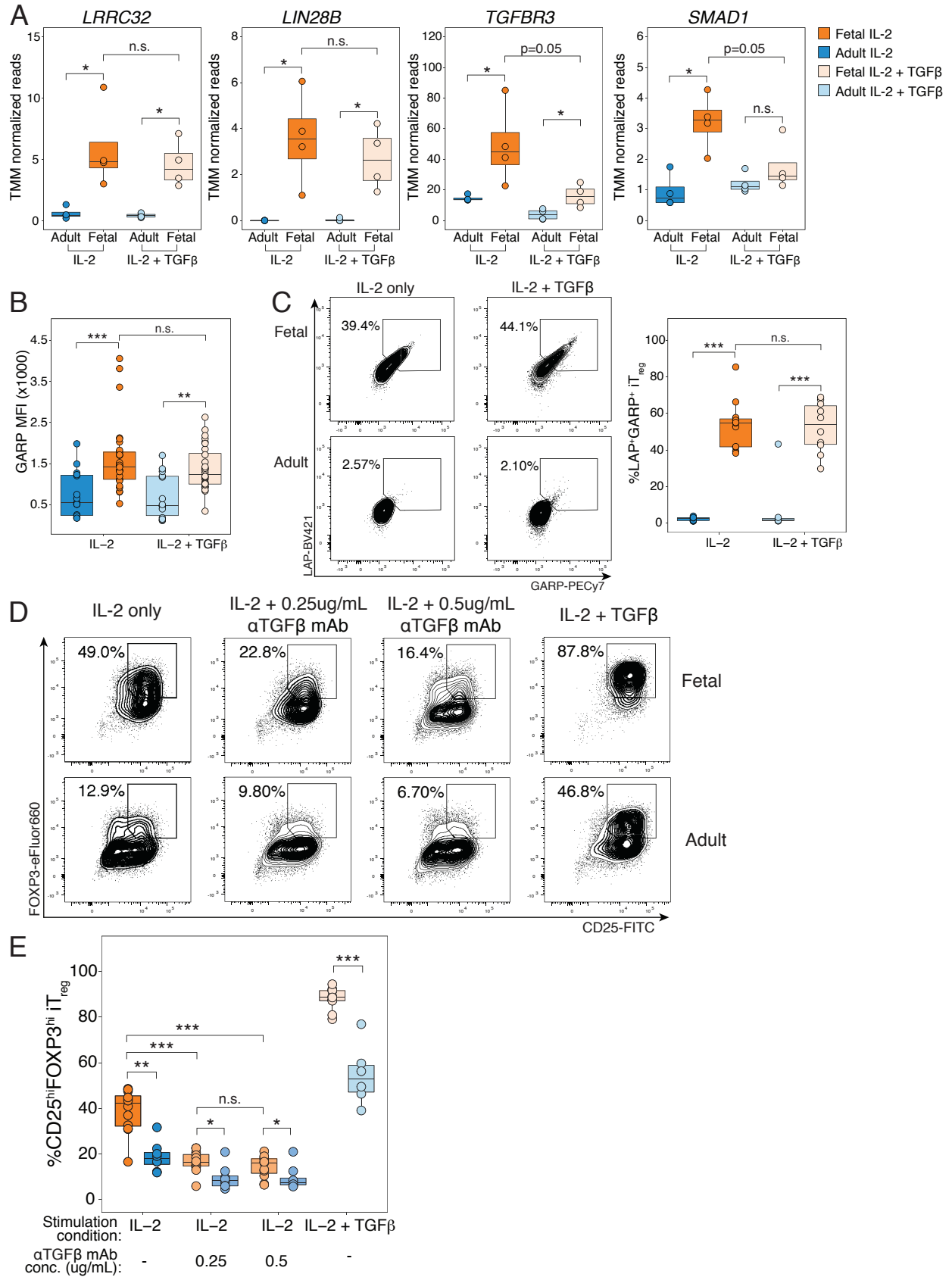


Figure 6. Fetal induced Treg cells have increased sensitivity to TGFβ signaling.

(A) Fetal induced T_{reg} (iT_{reg}) cells have increased expression of genes involved in downstream TGFβ signaling. Boxplots show log₂ trimmed mean of M values of normalized RNAseq reads for *LRRC32*, *LIN28B*, *TGFBR3* and *SMAD1* in fetal (orange) or adult (blue) iTreg differentiated in IL-2 alone (IL-2-iT_{reg}) or with exogenous TGFβ added (TGFβ-iT_{reg}), n=4 for all conditions.

(B) Fetal, but not adult, iT_{reg} cells have increased GARP(*LRRC32*) expression. Boxplots show mean fluorescence intensity (MFI) of GARP by flow cytometry staining in adult and fetal IL-2-iT_{reg} cells (n=15, 28 respectively) and TGFβ-iT_{reg} cells (n=14, 28 respectively).

(C) Fetal, and not adult iT_{reg} cells highly upregulate GARP and latency associated peptide (LAP). Representative flow cytometry plots (left) are shown for one experiment gated on live, CD4⁺CD25^{hi}FOXP3^{hi} iT_{reg} cells. Boxplots show quantification of GARP⁺LAP⁺ adult and fetal IL-2-iT_{reg} (n=7, 11 respectively) and TGFβ-iT_{reg} cells (n=7, 10 respectively).

(D) Fetal naïve T cells still retain an increased ability for T_{reg} cell differentiation over adult naïve T cells with TGFβ neutralization. Representative flow cytometry plots show one experiment for live, CD4⁺ cells.

(E) Quantification of percentages of CD25^{hi}FOXP3^{hi} iT_{reg} cells as shown in **(D)**. Sorted adult and fetal naïve T cells were stimulated with αCD3/αCD28/αCD2 tetramers either in the presence of IL-2 only (n=8, 12 respectively), IL-2 with 0.25 μg/mL (n=8, 12) or 0.5 μg/mL αTGFβ blocking antibody (n = 8, 11), or IL-2 with TGFβ (n = 8, 11). All statistics were calculated by unpaired two-sided Mann-Whitney test, ***p<0.001, **p<0.01, n.s. p>0.05. Boxplots show median (center line), interquartile range (box) and tenth and ninetieth percentiles (whiskers).

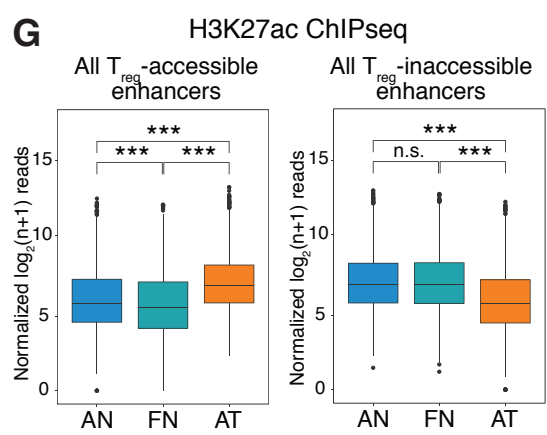
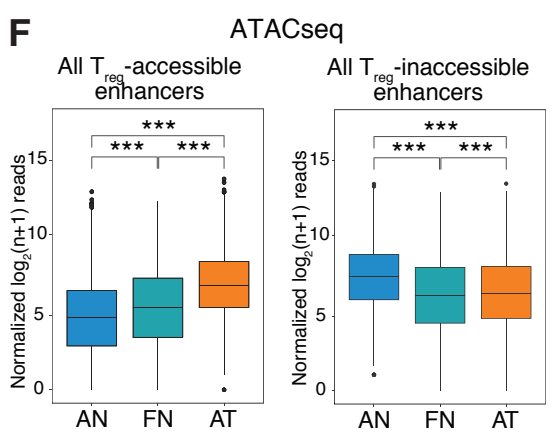
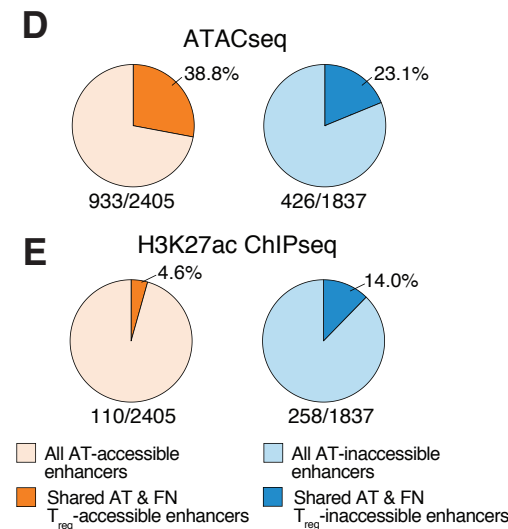
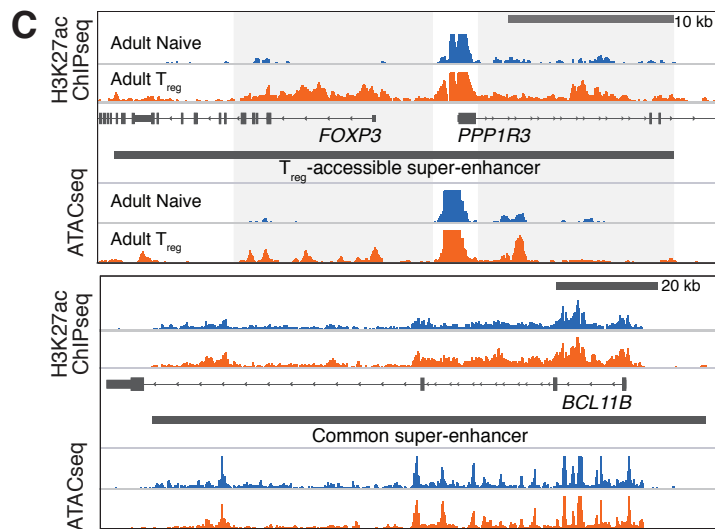
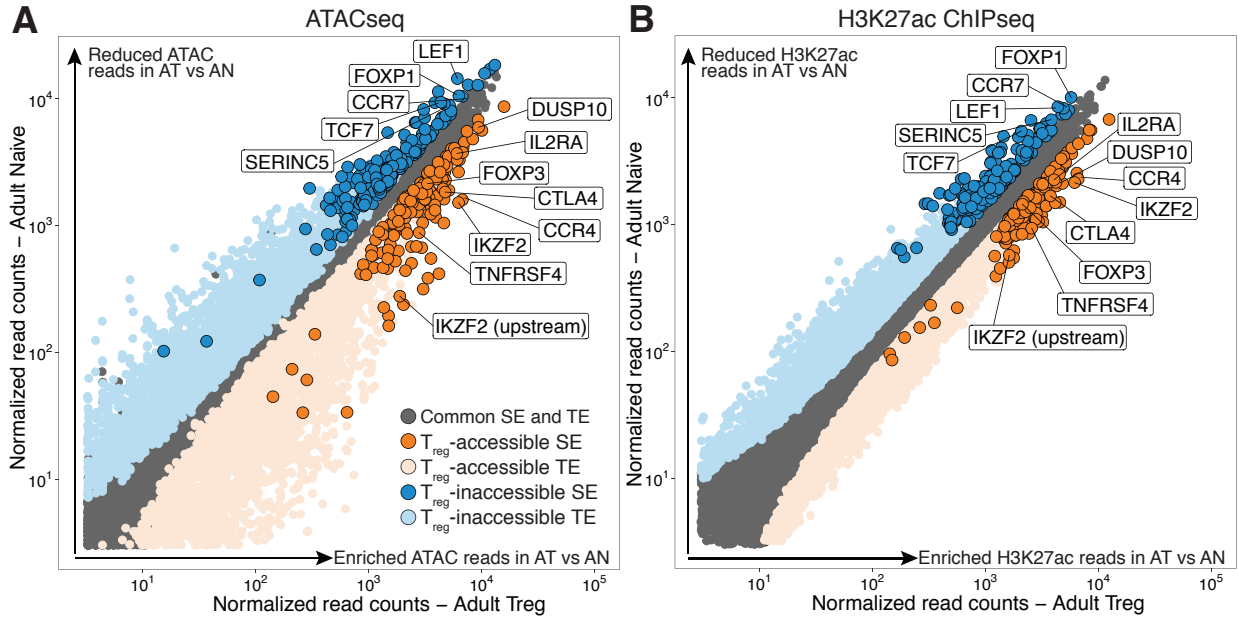


Figure 7. Identification of T_{reg}-accessible and inaccessible enhancers.

(A,B) Definition of the T_{reg}-accessible/inaccessible enhancer signature. Scatterplots show DESeq2 normalized **(A)** ATAC reads and **(B)** H3K27ac reads at all stitched superenhancers (SEs) and transcriptional enhancers (TEs) for adult T_{reg} cells (x-axis) plotted against adult naïve T cells (y-axis). Differentially enriched SEs (dark orange) and TEs (light orange) in T_{reg} cells and naïve T cells (dark blue and light blue respectively) are colored. Enhancers proximal to genes previously associated with T_{reg} and naïve T cell function are labeled.

(C) Shared T_{reg}-accessible enhancers are defined as enhancers with both increased ATAC and H3K27ac signal in adult T_{reg} cells relative to adult naïve T cells with fold change > 1.5 and false discovery rate (FDR) < 0.05 (see Supplementary Methods and Materials for further details). Tracks show an example of a T_{reg}-accessible SE at the *FOXP3* locus (right), and a common SE at the *BCL11B* locus (left). This was also utilized to define T_{reg}-inaccessible enhancers with decreased ATAC and H3K27ac reads.

(D) Fetal naïve T cells have increased chromatin accessibility relative to adult naïve T cells at T_{reg}-accessible enhancers and vice versa. Pie charts show percentage of T_{reg}-accessible enhancers with increased chromatin accessibility (left) or T_{reg}-inaccessible enhancers with decreased chromatin accessibility (right) in fetal naïve T cells.

(E) Fetal naïve T cells do not have H3K27ac enrichment relative to adult naïve T cells at T_{reg}-accessible enhancers and vice versa. Pie charts show percentages and averaged H3K27ac normalized log₂(n+1) reads across enhancers as with **(D)**.

(F,G) Boxplots show averaged ATAC **(F)** and H3K27ac **(G)** normalized log₂(n+1) transformed reads across T_{reg}-accessible enhancers (left) and T_{reg}-inaccessible enhancers (right). Boxplots show median (center line), interquartile range (box) and tenth and ninetieth percentiles (whiskers). All statistics were calculated using the Kruskal-Wallis test followed by Dunn's multiple comparison test with Bonferroni correction for multiple testing. ***p<0.001, n.s. p>0.05.

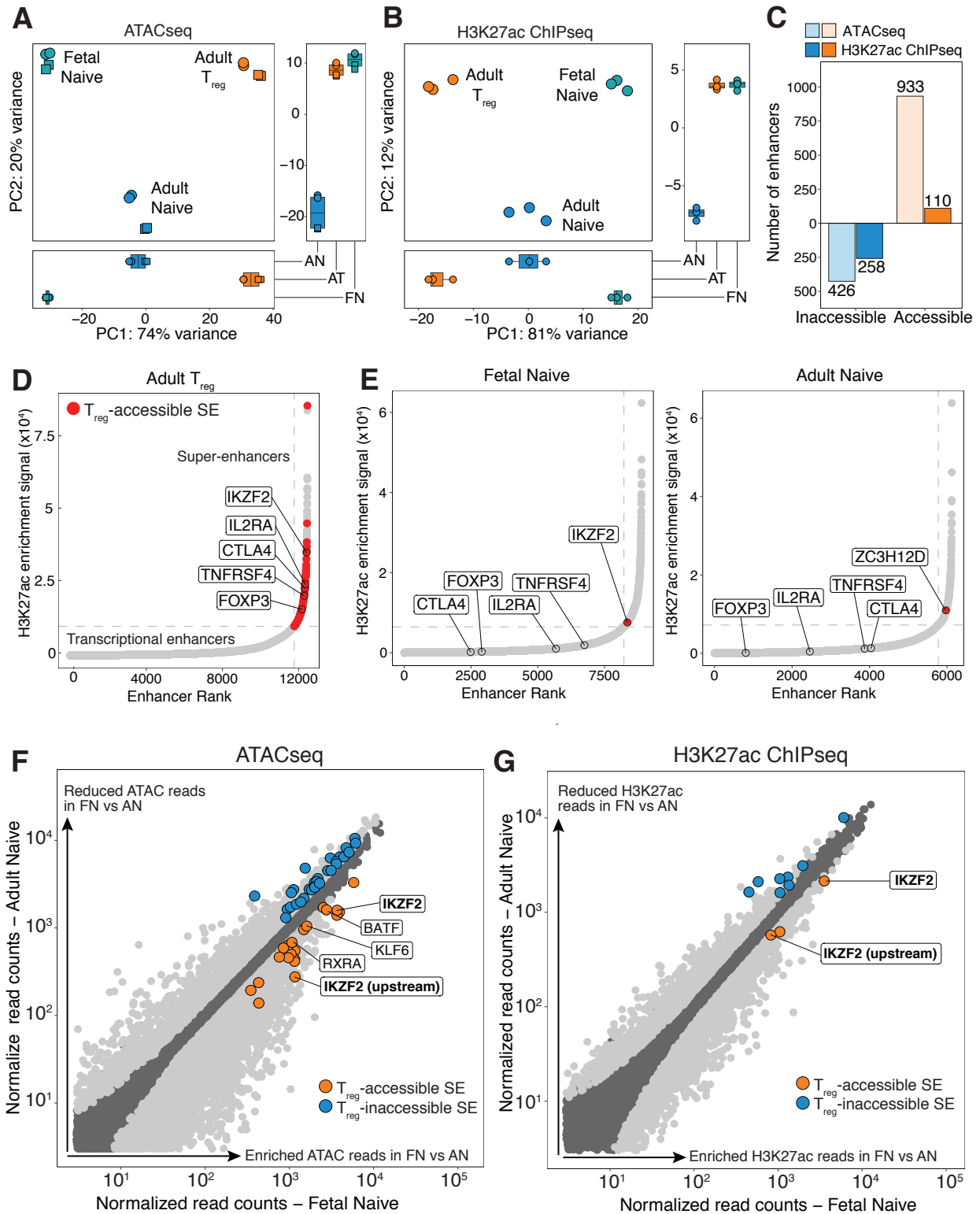


Figure 8. Fetal naïve T cells have increased ATAC and H3K27ac enrichment at two T_{reg}-accessible superenhancers associated with Helios

(A,B) A subset of enhancers is shared between adult T_{reg} and fetal naïve T cells. Principal component analysis performed on all super- (SE) and transcriptional enhancers (TE) with mapped **(A)** ATAC or **(B)** H3K27ac reads. Cells segregate first by age and functional subtype (Principal Component, PC1). Fetal naïve T cells (FN) and adult T_{reg} cells (AT) then cluster together away from adult naïve T cells (AN) on PC2. Boxplots show scores for PC1 and PC2 (bottom and right respectively).

(C) Fetal naïve T cells have increased/decreased enrichment of epigenetic marks at a subset of T_{reg} accessible/inaccessible enhancers. Barplots show number of T_{reg}-accessible/inaccessible enhancers with increased (orange) or decreased (blue) ATAC/H3K27ac signal in fetal naïve T cells relative to adult naïve T cells (T_{reg}-accessible/inaccessible enhancers defined in Supplementary Methods and Materials).

(D) Key T_{reg} genes are associated with superenhancers in adult T_{reg} cells. Cumulative H3K27ac signal at stitched enhancers within 12.5kb are plotted against enhancer rank, and SEs defined where the tangent of the plotted curve is 1. Dotted lines (grey) show cutoff for SEs for one representative sample each for adult T_{reg} (n = 3). SEs defined as T_{reg}-accessible and meet fold change (FC) > 1.5 and false discovery rate (FDR) <0.05 cut-offs are colored in red, and SEs associated with key T_{reg} genes are labeled.

(E) Fetal naïve T cells have a T_{reg}-accessible SE associated with Helios. Plots as with **(D)** show one representative sample for fetal (left) and adult (right) naïve T cells (n = 3). T_{reg}-accessible SEs identified in **(D)** was assessed for differential enrichment in fetal naïve against adult naïve T cells and vice versa. Differentially enriched T_{reg}-SEs in each sample with FC>1.5 and FDR<0.05 are colored red and labeled. TEs associated with key T_{reg} genes in **(D)** are also labeled. **(F,G)** Fetal naïve T cells have increased ATAC and H3K27ac enrichment at two T_{reg}-accessible SEs associated with Helios. Scatterplots of normalized **(F)** ATACseq reads and **(G)** H3K27ac reads at all stitched enhancer regions of fetal naïve T against adult naïve T cells. Differentially enriched SEs and TEs with FC>1.5 and FDR<0.05 are shown in light grey, with T_{reg}-accessible SEs (orange) and T_{reg}-inaccessible SEs (blue). T_{reg}-accessible SEs associated with transcription factors labeled; Helios (*IKZF2*) labeled in bold.

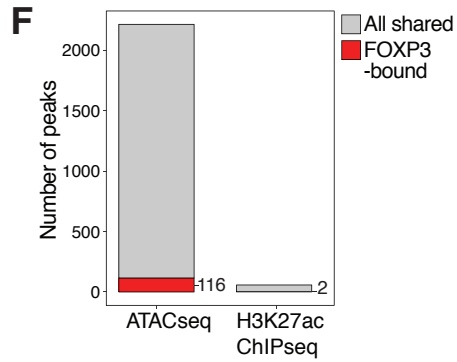
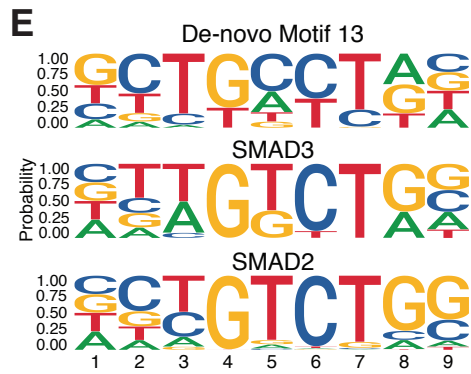
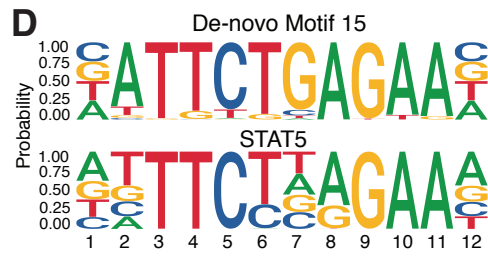
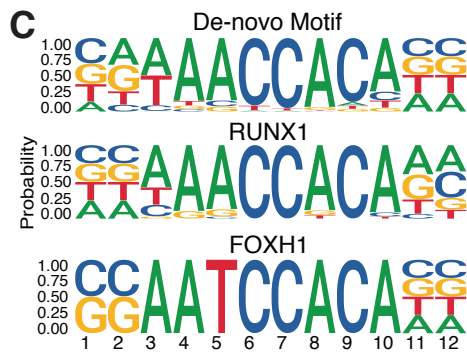
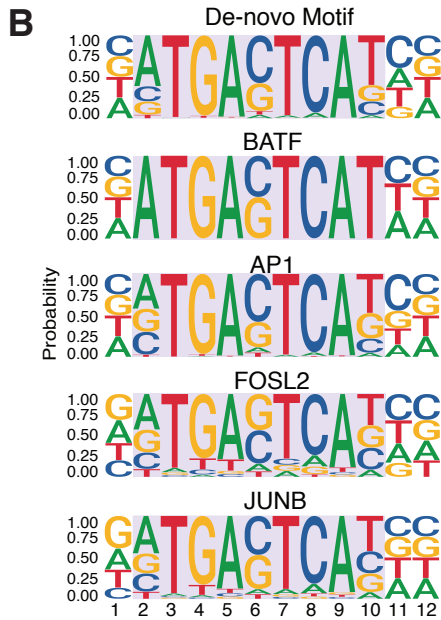
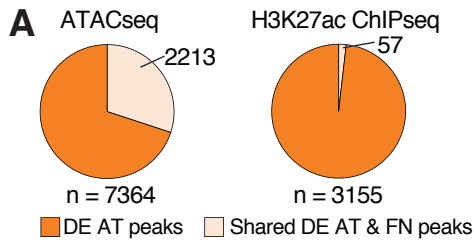


Figure 9. Binding motifs for downstream effectors of T_{reg} differentiation are enriched within shared T_{reg}-accessible peaks in fetal naïve T cells.

(A) Fetal naïve T cells have increased chromatin accessibility at a third of all defined T_{reg}-accessible peaks. Pie charts depict percentages of T_{reg}-accessible peaks (See Supplementary Methods and Materials for definition of T_{reg}-accessible peaks) that similarly have increased chromatin accessibility (left) or H3K27ac enrichment (right) in fetal naïve T cells relative to adult naïve T cells.

(B) The top *de novo* enriched motif is bound by BATF and the AP-1 complex. DNA motif analysis of shared T_{reg}-accessible peaks between fetal naïve and adult T_{reg} cells, with alignment of BATF, AP1, FOSL2 and JUNB motifs against the top *de novo* motif enriched. Other binding motifs enriched include **(C)** RUNX1 and FOXH1, **(D)** STAT5 and **(E)** SMAD3 and SMAD2.

(F) Only a small fraction of T_{reg}-accessible peaks shared between fetal naïve and adult T_{reg} cells intersect with FOXP3 binding sites. Bar plots show number of T_{reg}-accessible peaks with increased chromatin accessibility and H3K27ac enrichment in fetal naïve T cells, number of intersecting FOXP3-bound peaks in red and annotated (see Methods for definition of FOXP3-bound peaks).

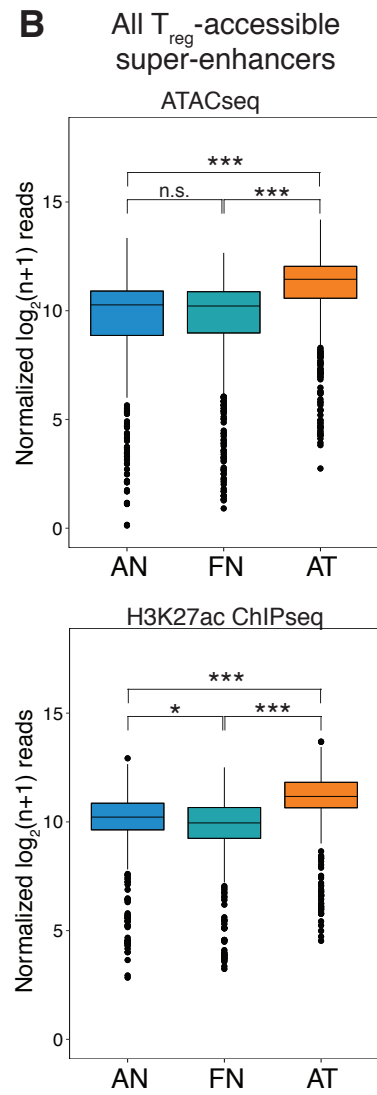
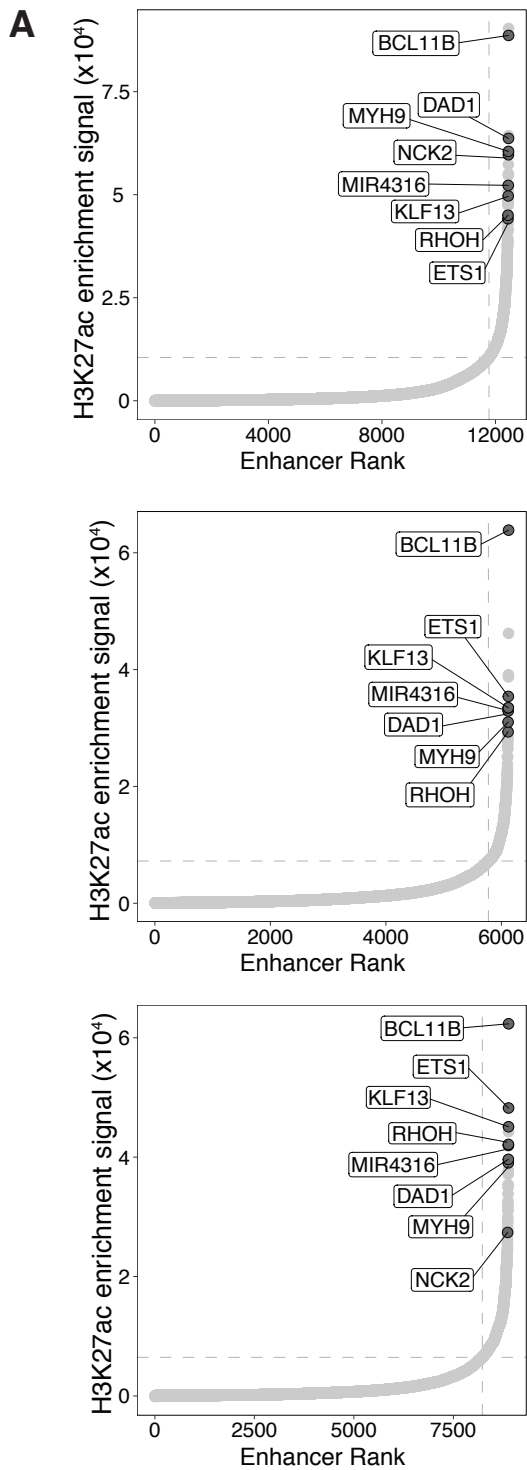


Figure 10. The highest ranked super-enhancers shared across all cell populations are associated with T cell development and function.

(A) Shared super-enhancers (SEs) across all cell populations are associated with genes involved in T cell development. Shared SEs across adult T_{reg} (top), fetal naïve (center) and adult naïve (bottom) T cells within the top 25 SEs for each population are colored in dark grey and labelled. Dashed lines (light grey) mark the SE cut-offs.

(B) Fetal naïve T cells do not have enrichment over adult naïve T cells at T_{reg}-accessible SEs. Boxplots show averaged ATAC signals (top) and H3K27ac signals (bottom) across 121 T_{reg}-accessible SEs in adult naïve (AN), fetal naïve (FN) and adult T_{reg} cells (AT).

Boxplots show median (centre line), interquartile range (box) and tenth and ninetieth percentiles (whiskers). All statistics were calculated using the Kruskal-Wallis test followed by Dunn's multiple comparison test with Bonferroni correction for multiple testing. ***p<0.001, n.s. p>0.05.

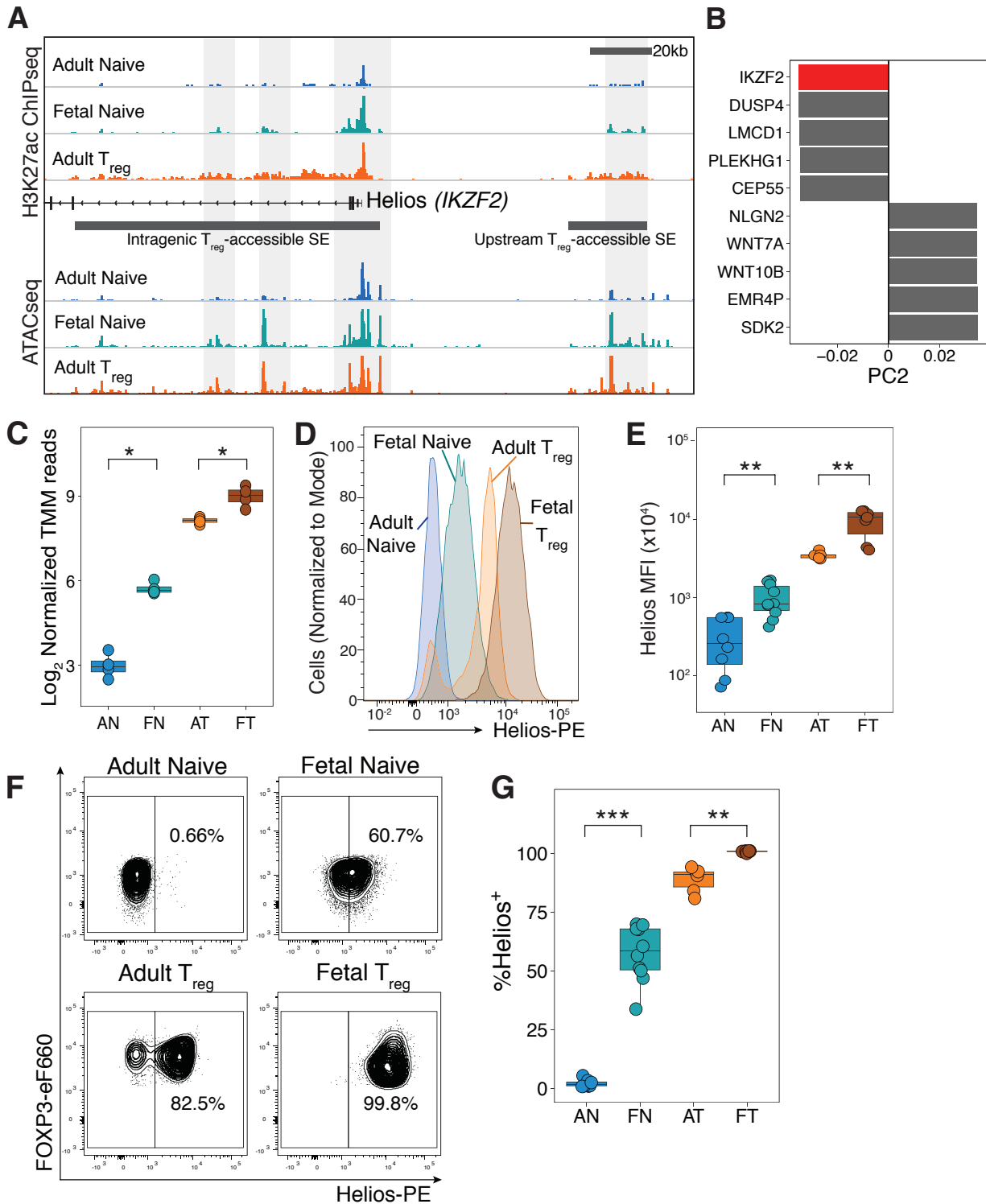


Figure 11. Helios expression is increased in fetal naïve T cells.

(A) H3K27ac and ATAC signals at two T_{reg} accessible super-enhancers (SEs) associated with the Helios (*IKZF2*) locus are differentially enriched in fetal naïve T cells relative to adult naïve T cells. Representative tracks of one replicate shown (H3K27ac ChIPseq, n=3, ATACseq, n=2).

(B) Helios is the top gene contributing to the negative directionality of principal component 2 (PC2). The top 5 genes contributing to PC2, which segregates cells by functional subtype (naïve versus T_{reg}) are plotted for both directions; Helios (*IKZF2*) highlighted in red.

(C) Transcription of Helios is increased in fetal naïve T cells. Boxplot shows \log_2 trimmed mean of M values of normalized RNAseq reads for Helios in adult naïve (AN), fetal naïve (FN), adult T_{reg} (AT) and fetal T_{reg} (FT) cells (n=4).

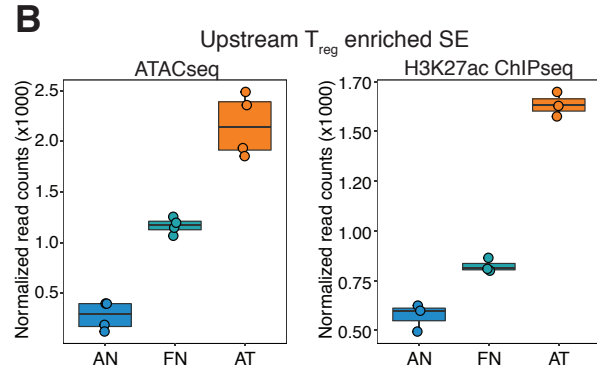
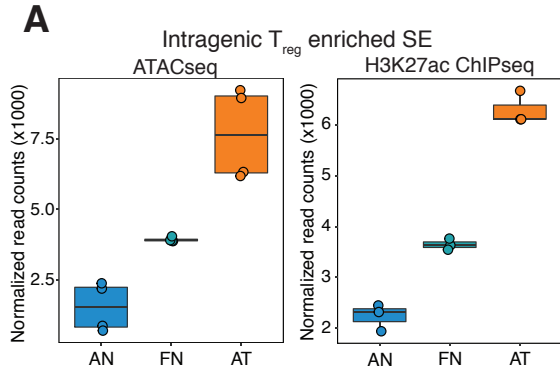
(D) Helios protein expression is increased in fetal naïve T cells. Helios staining intensity in sorted $CD4^+CD25^-CD27^+CD45RA^+$ adult (blue) and fetal naïve (green), and adult $CD25^{hi}CD127^{lo}FOXP3$ (orange) and fetal T_{reg} (brown).

(E) Boxplot shows quantification of mean fluorescence intensity of Helios for adult naïve (AN, n=8), fetal naïve (FN, n=10), adult T_{reg} (AT, n=8), and fetal T_{reg} (FT, n=10) cells.

(F) Flow cytometry analyses of sorted populations in **(D)** show that a large proportion of fetal naïve T cells are Helios⁺. Helios⁺ and Helios⁻ gates were set based on negative and positive populations in adult T_{reg} samples (bottom left). Adult naïve T cells were universally Helios⁻.

(G) Quantification of Helios⁺ cells among sorted populations in **(F)**.

All statistics were calculated by unpaired two-sided Mann-Whitney test. ***p<0.001, **p<0.01, *p<0.05. All boxplots show median (centre line), interquartile range (box) and tenth and ninetieth percentiles (whiskers)



C

Gene ID	Log ₂ FC	FDR	Enhancer
VANGL1	-3.65699441	1.07E-50	TE
MICAL2	-2.579985021	1.89E-32	SE
TOX	-2.958720161	3.28E-31	TE
CDCA7	-3.778717218	7.46E-31	TE
SEC14L1	-1.936185748	4.90E-28	TE
CCR4	-4.072089764	9.62E-28	SE
IKZF2	-2.530832857	9.29E-26	SE
ATP2B1	-1.951244278	2.39E-22	TE
LMNB1	-1.966818663	4.10E-22	TE
SPSB1	-3.683240249	8.91E-21	TE
SLC7A5	-4.814867521	9.98E-21	TE
ZNRF1	-2.27747697	9.98E-21	TE
TPPP	-3.557114216	1.23E-16	TE
NAMPT	-2.301973979	2.64E-15	TE
CORO1C	-2.299784681	4.39E-15	TE
CYTH3	-1.859506595	5.41E-14	TE
TFEB	-2.113772111	4.16E-13	TE
PRC1	-1.66993509	1.55E-11	TE
CTIF	-1.99493637	2.83E-11	TE
DUSP4	-2.790411194	1.13E-10	TE
AGPAT4	-2.15003174	1.91E-10	TE
TOX2	-2.000875577	3.66E-10	TE
IKZF4	-2.268186068	2.60E-08	TE
FOSL2	-4.028531602	1.13E-07	TE
HIVEP3	-1.634885545	3.23E-07	TE
SWAP70	-1.911228799	6.94E-07	TE
MEOX1	-2.10641286	1.50E-06	TE
SNX10	-1.505506174	3.67E-06	TE
VAV3	-1.520110027	4.43E-06	TE
BATF	-1.796089867	2.08E-05	SE
KLF11	-1.827599244	6.12E-05	TE
CTSH	-1.981616193	0.000134763	TE
PRDM1	-1.773165167	0.007635573	TE

D

Gene ID	Log ₂ FC	FDR	Enhancer
MICAL2	-2.579985021	1.89E-32	SE
TOX	-2.958720161	3.28E-31	TE
IKZF2	-2.530832857	9.29E-26	SE
TPPP	-3.557114216	1.23E-16	TE
CTIF	-1.99493637	2.83E-11	TE
IKZF4	-2.268186068	2.60E-08	TE
MEOX1	-2.10641286	1.50E-06	TE
VAV3	-1.520110027	4.43E-06	TE
RGS1	-2.130090123	0.001145178	TE

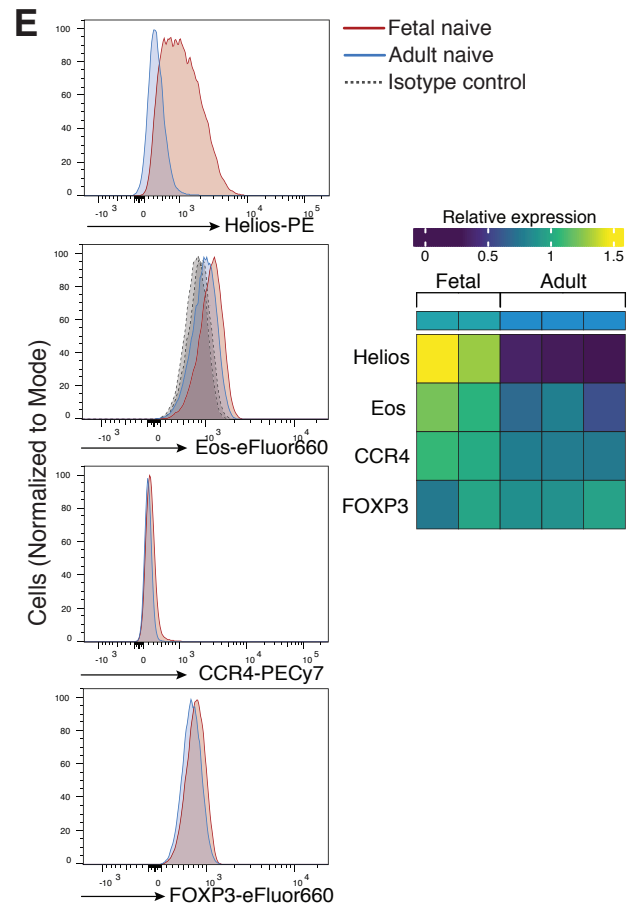


Figure 12. Chromatin accessibility and H3K27ac enrichment at the Helios locus in fetal naïve T cells correlate with increased RNA and protein expression.

(A) Normalized H3K27ac (left, n=3) and ATAC read counts (right, n=2 with 2 technical replicates) at the intragenic T_{reg}-accessible SE at the Helios locus for adult naïve (AN), fetal naïve (FN) and adult T_{reg} samples.

(B) Normalized H3K27ac (left) and ATAC read counts (right) at the upstream T_{reg}-accessible SE at the Helios locus for AN, FN and AT.

(C) Intersect of T_{reg}-specific genes associated with: (1) increased ATAC signal at T_{reg}-accessible enhancers and (2) increased RNA expression in fetal naïve T cells relative to adult naïve T cells. Genes assessed for protein expression in **(E)** highlighted in bold.

(D) Intersect of T_{reg}-specific genes associated with: (1) increased H3K27ac signal at T_{reg}-accessible enhancers and (2) increased RNA expression in fetal naïve T cells relative to adult naïve T cells. Genes assessed for protein expression in **(E)** highlighted in bold.

(E) Differential protein expression of Helios is present in fetal naïve T cells relative to adult naïve T cells. Flow cytometry plots (right) show staining intensity of Helios (*IKZF2*), Eos (*IKZF4*), CCR4, and FOXP3 in gated CD4⁺CD25⁻CD27⁺CD45RA⁺ adult (blue) and fetal naïve (red) cells. Staining intensity for isotype controls for Eos are shown in grey. Mean fluorescence intensity was quantified, scaled, and plotted as a heatmap (right) for fetal (n=2) and adult (n=3) naïve T cells.

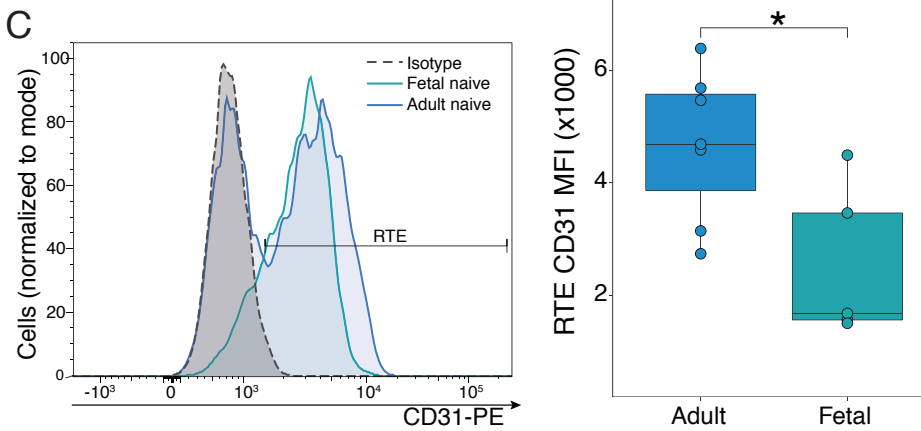
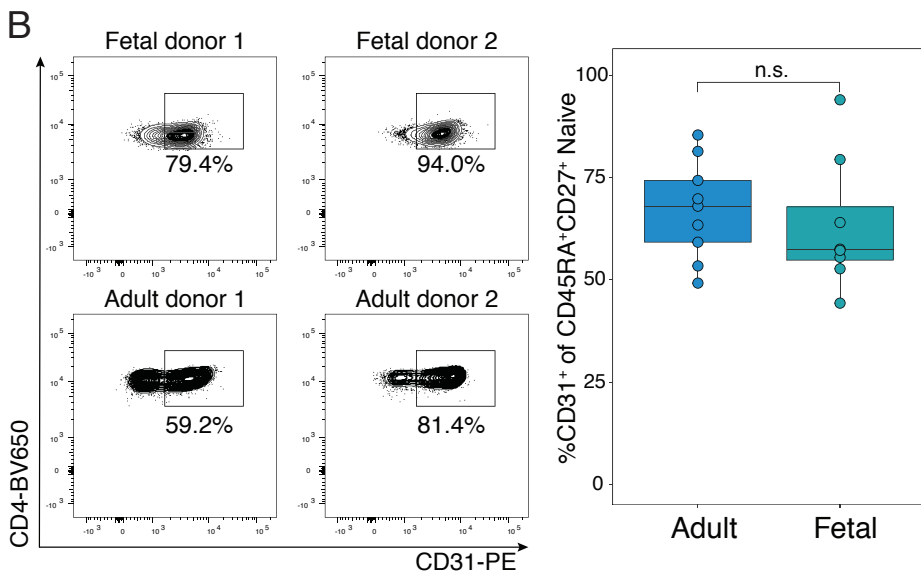
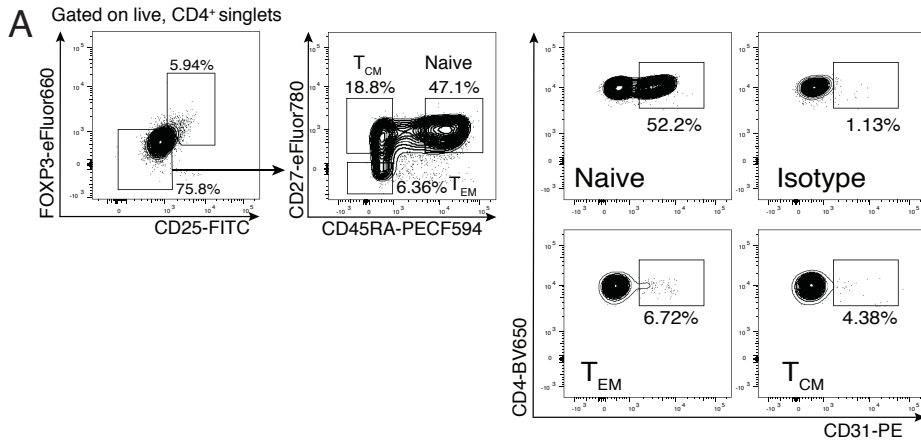


Figure 13. Fetal naïve T cells do not have an increased proportion of CD31⁺ recent thymic emigrants (RTE) relative to adult naïve T cells.

(A) Gating strategy for defining CD31⁺ RTEs based on magnetically sorted CD4⁺ adult T cells. The CD31 positive gate was set by excluding the negative population defined in combination by the isotype staining control, effector memory (T_{EM}) and central memory (T_{CM}) populations.

(B) Fetal naïve T cells do not have an increased proportion of RTEs as defined by CD31. Flow cytometry plots showing CD31 positive gating on sorted CD25⁻CD27⁺CD45RA⁺ naïve T cells from two representative fetal and adult samples (left). Boxplots show quantification of CD31⁺ RTE frequency (right) for adult (n=6) and fetal naïve T cells (n=8).

(C) Fetal RTEs have decreased CD31 expression. Histogram (left) show CD31 staining within sorted naïve T cells for one representative fetal (green) and adult (blue) sample with an isotype staining control (grey). The RTE gate is outlined. Boxplots (right) show quantification of CD31 mean fluorescence intensity of the CD31⁺ RTE population as gated in histogram for adult (n=6) and fetal (n=8). All statistics were calculated by unpaired two-sided Mann-Whitney test, *p<0.05, n.s. p>0.05. Boxplots show median (center line), interquartile range (box) and tenth and ninetieth percentiles (whiskers).

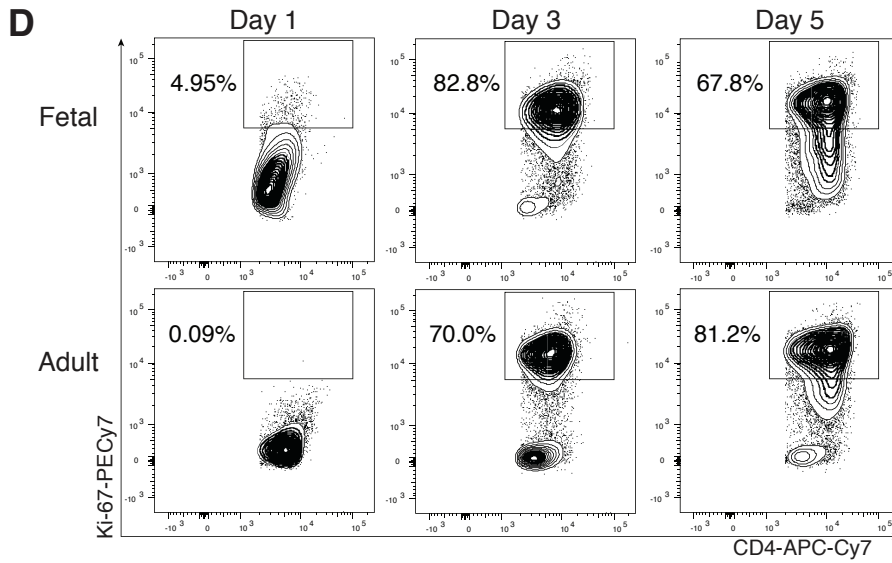
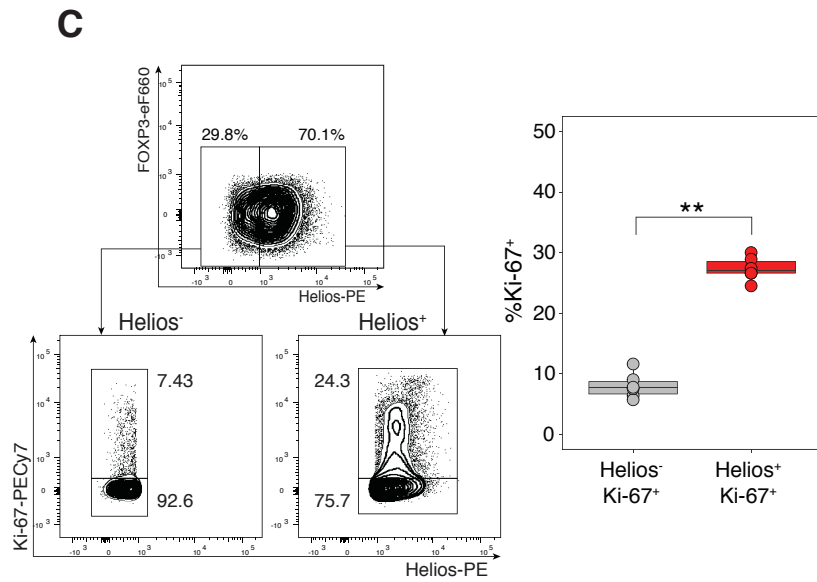
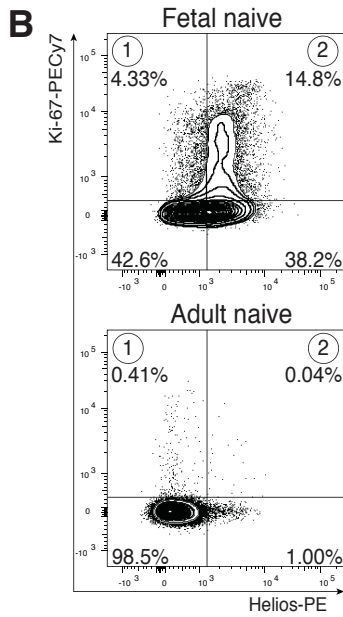
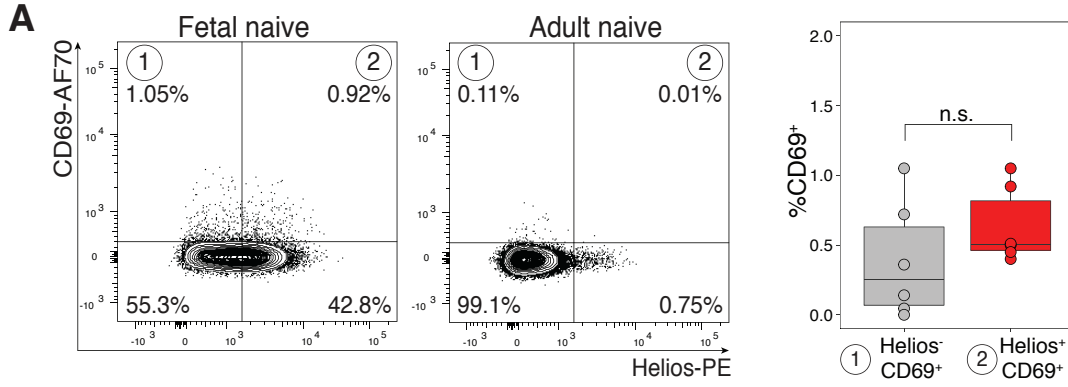


Figure 14. A fraction of fetal naïve T cells are highly proliferative.

(A) Fetal naïve T cells are not activated at steady state. Representative flow cytometry plots (left) of one experiment show CD69 staining for sorted fetal and adult CD25⁻CD27⁺ CD45RA⁺ naïve T cells. Boxplot (right) quantifies (1) Helios⁻CD69⁺ (grey) and (2) Helios⁺CD69⁺ (red) quadrants as shown for fetal samples (n=6).

(B) A fraction of fetal naïve T cells are actively proliferating. Representative flow cytometry plots of one experiment show Ki-67 staining for sorted fetal and adult naïve T cells.

(C) The Helios⁺ fraction contains the majority of actively proliferating cells. Representative flow cytometry plots (left) of one experiment gating for Ki-67 expression within Helios⁻ and Helios⁺ fractions within fetal naïve T cells. Boxplot (right) quantifies the percentages of Ki67⁺ cells shown in the flow cytometry plots. All statistics were calculated by two-sided Wilcoxon signed-rank test, *p<0.05, n.s. p>0.05. Boxplots show median (center line), interquartile range (box) and tenth and ninetieth percentiles (whiskers).

(D) Fetal and adult naïve T cells both highly upregulate Ki-67 by Day 5 of stimulation. Sorted fetal and adult naïve T cells stimulated with αCD3/αCD28/αCD2 tetramers and IL-2 alone over 1, 3 and 5 days. Flow cytometry plots are representative of one experiment for live, CD4⁺ cells. Positive gate defines the Ki-67^{hi} population.

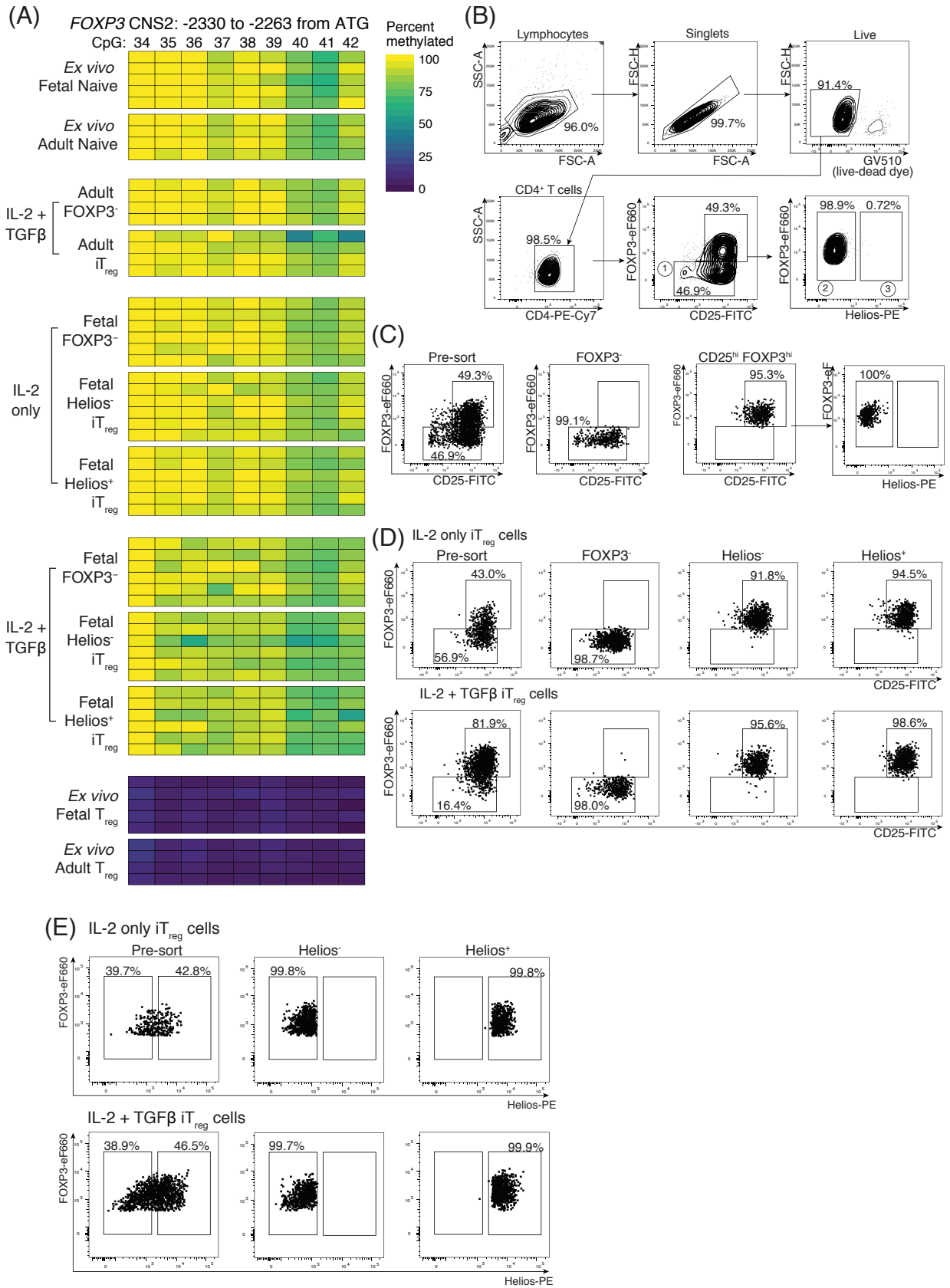


Figure 15. Fetal naïve T cells do not have demethylation at the *FOXP3* CNS2 (conserved non-coding sequence 2) Treg-specific demethylated region (TSDR).

Sorted fetal and adult *ex vivo* naïve and T_{reg} cells, along with differentiated *in vitro* induced T_{reg}⁻ (iT_{reg}) cells, were assessed for CpG demethylation at the *FOXP3* CNS2 TSDR locus.

(A) Fetal and adult naïve T cells show no difference in the extent of CpG demethylation at the TSDR. Heatmap shows percentage methylation of CpGs 34-42 at the *FOXP3* CNS2, defined as 2263-2330 basepairs upstream of the ATG start codon. More information on sequenced populations are in Supplementary Materials and Methods.

(B) Flow cytometry plots from one representative adult iT_{reg} sample differentiated in IL-2 and TGFβ showing gating strategy for fluorescence activated cell sorting (FACS) of (1) FOXP3⁻, (2) FOXP3⁺Helios⁻ and (3) FOXP3⁺Helios⁺ populations.

(C) Flow cytometry plots show purity of sorted FOXP3⁻ and FOXP3⁺Helios⁻ populations for one representative adult iT_{reg} sample differentiated in IL-2 and TGFβ.

(D) Flow cytometry plots show FOXP3 staining within sorted FOXP3⁻, FOXP3⁺Helios⁻ and FOXP3⁺Helios⁺ populations for one representative fetal iT_{reg} sample differentiated in IL-2 alone (top row) or in IL-2 and TGFβ (bottom row).

(E) Flow cytometry plots show Helios staining within sorted FOXP3⁺Helios⁻ and FOXP3⁺Helios⁺ populations for one representative fetal iT_{reg} sample differentiated in IL-2 alone (top row) or in IL-2 and TGFβ (bottom row).

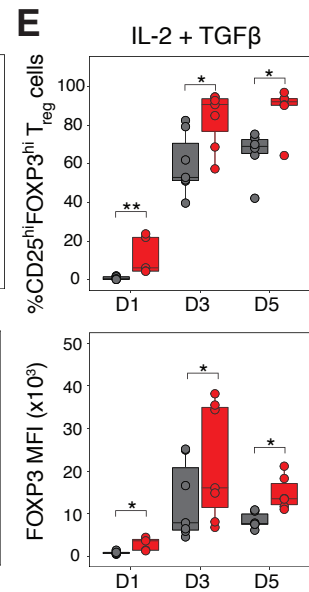
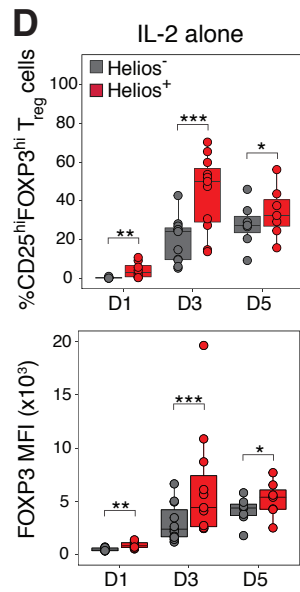
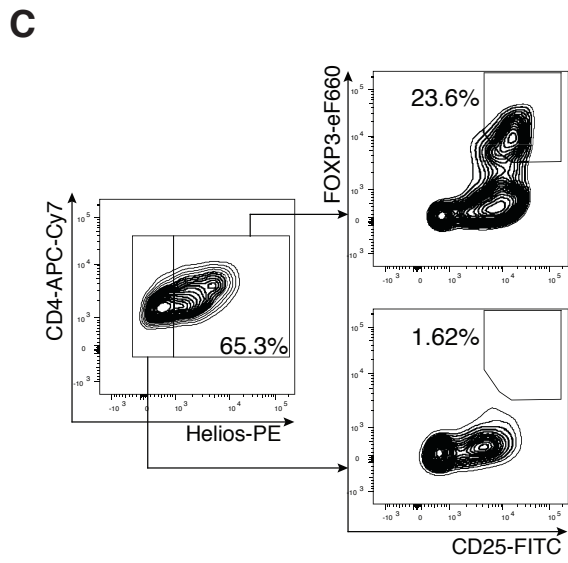
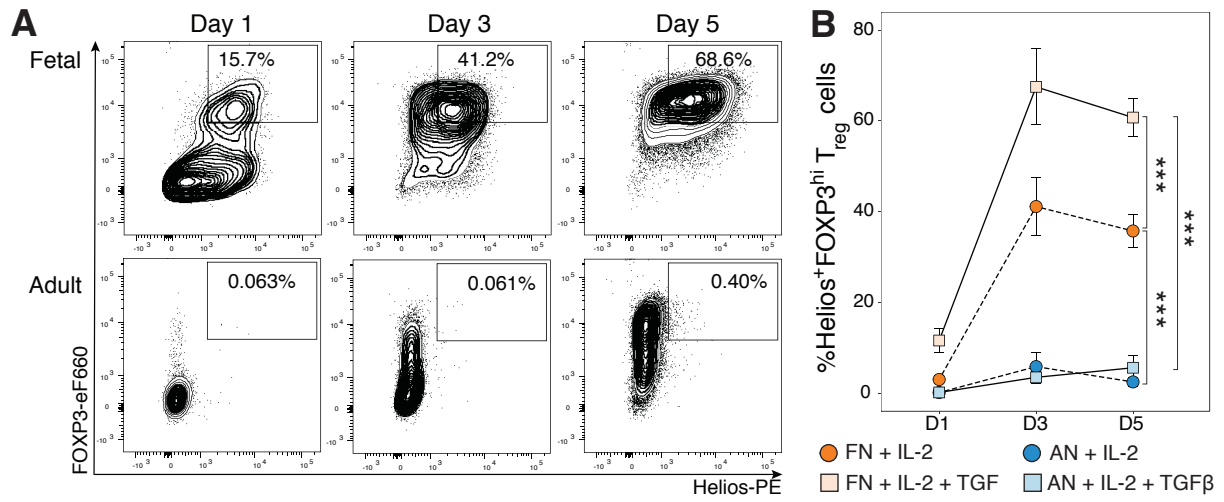


Figure 16. Helios⁺ fetal induced T_{reg} cells have increased FOXP3 expression

Sorted fetal and adult naïve T cells were stimulated with αCD3/αCD28/αCD2 tetramers and IL-2 in the absence or presence of TGFβ over 1, 3 or 5 days, and analyzed by flow cytometry. The number of biological replicates for each time point and stimulation condition are specified in table S8.

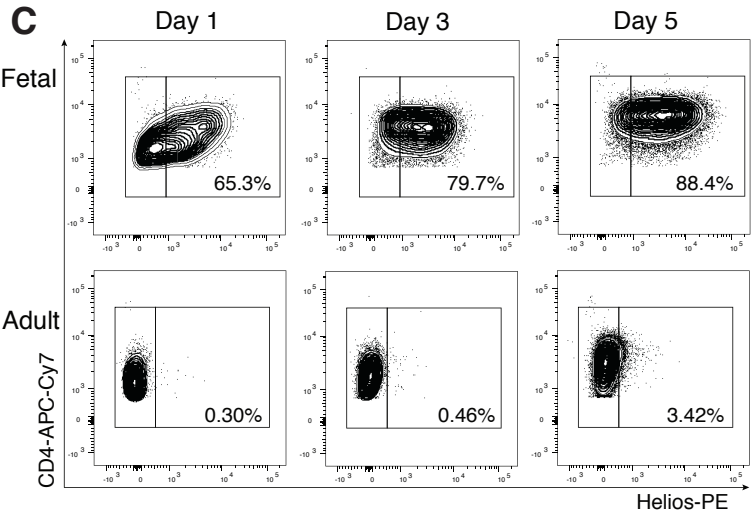
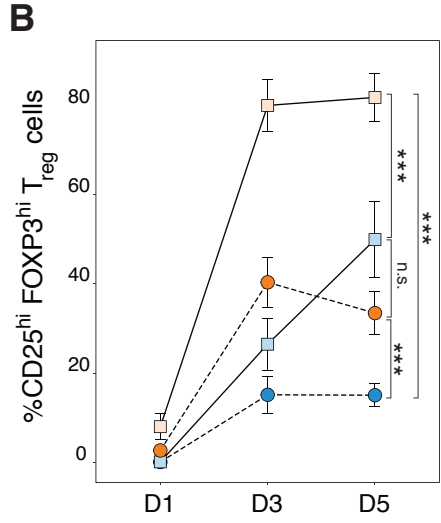
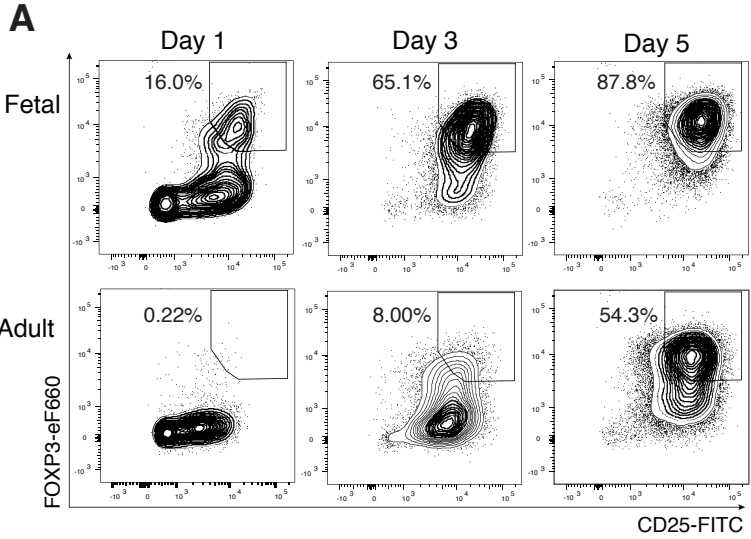
(A) Fetal naïve T cells, but not adult naïve T cells, rapidly upregulate Helios and FOXP3 upon T cell receptor stimulation. Representative flow cytometry plots show T_{reg} induction in the presence of IL-2 and TGFβ for fetal (top) and adult (bottom) naïve T cells respectively gated on live, CD4⁺ T cells.

(B) Fetal induced T_{reg} (iT_{reg}) cells, and not adult iT_{reg} cells, retain Helios expression. Quantification of percentage of Helios⁺FOXP3⁺ iT_{reg} cells gated in **(A)** for adult (AN) and fetal naïve (FN) T cells stimulated in the presence or absence of TGFβ. Statistics calculated using 2-way ANOVA with Tukey's honest significant difference post-test, ***p<0.001. Error bars denote mean ± s.d.

(C) The Helios⁺ population contains the majority of the fetal iT_{reg} cells. Representative flow cytometry plots shown for one fetal sample stimulated with IL-2 and TGFβ at day 1.

(D) Quantification of the proportion of fetal T_{reg} cells in the Helios⁺ or Helios⁻ population as gated in **(C)** over 1, 3 and 5 days in the absence (left) or presence (right) of TGFβ.

(E) FOXP3 mean fluorescence intensity was increased in Helios⁺ iT_{reg} cells relative to Helios⁻ iT_{reg} cells as gated in **(C)** across all time points in the absence (left) or presence (right) of TGFβ. Statistics for **(D,E)** were calculated by two-sided Wilcoxon signed-rank test, ***p<0.001, **p<0.01, *p<0.05. All boxplots show median (centre line), interquartile range (box) and tenth and ninetieth percentiles (whiskers)



● FN + IL-2 ● AN + IL-2
■ FN + IL-2 + TGFβ ■ AN + IL-2 + TGFβ

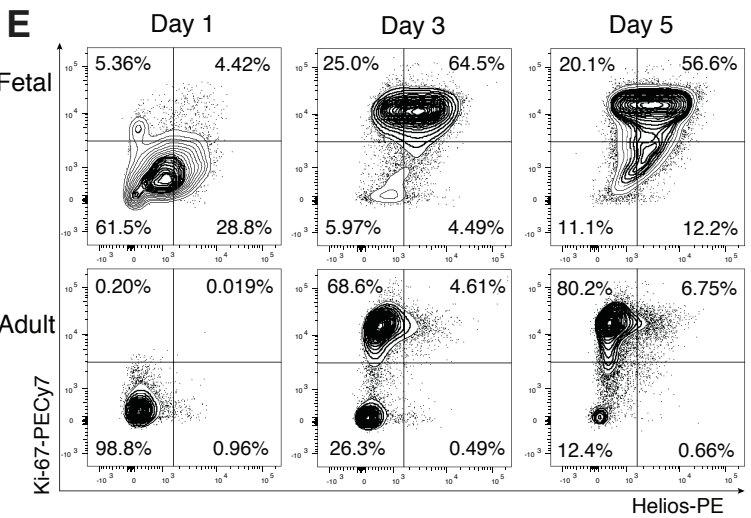
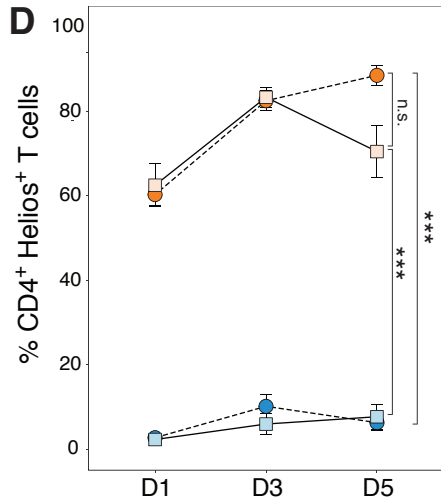


Figure 17. Fetal naïve T cells upregulate Helios during T_{reg} induction.

Fetal and adult naïve T cells were stimulated with α CD3/ α CD28/ α CD2 tetramers and IL-2 in the presence or absence of TGF β . The numbers of biological replicates for each time point and stimulation condition are specified in table S8. Cells were analysed by flow cytometry at 1, 3 and 5 days.

(A) A larger fraction of fetal naïve T cells differentiate into T_{reg} cells relative to adult naïve T cells over 1,3 or 5 days of T cell receptor stimulation. Representative flow cytometry plots are shown for one experiment for live, CD4⁺ T cells.

(B) Quantification of percentages of induced T_{reg} (iT_{reg}) gated in **(A)** for adult (AN) and fetal (FN) cells.

(C) A large fraction of fetal naïve T cells upregulate and maintain Helios expression over all time points. Representative flow cytometry plots are shown for one experiment for live, CD4⁺ T cells. Helios⁺ and Helios⁻ gates were set to staining levels of adult naïve T cells at day 1.

(D) Quantification of percentages of Helios⁺ cells gated in **(C)** for AN and FN cells.

All statistics were calculated with 2-way ANOVA with Tukey's HSD post-test, ***p<0.001, n.s. p>0.05. Error bars denote mean \pm s.d.

(E) Fetal and adult naïve T cells increase Ki-67 expression to the same extent after proliferation regardless of Helios expression. Representative flow cytometry plots of one experiment show Ki-67 and Helios staining for live, CD4⁺ cells.

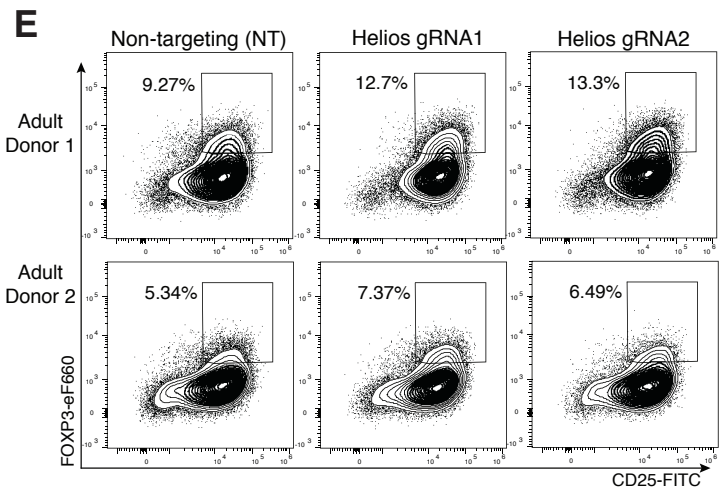
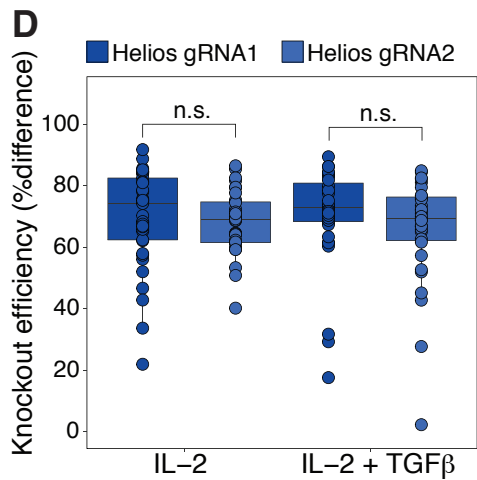
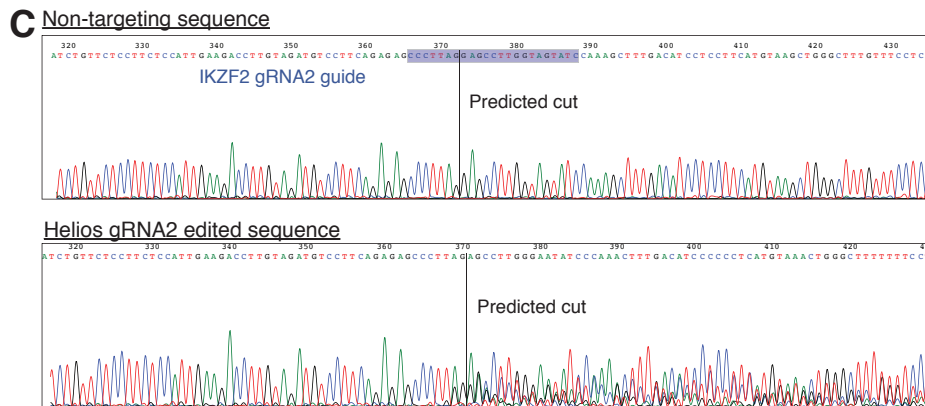
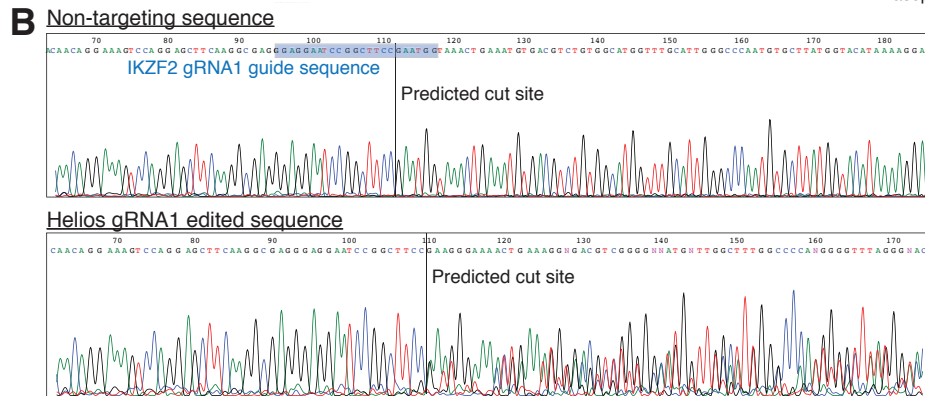
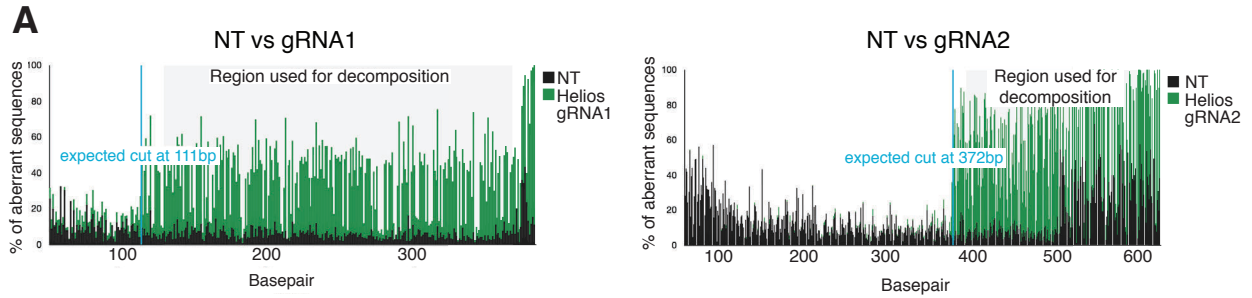


Figure 18. Validation of CRISPR-Cas9 editing at the Helios locus

Primers amplifying across cut sites for gRNA1 and gRNA2 were used to amplify the Helios locus and were sequenced. Sequencing traces were analyzed with the Tracking of Indels by DEcomposition (TIDE) webtool (<http://tide.nki.nl/>) to verify editing.

(A) Histogram shows percentage of sequence aberration found comparing sequencing chromatograms of amplicons from cells treated with the non-targeting (NT) gRNA and Helios gRNA1 (left) or gRNA2 (right). The blue line shows the predicted cut site; the region following the cut site was used for decomposition by TIDE.

(B) Chromatograms of amplicons from NT gRNA (top) and gRNA1 (bottom) nucleofections. The full sequence of gRNA1 is highlighted in blue, and black lines denote the TIDE predicted cut site. Frameshifts in the sequence resulting in jumbled sequences after the cut site were only observed with gRNA1 mediated editing.

(C) Chromatograms of amplicons from NT gRNA (top) and gRNA2 (bottom) nucleofections. The full sequence of gRNA2 is highlighted in blue, and black lines denote the TIDE predicted cut site. Frameshifts in the sequence resulting in jumbled sequences after the cut site were only observed with gRNA2 mediated editing.

(D) Assessment of efficiency of Helios editing by intracellular flow cytometry. Efficiency was calculated by taking the percentage of Helios⁺ cells gated in gRNA-edited cells divided by percentage of Helios⁺ in NT controls. Boxplot shows percentage efficiency for gRNA1 and 2 across both stimulation conditions at day 6 post-editing. Statistics were calculated by unpaired two-sided Mann-Whitney test, n.s. $p > 0.05$.

(E) Flow cytometry plots show adult iT_{reg} cells which received NT, gRNA1 and gRNA2 guides used to set CD25^{hi}FOXP3^{hi} T_{reg} gates for two different representative donors.

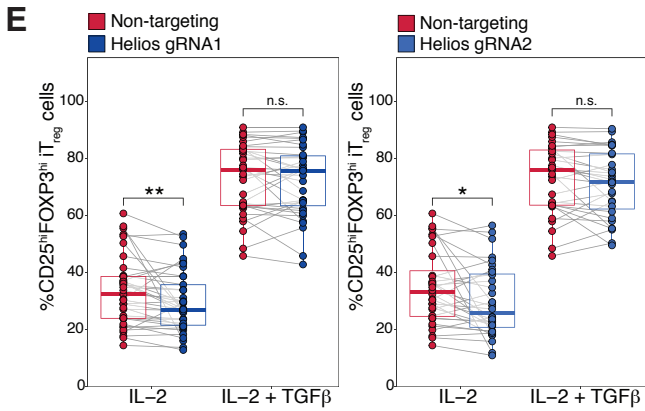
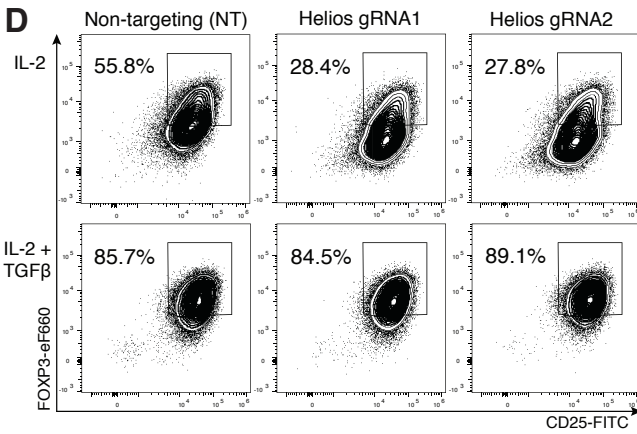
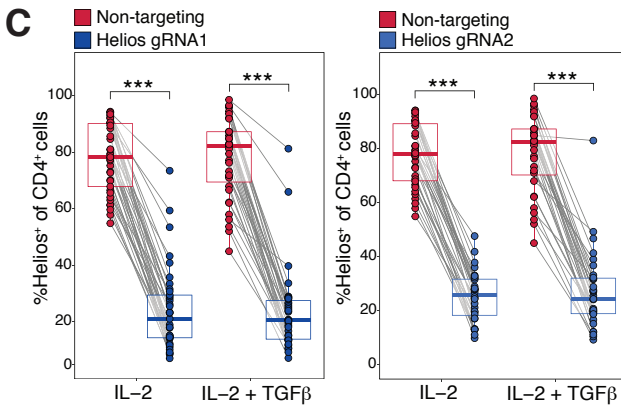
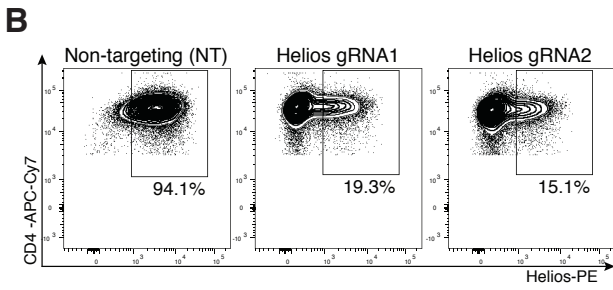
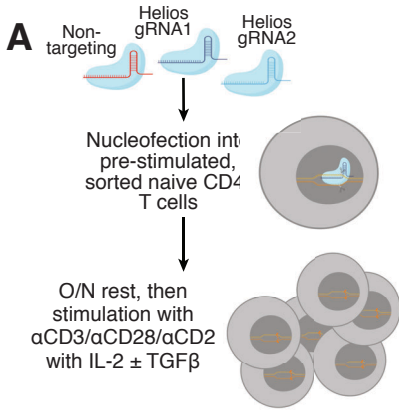


Figure 19. CRISPR-Cas9 mediated knockout of Helios in fetal naïve T cells reduces their preferential differentiation into T_{reg} cells.

(A) Schematic showing experimental design. CRISPR-Cas9 editing at the Helios locus with two independent guide RNAs (gRNA1, gRNA2, see Supplementary Materials & Methods) was carried out in pre-stimulated fetal naïve T cells, with a non-targeting (NT) gRNA as a control. Edited cells were stimulated with α CD3/ α CD28/ α CD2 tetramers in the absence or presence of TGF β . T_{reg} induction was assessed at 6 days. The numbers of biological replicates for each guide and stimulation condition are specified in table S9.

(B) CRISPR-Cas9 editing at the Helios locus reduces Helios expression in fetal naïve T cells relative to the non-targeting (NT) guide as evaluated by intracellular flow cytometry. Representative plots of one experiment are shown gated on live, CD4⁺ T cells.

(C) Quantification of Helios expression post-editing in fetal naïve T cells after T_{reg} induction as in

(B). Boxplots show paired samples for gRNA1 (left) and gRNA2 (right).

(D) Helios ablation in fetal naïve T cells reduces T_{reg} induction in response to TCR signaling alone. This effect was abolished by the addition of TGF β . Representative plots of one experiment are shown gated on live, CD4⁺ T cells.

(E) Quantification of induced T_{reg} proportions in edited fetal naïve T cells as in **(D)**. Boxplots show paired samples for gRNA1 (left) and gRNA2 (right). All statistics were calculated by two-sided Wilcoxon signed-rank test, ***p<0.001, **p<0.01, *p<0.05. All boxplots show median (center line), interquartile range (box) and tenth and ninetieth percentiles (whiskers).

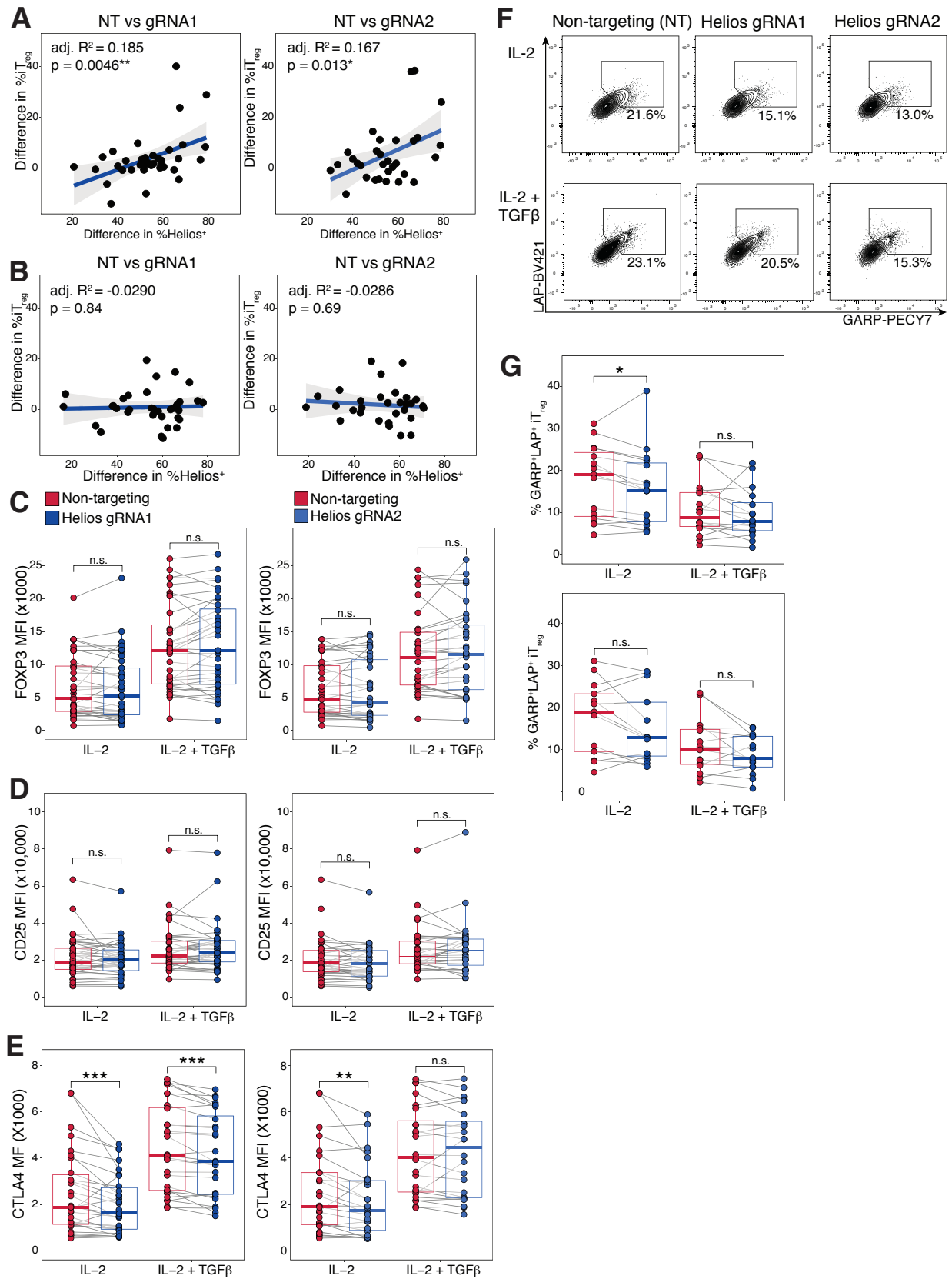


Figure 20. The effect of CRISPR-Cas9 knockout of Helios on protein expression of T_{reg} functional markers is variable.

(A) The reduction in T_{reg} differentiation in fetal naïve T cells differentiated in response to TCR signaling alone is correlated with the difference in Helios percentage after editing. Scatterplots show correlation between the difference in percentages of CD25^{hi}FOXP3^{hi} T_{reg} against the difference in percentages of Helios⁺ T cells for cells edited with gRNA1 (left) or gRNA2 (right) versus NT gRNA.

(B) The reduction in T_{reg} differentiation in fetal naïve T cells differentiated in IL-2 and TGFβ is not correlated with the difference in Helios percentage after editing. Scatterplots show correlation between the difference in percentages of CD25^{hi}FOXP3^{hi} T_{reg} against the difference in percentages of Helios⁺ T cells for cells edited with gRNA1 (left) or gRNA2 (right) versus NT gRNA. Adjusted R² and p values for **(A,B)** were calculated by simple linear regression, n.s., p>0.05.

CRISPR-Cas9 editing of the Helios locus with gRNA1 (left), gRNA2 (right) had no effect on the mean fluorescence intensity (MFI) of **(C)** FOXP3, **(D)** CD25 in comparison to the NT control in fetal iT_{reg} cells. MFI of **(E)** CTLA-4 is reduced in edited fetal induced T_{reg} (iT_{reg}) cells treated with Helios gRNA compared to NT controls. Boxplots show MFI of live, CD4⁺ T cells 6 days post induction in the presence of absence of TGFβ.

(F) Helios knockout may reduce upregulation of GARP and LAP in fetal iT_{reg} cells.

Representative flow cytometry plots shown for one experiment for live, CD4⁺CD25^{hi}FOXP3^{hi} T_{reg} cells differentiated in the presence (top) or absence (bottom) of TGFβ.

(G) Quantification of GARP⁺LAP⁺ fetal iT_{reg} cells after Helios knockout as in **(F)** for cells treated with gRNA1 (top) or gRNA2 (bottom). All statistics for **(C, D, E, G)** were calculated by two-sided Wilcoxon signed-rank test, ***p<0.001, *p<0.05, n.s. p>0.05. All boxplots show median (centre line), interquartile range (box) and tenth and ninetieth percentiles (whiskers).

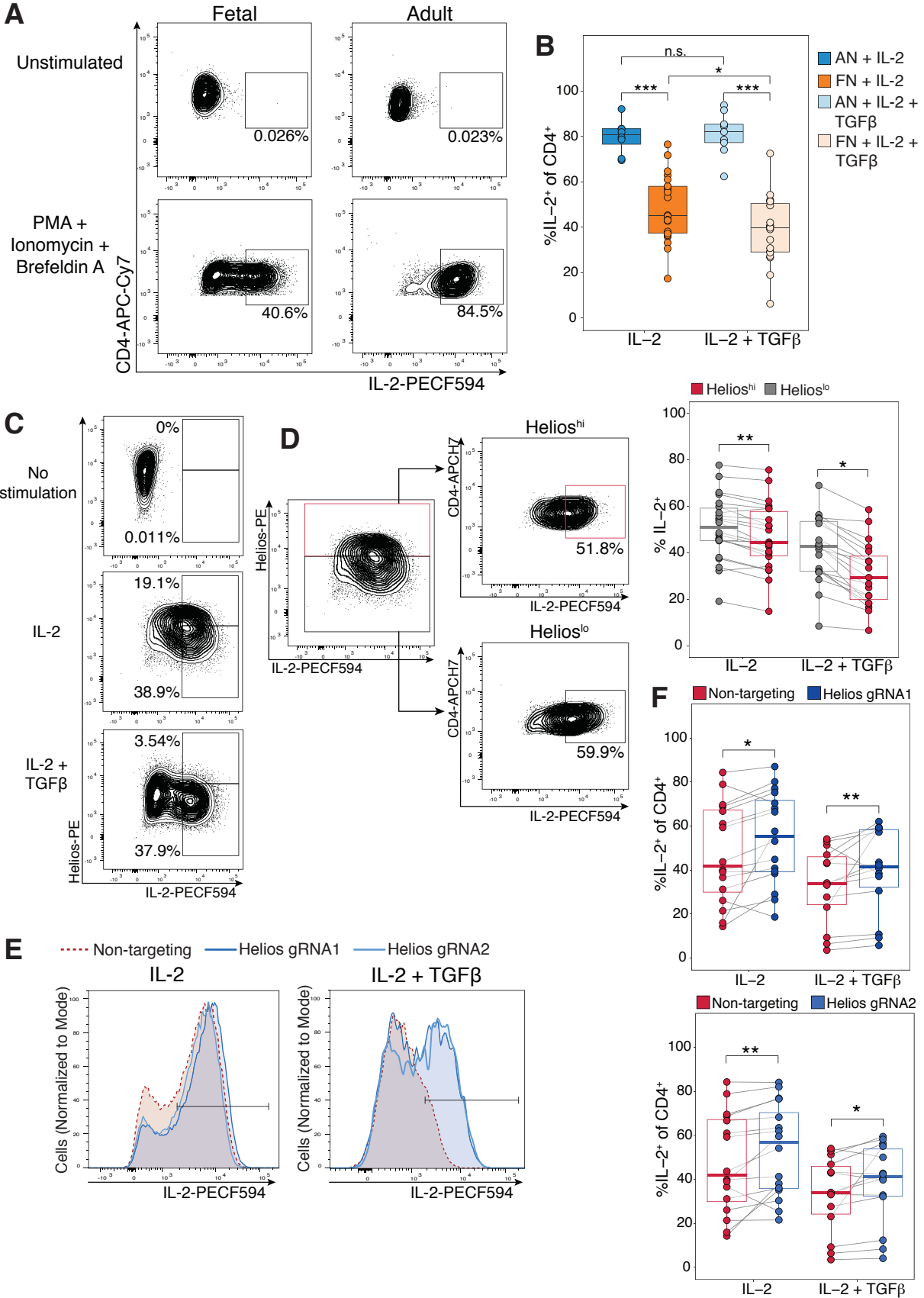


Figure 21. Fetal, but not adult, induced T_{reg} cells have suppressed IL-2 production after restimulation

Fetal and adult iT_{reg} differentiated with IL-2 in the presence or absence of TGFβ for 5 days were restimulated with Phorbol 12-Myristate 13-Acetate (PMA), ionomycin, and Brefeldin A for 5 hours to measure cytokine production.

(A) Fetal induced T_{reg} (iT_{reg}) cells have reduced IL-2 production upon restimulation. Flow cytometry plots show staining for intracellular IL-2 in unstimulated controls (top) in comparison to restimulated cells (bottom). Plots show one representative experiment for fetal and adult iT_{reg} cells differentiated with IL-2 alone gated on live CD4⁺ T cells.

(B) Quantification of IL-2 production in fetal and adult iT_{reg} cells after restimulation in **(A)** after T_{reg} induction in IL-2 alone (fetal, n=22, adult, n=8) or with added TGFβ (fetal, n=19, adult, n=9). Statistics calculated with unpaired two-sided Mann-Whitney test, ***p<0.001, *p<0.05, n.s., p>0.05.

(C) Reduction of IL-2 production is greater in Helios^{hi} fetal iT_{reg} population. Flow cytometry plots show staining for intracellular IL-2 in unstimulated controls (top) and restimulated fetal iT_{reg} differentiated in IL-2 alone (center) and in the presence of added TGFβ (bottom) for one representative experiment gated on live CD4⁺ T cells.

(D) Helios^{hi} iT_{reg} cells produce more IL-2 than Helios^{lo} iT_{reg} cells. Flow cytometry plots show gating for Helios^{hi} and Helios^{lo} populations, after staining for intracellular IL-2 was assessed for one representative sample cultured in IL-2 alone. Boxplots show quantification for Helios^{lo} (grey) and Helios^{hi} (red) fetal iTreg differentiated in IL-2 alone (n=22) or with TGFβ added (n=19). Statistics calculated by two-sided Wilcoxon signed-rank test, ** p<0.01, *p<0.05.

(E) The ablation of Helios expression in fetal iT_{reg} cells result in increased IL-2 production regardless of induction condition. Histograms show gating for one representative sample cultured in IL-2 alone (right) and with added TGFβ (left) for live CD4⁺ T cells.

(F) Quantification of IL-2 after Helios ablation by CRISPR editing as in **(E)** for iT_{reg} cells differentiated in IL-2 alone or with added TGFβ (NT, n = 16, sgRNA1, n=14, sgRNA2, n = 16 for both stimulation conditions). Statistics calculated by two-sided Wilcoxon signed-rank test, **p<0.01, *p<0.05. All boxplots show median (centre line), interquartile range (box) and tenth and ninetieth percentiles (whiskers).

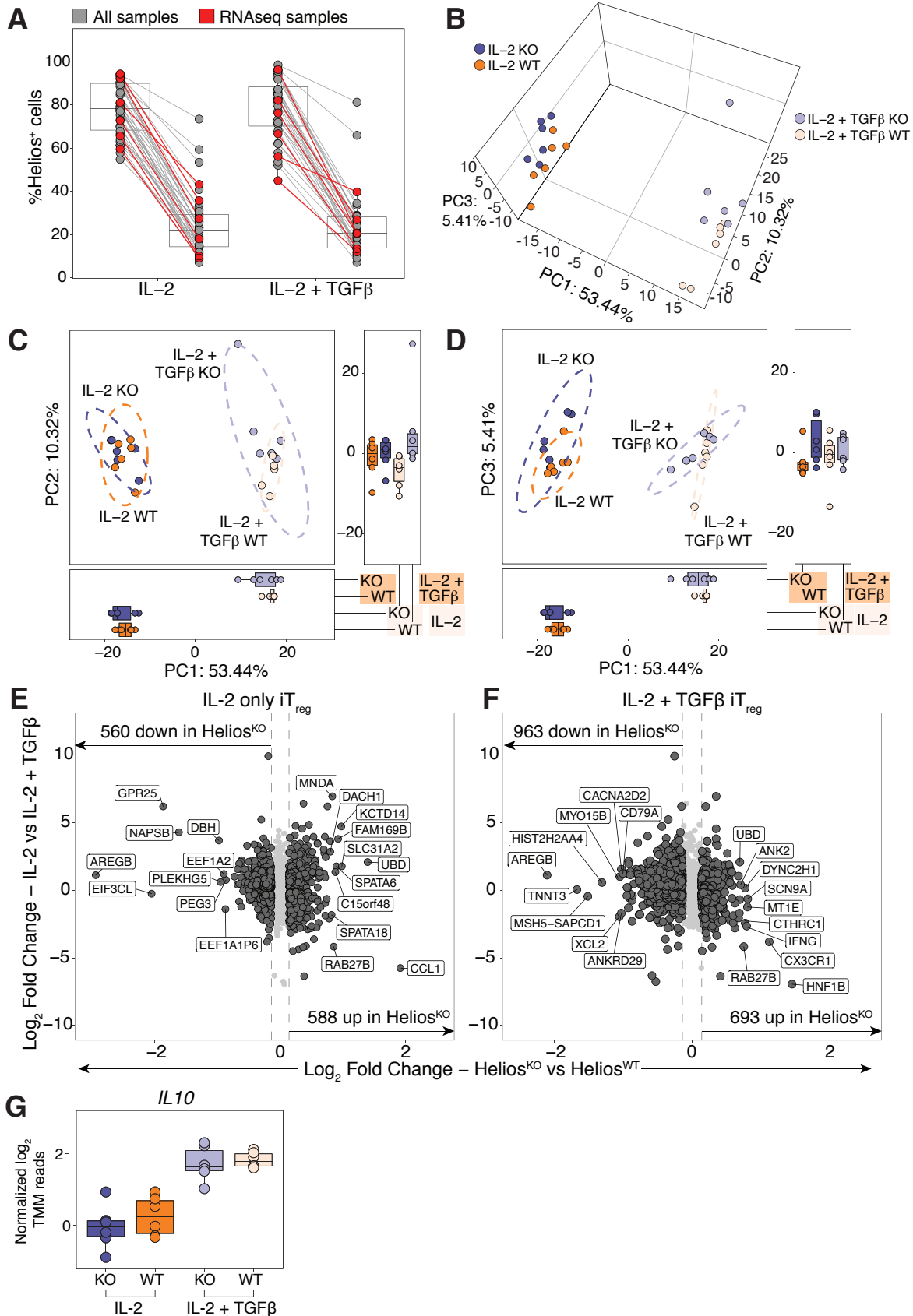


Figure 22. Helios knockout in fetal iT_{reg} cells result in a subtle shift in the underlying transcriptome

(A) Paired lineplots quantify differences in Helios expression measured by flow cytometry in fetal iT_{reg} cells nucleofected with Helios gRNA1 (Helios^{KO}) relative to the non-targeting control (Helios^{WT}) in the presence of IL-2 alone or with exogenous TGFβ. Samples sequenced shown in red (n=6). **(B)** Principal component analysis (PCA) reveals a subtle separation of Helios^{KO} and Helios^{WT} populations. Three-dimensional PCA plot show separation of populations first by T_{reg} differentiation conditions (Principal component, PC1, IL-2 versus IL-2 and TGFβ), and then by the absence or presence of Helios knockout (PC2, 3, Helios^{KO} vs Helios^{WT}). **(C)** Two-dimensional PCA plot of PC1 and PC2 shown in **(B)** show that PC2 segregates Helios^{WT} and Helios^{KO} iT_{reg} cells differentiated in the presence of TGFβ. Boxplots show scores for PC1 and 2 (bottom and right respectively). **(D)** Two-dimensional PCA plot of PC1 and PC3 shown in **(B)** show that PC3 segregates Helios^{WT} and Helios^{KO} iT_{reg} cells differentiated in the absence of TGFβ. Boxplots show scores for PC1 and 2 (bottom and right respectively). **(E,F)** Changes in the overall transcriptome in Helios^{KO} relative to Helios^{WT} iT_{reg} cells are modest but detectable in both differentiation conditions. Scatterplots plots log₂FC values for comparisons for the absence or presence of exogenous TGFβ during the differentiation process (y axis) and Helios^{KO} against Helios^{WT} iTreg (x axis) that underwent differentiation in IL-2 alone **(E)** or with exogenous TGFβ added **(F)**. Dotted lines in grey denote log₂FC cut-offs. Genes with false discovery rate (FDR) <0.05 and fold change (FC) > 1.1 are in dark grey, with top ten genes with the highest fold changes in both conditions labeled. **(G)** Helios^{WT} iT_{reg} cells have increased *IL10* transcription over Helios^{WT} cells. Boxplots show trimmed mean of M values of log₂ normalized RNAseq reads for *IL10*. All boxplots show median (centre line), interquartile range (box) and tenth and ninetieth percentiles (whiskers).

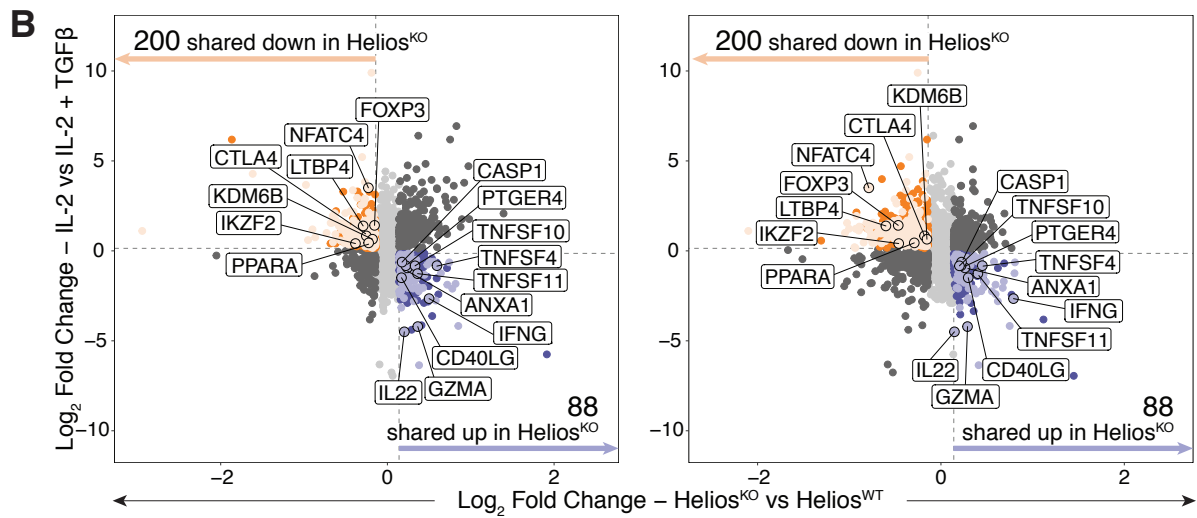
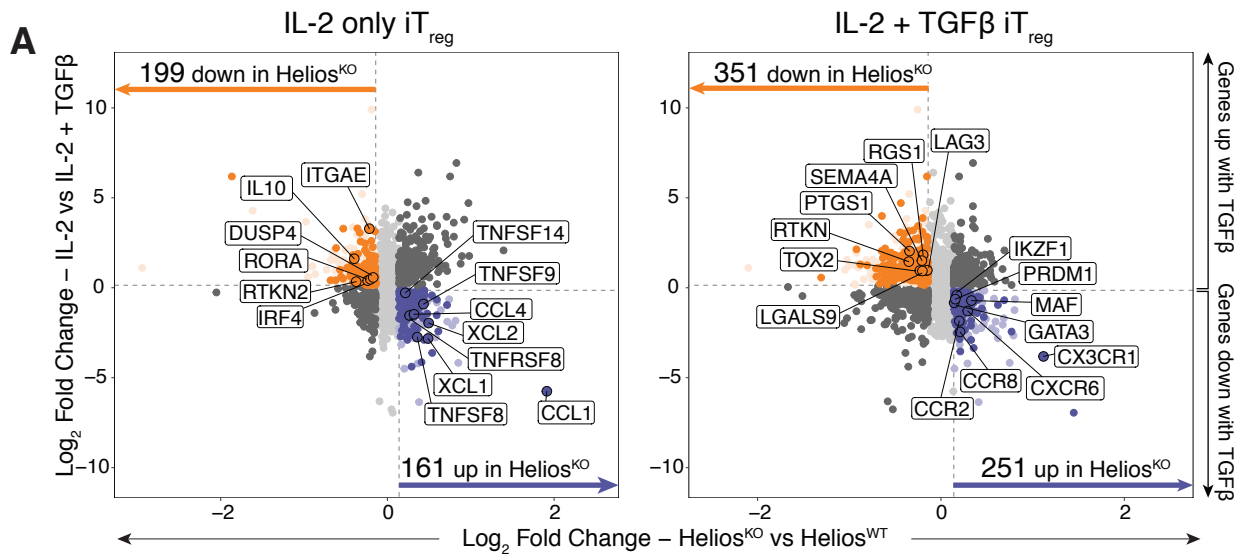


Figure 23. Ablation of Helios in fetal iT_{reg} results in downregulation of T_{reg}-specific genes, and the concurrent upregulation of pro-inflammatory genes.

CRISPR-Cas9 editing was carried out in fetal naïve T cells (n=6) with Helios gRNA1 (Helios^{KO}) or the non-targeting control guide (Helios^{WT}). Edited cells stimulated with αCD3/αCD28/αCD2 tetramers in the absence or presence of TGFβ for 6 days, after which changes in their overall transcriptome was assessed by RNAseq.

(A) Helios ablation results upregulation of pro-inflammatory genes and downregulation of genes associated with T_{reg} phenotype and function in parallel or addition to TGFβ signaling. Scatterplot plots log₂ fold change (log₂FC) values comparing the absence or presence of exogenous TGFβ during the differentiation process (y-axis) and Helios^{KO} against Helios^{WT} iT_{reg} (x-axis) that underwent differentiation in IL-2 alone (left, IL-2 only iT_{reg}) or with exogenous TGFβ added (right, IL-2 + TGFβ-iT_{reg}). Dotted lines in grey denote log₂FC cut-offs. Genes upregulated (dark purple) or downregulated (dark orange) in Helios^{KO} relative to Helios^{WT} iT_{reg} cells are colored (fold change, FC>1.1, false discovery rate, FDR<0.05). Genes associated with T_{reg} or pro-inflammatory immune functions are outlined and labeled.

(B) Helios controls the transcription of a core set of T_{reg}-specific genes across both stimulation conditions. Scatterplot plots are similar to **(A)** for IL-2 only iT_{reg} cells (left) and IL-2 + TGFβ-iT_{reg} cells (right). Shared genes meeting cutoffs (FC>1.1, FDR<0.05) that were upregulated (light purple) or downregulated (light orange) in Helios^{KO} relative to Helios^{WT} iT_{reg} cells are colored. Genes associated with T_{reg} or pro-inflammatory immune functions within the shared Helios-regulated transcriptome are outlined and labeled.

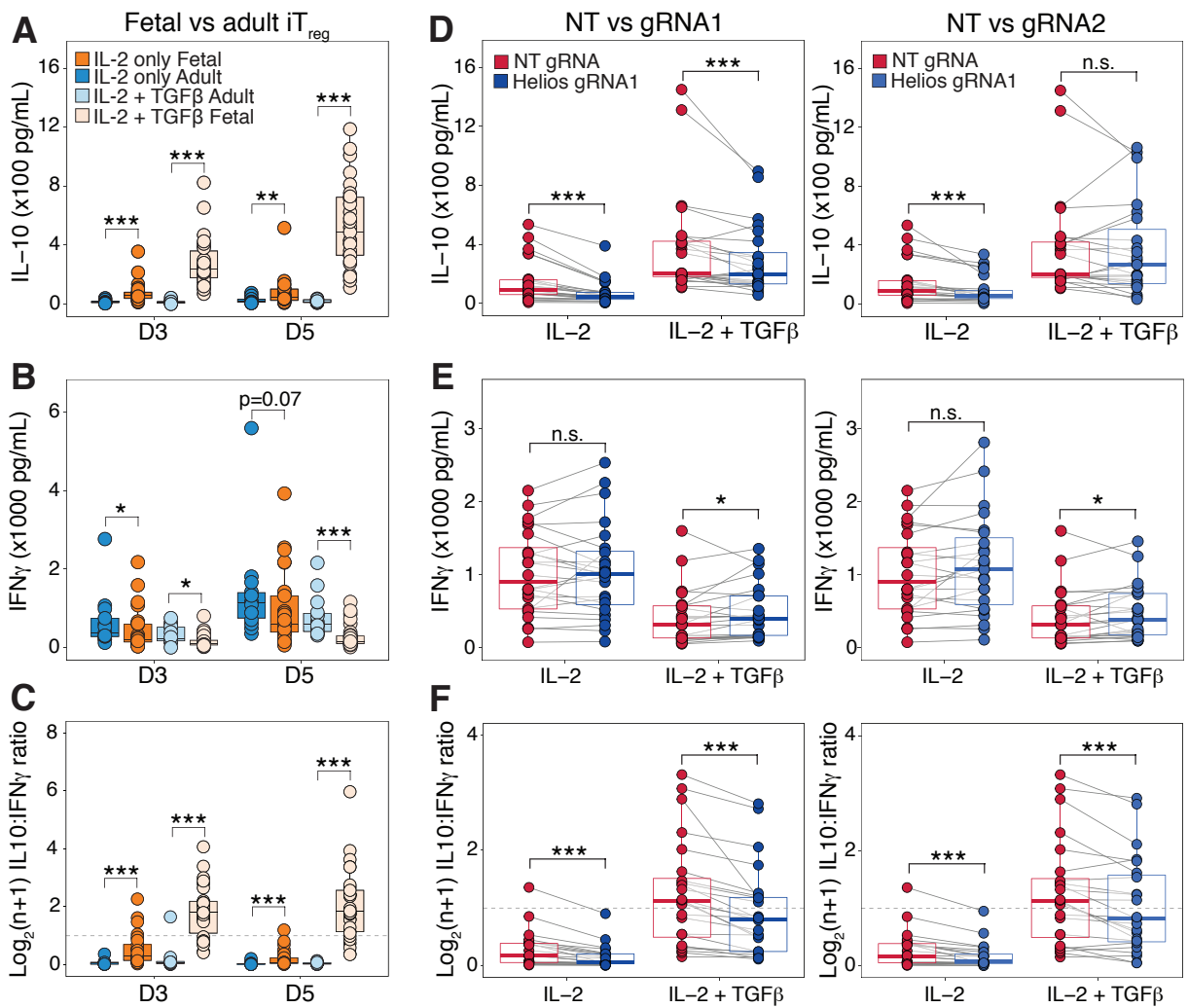


Figure 24. Fetal Helios knockout iT_{reg} cells have decreased IL-10 and increased IFN γ cytokine production.

(A) Fetal, but not adult iT_{reg} cells produce IL-10 during iT_{reg} differentiation. Boxplots quantify IL-10 cytokine concentration within culture supernatants collected at day 3 and 5 of differentiation for adult (blue, n=27) or fetal iT_{reg} cells (orange, n=58) differentiated in IL-2 alone (IL-2 iT_{reg}), as well as adult (light blue, n=27) or fetal (light orange, n=55) iT_{reg} cells differentiated with added TGF β (TGF β -iT_{reg}).

(B) Fetal iT_{reg} cells suppress IFN γ production over the course of iT_{reg} differentiation. Boxplots quantify IFN γ cytokine concentrations for samples as in **(A)**.

(C) Fetal TGF β -iT_{reg} cells produce more IL-10 than IFN γ . Boxplots show log₂(n+1) ratio of IL-10 to IFN γ cytokine concentration for samples as in **(A)**. Dotted line marks the ratio at which cells produce IL-10 and IFN γ at 1:1. All statistics for **(A,B,C)** calculated by unpaired two-sided Mann-Whitney test, *** p<0.001, ** p<0.01, *p<0.05.

(D) Helios ablation reduces IL-10 production by fetal IL-2-iT_{reg} cells. Boxplots quantify IL-10 cytokine concentrations at day 5 of differentiation for iT_{reg} cells that received the non-targeting guide (Helios^{WT}, red) or for Helios knockout (Helios^{KO}, blue) with gRNA1 (left, n=24) and gRNA2 (right, n=23).

(E) Helios ablation increases IFN γ production in fetal TGF β -iT_{reg} cells. Boxplots quantify IFN γ cytokine concentrations for samples in **(D)**.

(F) Helios ablation tips the balance from immunosuppressive IL-10 towards pro-inflammatory IFN γ production in fetal iT_{reg} cells. Boxplots show log₂(n+1) ratio of IL-10 to IFN γ cytokine concentration for samples as in **(D)**. Dotted line marks the ratio where cells produce IL-10 and IFN γ at 1:1. All statistics for **(D,E,F)** calculated by two-sided Wilcoxon signed-rank test, *** p<0.001, * p<0.05, n.s. p>0.05. All boxplots show median (centre line), interquartile range (box) and tenth and ninetieth percentiles (whiskers).

2.7 TABLES

Table 2.7.3. Statistics from GSEA testing

Fetal versus adult iT_{reg} cells differentiated in IL-2 alone								
GENESET NAME	SIZE	ES	NES	FDR q-val	LEADING EDGE	RANK AT MAX	NOM p-val	FWER p-val
GSE7460_TREG_VS_TCONV_ACT_UP	169	0.64	1.66	6.30E-03	tags=22%, list=7%, signal=23%	907	4.13E-04	6.00E-03
UP_IN_HUMAN_MTREG	142	0.64	1.64	4.52E-03	tags=50%, list=13%, signal=57%	1751	7.06E-04	8.50E-03
GSE7460_TREG_VS_TCONV_ACT_WITH_TGFB_UP	134	0.60	1.51	2.46E-02	tags=25%, list=9%, signal=27%	1205	8.89E-03	6.53E-02
UP_IN_HUMAN_NTREG	55	0.65	1.48	2.65E-02	tags=42%, list=7%, signal=45%	935	3.50E-02	9.38E-02
CLUSTER 1.2	108	0.62	1.54	2.84E-02	tags=27%, list=8%, signal=29%	1067	9.22E-03	3.73E-02
DOWN_IN_HUMAN_MTREG	152	-0.61	-1.78	5.62E-04	tags=33%, list=8%, signal=35%	1084	0.00E+00	9.00E-04
CLUSTER 1.3	50	-0.75	-1.86	0.00E+00	tags=38%, list=8%, signal=41%	1131	0.00E+00	0.00E+00
Fetal versus adult iT_{reg} cells differentiated in IL-2 and TGFβ								
GENESET NAME	SIZE	ES	NES	FDR q-val	LEADING EDGE	RANK AT MAX	FWER p-val	NOM p-val
UP_IN_HUMAN_NTREG	55	0.77	1.77	1.13E-03	tags=49%, list=8%, signal=53%	1122	1.10E-03	6.54E-04
UP_IN_HUMAN_MTREG	142	0.64	1.66	4.80E-03	tags=53%, list=13%, signal=60%	1737	9.90E-03	4.39E-04
GSE7460_TREG_VS_TCONV_ACT_UP	169	0.55	1.45	4.60E-02	tags=22%, list=7%, signal=24%	901	1.31E-01	1.51E-02
GENESET NAME	SIZE	ES	NES	FDR q-val	LEADING EDGE	RANK AT MAX	NOM p-val	FWER p-val
CLUSTER 1.2	108	0.62	1.55	2.54E-02	tags=29%, list=8%, signal=31%	1033	3.27E-02	8.55E-03

CLUSTER 1.1	114	0.58	1.47	3.21E-02	tags=33%, list=10%, signal=37%	1442	8.00E-02	2.37E-02
DOWN_IN_HUMAN_MTREG	152	-0.64	-1.85	6.16E-05	tags=41%, list=11%, signal=46%	1464	1.00E-04	0.00E+00
CLUSTER 1.3	50	-0.79	-1.93	2.38E-04	tags=38%, list=8%, signal=41%	1147	1.00E-04	2.52E-04
CLUSTER 1.4	52	-0.65	-1.61	5.37E-03	tags=33%, list=7%, signal=35%	901	7.60E-03	8.22E-03

Table 2.7.7 Top Shared superenhancers between adult naïve, adult T_{reg} and fetal naïve T cell

Cell Type	GeneID	enhancerRank	EnrichSignal
Adult Treg	FAM53B	1	90338.9016
Adult Treg	BCL11B	2	88642.2576
Adult Treg	RALGDS	3	64304.3212
Adult Treg	DAD1	4	63653.2075
Adult Treg	MYH9	5	60492.6471
Adult Treg	CCDC88C	6	60475.5936
Adult Treg	NCK2	7	59680.5552
Adult Treg	MIR4632	8	57337.7156
Adult Treg	HIVEP2	9	55030.746
Adult Treg	PHF19	10	54694.6618
Adult Treg	MIR3188	11	52317.5121
Adult Treg	MIR4316	12	52256.4735
Adult Treg	IRF1	13	51019.5564
Adult Treg	KLF13	14	49691.2472
Adult Treg	MOB3A	15	49002.3585
Adult Treg	SEMA4D	16	48454.0416
Adult Treg	ANKRD44	17	48299.398
Adult Treg	MIR29A	18	47766.4477
Adult Treg	RARA	19	47397.6506
Adult Treg	SKI	20	45210.7782
Adult Treg	RHOH	21	45002.461
Adult Treg	FAM107B	22	44423.1774
Adult Treg	ETS1	23	44146.8885
Adult Treg	RAPGEF1	24	43940.3737
Adult Treg	CELF2	25	43713.0204
Adult Naïve	BCL11B	1	63863.2072
Adult Naïve	HIVEP2	2	46193.8302
Adult Naïve	<i>ITPKB</i>	3	39119.603
Adult Naïve	CCR7	4	38740.2096
Adult Naïve	ETS1	5	35402.6181
Adult Naïve	KLF13	6	33468.4465
Adult Naïve	MIR4316	7	33431.275
Adult Naïve	DAD1	8	32912.275
Adult Naïve	MYH9	9	31014.6954
Adult Naïve	RHOH	10	29338.9504
Adult Naïve	<i>ADGRE5</i>	11	28999.8467
Adult Naïve	<i>CD247</i>	12	28462.6503
Adult Naïve	CRIP1	13	27972.432
Adult Naïve	<i>LEPROTL1</i>	14	27798.9002

Cell Type	GeneID	enhancerRank	EnrichSignal
Adult Naïve	MOB3A	15	27160.3896
Adult Naïve	KDM6B	16	26527.4289
Adult Naïve	CCDC88C	17	26451.0077
Adult Naïve	MIR3188	18	25147.0695
Adult Naïve	ZFP36L2	19	25009.6167
Adult Naïve	PER1	20	23827.7492
Adult Naïve	NCK2	21	23032.646
Adult Naïve	<i>TCF7</i>	22	22649.3449
Adult Naïve	<i>LRRFIP1</i>	23	22335.3472
Adult Naïve	PITPNC1	24	22171.8928
Adult Naïve	<i>NEAT1</i>	25	22154.526
Fetal Naïve	BCL11B	1	62343.7038
Fetal Naïve	ETS1	2	48234.8667
Fetal Naïve	KLF13	3	45096.9791
Fetal Naïve	<i>ITPKB</i>	4	44268.8808
Fetal Naïve	RHOH	5	42130.726
Fetal Naïve	MIR4316	6	41956.7058
Fetal Naïve	DAD1	7	39631.488
Fetal Naïve	MYH9	8	39038.6605
Fetal Naïve	CHIT1	9	37766.114
Fetal Naïve	<i>ADGRE5</i>	10	37329.1296
Fetal Naïve	<i>CD247</i>	11	37142.628
Fetal Naïve	<i>NEAT1</i>	12	35427.2636
Fetal Naïve	MIR4492	13	34963.1721
Fetal Naïve	BACH2	14	33860.3712
Fetal Naïve	PTPRC	15	32658.696
Fetal Naïve	KDM6B	16	32127.0662
Fetal Naïve	<i>LRRFIP1</i>	17	31812.7375
Fetal Naïve	<i>LEPROTL1</i>	18	31129.635
Fetal Naïve	<i>TCF7</i>	19	30975.966
Fetal Naïve	PLEC	20	29933.813
Fetal Naïve	SKI	21	29440.3344
Fetal Naïve	CYTIP	22	28938.1605
Fetal Naïve	RARA	23	28142.8194
Fetal Naïve	EVL	24	27667.328
Fetal Naïve	NCK2	25	27386.0205

Table 2.7.8 Experimental setup for T_{reg} induction time course carried out for adult and fetal naïve T cells.

Cell origin	Stimulation condition	Day	Number of biological replicates
Fetal	IL-2	1	8
	TGFβ	1	5
Adult	IL-2	1	7
	TGFβ	1	5
Fetal	IL-2	3	11
	TGFβ	3	7
Adult	IL-2	3	8
	TGFβ	3	6
Fetal	IL-2	5	5
	TGFβ	5	5
Adult	IL-2	5	7
	TGFβ	5	6

Table 2.7.9. Experimental setup for Helios CRISPR-Cas9 mediated editing for subsequent T_{reg} induction carried out for fetal naïve T cells.

Stimulation condition	Guide	Number of biological replicates
IL-2	Non-targeting	39
IL-2	gRNA1	38
IL-2	gRNA2	33
TGFβ	Non-targeting	36
TGFβ	gRNA1	36
TGFβ	gRNA2	32

CHAPTER 3 – MATERIALS AND METHODS

Material for this chapter was modified from a manuscript currently in revision:

Ng MSF, Roth TL, Mendoza VF, Marson A, Burt TD. Helios predisposes human fetal CD4⁺ naïve T cells towards regulatory T cell differentiation. 2019 (in revision)

3.1 Study design

The objective of this study was to determine the molecular mechanisms that underlie preferential T_{reg} cell differentiation in human fetal naïve T cells. As such, primary human CD4⁺ naïve T and T_{reg} cells from fetal spleen and adult peripheral blood mononuclear cells were the primary cell sources used for this study. Transcriptional and epigenetic profiling was carried out utilizing RNAseq, H3K27ac ChIPseq and ATACseq. Flow cytometry was utilized to confirm observations from sequencing datasets, to validate of expression levels at baseline, and to assess the activation and subsequent differentiation of fetal and adult naïve T cells in *in vitro* experiments. CRISPR-mediated knockout was used to confirm the results of the observational studies. The sample size (n = 2-6) for the sequencing datasets was determined to be the optimal size for statistical analysis and to allow for independent repeats, given the scarcity of tissue available for fetal samples. The sample size and experimental replicates for *in vitro* experiments are subsequently indicated all accompanying figure legends. Sample size was determined to be adequate based on the magnitude and consistency of measurable differences between groups. Investigators were not blinded, and samples were equally divided between treatments, i.e. gRNA received.

3.2 Cell isolation and purification

Fetal splenocytes were obtained under the auspices of the UCSF Committee on Human Research (CHR) at 18-23 gestational weeks from the Department of Obstetrics, Gynecology and Reproductive Science, San Francisco General Hospital. Global consent for research was obtained by medical providers, medical information abstracted, and any Personal Health Information removed prior to any contact with researchers. Samples were transported in media on ice and processed within 2-3 hours after collection. Tissue was mechanically dispersed and digested with 3mg/ml Collagenase IV (Life Technologies) and 1mg/ml DNase (Roche) in RPMI-

1640 supplemented with 10% HI-FBS (heat inactivated fetal bovine serum), 300mg/mL L-glutamine, 10U/mL Penicillin, and 10ug/mL Streptomycin (supplemented RPMI) for 30 minutes in shaking water bath. Single cell suspensions were created by passage through a 70uM filter, and the lymphocyte fraction was isolated by density centrifugation of a Ficoll-Hypaque gradient (Amersham Biosciences). Residues from TRIMA Apheresis collection kits were obtained from the Blood Centers of the Pacific (San Francisco, CA), and adult peripheral blood mononuclear cells (PBMCs) were similarly isolated by density centrifugation. All samples were either utilized immediately post isolation or viably cryopreserved prior to use. No difference in function or phenotype was detected in samples before and after cryopreservation.

3.3 Magnetic isolation of CD4⁺ T cells and fluorescence activated cell sorting (FACS) for sequencing and cell culture

Prior to FACS, fetal splenocytes and adult PBMCs were pre-enriched for CD4⁺ T cells using the EasySep Human CD4⁺ T cell isolation kit (#17952, Stemcell Technologies) according to the manufacturer's instructions. In order to obtain sufficient numbers of adult regulatory T (T_{reg}) cells for epigenetic analyses, adult PBMCs were also pre-enriched for CD4⁺CD127^{lo} T cells using the Human CD4⁺CD127^{lo} T cell Pre-enrichment kit (#19231, Stemcell Technologies). Enriched cell fractions were then incubated in FACS staining buffer (Phosphate buffered saline, PBS, with 2% HI-FBS and 2mM EDTA) with flurochrome-conjugated anti-human surface monoclonal antibodies (mAbs). Antibodies used include: CD25 FITC (2A3, BD Biosciences), CD127 PE/BV421 (hIL-7R-M21, BD Pharmingen), CD45RA PE-CF594 (HI100, BD Horizon), CD4 PE-Cy7 (SK3, BD Pharmingen), CD27 eFluor780 (O323, ThermoFisher Scientific). All cells were stained with the live-dead marker (GhostDye Violet 510; Tonbo Biosciences) to exclude dead cells. Cells were sorted into supplemented RPMI (10% HI-FBS, 300mg/mL L-glutamine, 10U/mL

Penicillin, and 10ug/mL Streptomycin) based on gating in Supplementary Figure 1. All cells were sorted on a BD FACS Aria III.

3.4 RNA sequencing for *ex vivo* sorted cells

RNAseq was carried out for 4 biological replicates of adult and fetal naïve and T_{reg} cells, with 2.5x10⁵ cells per sample. RNA was extracted and purified with the Nucleospin RNA kit (Machery-Nagel) and assessed for quality by RNA Pico (Agilent Technologies). Library preparation and sequencing on a HiSeq300 were carried out by the Technology Center for Genomics and Bioinformatics (TCGB) core at University of California, Los Angeles. 50bp single-end reads were aligned to hg19 using Bowtie2, and read counts per gene were obtained using RSEM. The EdgeR package for Bioconductor (113, 114) was utilized to perform TMM normalization and differential expression analysis of samples, with each pairwise comparison performed. TMM normalized reads were pre-filtered prior to PCA analysis, where genes with read counts less than one in three or more replicates of all cell types were removed from analysis. PCA analysis was carried out in R using the prcomp function on log₂(n+1) transformed TMM normalized reads. Differentially expressed genes were identified from pairwise comparisons between all four populations as meeting the following cutoffs: false discovery rate (FDR) <0.05 and log₂ fold change (log₂FC) >1.5. The T_{reg} transcriptional signature is defined from the intersection of genes meeting the cutoffs above with increased/decreased transcription in pairwise comparisons of adult and fetal T_{reg} populations against adult naïve T cells.

3.5 RNA sequencing for adult and fetal induced T_{reg} populations

4 biological replicates of sorted adult or fetal naïve T cells were stimulated in U-bottomed 96 wells with 5ul of Immunocult Human T cell Activator (CD3/CD28/CD2 tetramers, Stemcell Technologies) in 200ul of culture media (RPMI-1640 supplemented with 10% HI-FBS (heat

inactivated fetal bovine serum), 300mg/mL L-glutamine, 10U/mL Penicillin, and 10ug/mL Streptomycin, 10mM HEPES, 1X MEM-NEAA, β -mercaptoethanol). Exogenous IL-2 (10ng/ml, Peprotech) and TGF β (50ng/ml, Peprotech) were added according to the relevant experimental setup. 100ul media changes were performed every two days starting from the first day of stimulation. At day 6 post-induction, RNA from 2.5×10^4 iT_{reg} cells was extracted and purified with the Nucleospin XS RNA kit (Machery-Nagel) and assessed for quality by RNA Pico (Agilent Technologies). Ribosomal RNA was removed using the NEBNext[®] Poly(A) mRNA Magnetic Isolation Module (New England Biolabs), and library preparation was carried out using the NEBNext[®] Ultra[™] II Directional RNA Library Prep Kit for Illumina[®] (New England Biolabs). Sequencing on a HiSeq4000 was carried out by the Center for Advanced Technology core at University of California, San Francisco. 50bp single-end reads were aligned to hg19 using Bowtie2, and read counts per gene were obtained using RSEM. The EdgeR package (v3.24.3) for Bioconductor (113, 114) was utilized to perform TMM normalization and differential expression analysis of samples. Due to the multifactorial experimental design, a generalized linear model (gLM) design was specified:

$$\sim \text{Stimulation} + \text{Celltype} + \text{Stimulation}:\text{Celltype}$$

This allowed for the assessment of the effect of stimulation condition (Stimulation: IL-2, IL-2 + TGF β), cell origin (Celltype: Adult or Fetal) and any possible interaction between the two factors. Negative binomial dispersion was estimated using the design specified, and genewise gLM was fit before likelihood ratio tests (LRTs) were utilized to determine differentially expressed genes. Differentially expressed genes were defined by $\text{FDR} < 0.05$ $\log_2 F > 1.5$. For PCA analysis, \log_2 TMM normalized reads were obtained with a prior count of 5. Reads were pre-filtered, where genes with read counts less than one in three or more replicates of all cell types were removed from analysis. PCA analysis was carried out in R using the prcomp function.

3.6 Gene set enrichment analysis (GSEA) for pairwise fetal versus adult iT_{reg} comparisons

GSEA was carried out using the javaGSEA program (v2.0.9) using the pre-ranked option with default parameters. Pre-ranked genelists were generated separately for fetal versus adult iT_{reg} comparisons that were differentiated with IL-2 only, or with added exogenous TGFβ. Genes were ranked by $-\log_{10}(\text{FDR})$ multiplied by the sign of the corresponding $\log_2\text{FC}$ to determine directionality. Four genesets: GSE7460_TREG_VS_TCONV_ACT_DN, GSE7460_TREG_VS_TCONV_ACT_UP, GSE7460_TREG_VS_TCONV_ACT_WITH_TGFB_DN, and GSE7460_TREG_VS_TCONV_ACT_WITH_TGFB_UP were obtained from the Molecular Signatures Database (MSigDB) from the C7 immunologic gene sets collection [cite Hill and MSigDB here]. Another four genesets were derived from microarrays (accession GSE76598) performed on CD4⁺CD4RA⁺ naïve and CD4⁺CD45RA⁻ memory human CD25⁻ conventional and CD25^{hi} T_{reg} cells activated for 40 hours with αCD3/αCD28 coated beads [cite Pensnacker et al.]. GEO2R (NCBI) was utilized to return associated FDR and adjusted p-values associated with all genes, and genesets used for GSEA were created by filtering genes by FDR<0.05 and $\log_2\text{FC}>1.5$ in both directions. Lastly, another four gene sets were defined from *k*-means clustering analysis on the T_{reg} transcriptional signature defined from *ex vivo* sorted human fetal and adult naïve and T_{reg} cells as detailed above. Normalized enrichment scores (NES) were used to compare between genesets. GSEA result outputs were plotted in R using the ReplotGSEA package [cite].

3.7 Assay for transposase-accessible chromatin (ATACseq)

ATACseq was performed as previously described (115, 116), for adult naïve, adult T_{reg} and fetal naïve T cells. Fetal T_{reg} cells were unable to be subjected to this assay due to limitation of cell

numbers. 5×10^4 sorted cells per sample were transposed with sequencing adapters using the Nextera DNA Library Prep kit (Illumina), and transposed chromatin purified with the MinElute PCR Purification Kit (Qiagen). Amplification cycles were first determined by quantitative PCR as described, and subsequently used to amplify prepared libraries using NEBNext High Fidelity 2X PCR Master Mix (New England Biolabs). Amplified libraries were then purified with the MinElute PCR Purification Kit (Qiagen). Sequencing was carried out on a HiSeq2500 (Institute for Human Genetics, UCSF). Sequence reads (25bp, paired-end) were mapped to hg19 using Bowtie2, and subsequently filtered for unique mappability ($\text{mapq} \geq 30$). For the generation of Bigwig files, tag densities were calculated as the number of tags that map to within 75bp of each 20bp genomic bin. Tag insertion positions were calculated as +4bp from the upstream end of positive strand tags and -5 bp from negative strand tags. Blacklist regions were also removed using known regions from the ENCODE consortium using the bedtools `–overlap` function. Regions with tag density greater than 40 were identified as accessible regions.

3.8 H3K27ac chromatin immunoprecipitation sequencing (ChIPseq)

A modified protocol adapted from Collas et al. (117) and the truChIP protocol (Covaris) was utilized for 5×10^5 sorted cells per sample for adult naïve, adult T_{reg} and fetal naïve T cells. Fetal T_{reg} cells were unable to be subjected to this assay due to limitation of cell numbers. Cells were counted and washed in 500ul of cold PBS buffer. Cross-linking, quenching and lysis were performed with the truChIP Chromatin Shearing Kit with Formaldehyde (Covaris) according to manufacturer's instructions, with the addition of protease inhibitor cocktails and 20mM sodium butyrate (Sigma-Aldrich) to all buffers. Sonication was carried out with an AFA-Focused Covaris S2 ultrasonicator in AFA microtubes (Covaris) for 6 minutes (duty cycle 10%, intensity 5, cycle-burst 200). Samples were subsequently diluted up to 1ml in RIPA buffer (10mM Tris-HCl pH 7.5, 140mM NaCl, 1mM EDTA, 1% Triton-X, 0.01% SDS, 0.1% Na-deoxycholate, 1X protease

inhibitors, 20mM sodium butyrate), and 100ul was set aside for the input control. For H3K27ac ChIP, 5ug of α H3K27ac rabbit pAb (ab4729, Abcam) was incubated for 2 hours at 4°C with an equal mix of protein A and protein G beads. Antibody-bound beads were then washed twice with RIPA buffer. 900ul of sonicated chromatin was then added, and incubated overnight at 4°C on a rotator to maximize immunoprecipitation. Beads with bound chromatin were then sequentially washed in 1ml of the following buffers (with 1X protease inhibitors and 20mM sodium butyrate added for all buffers) for 5mins on the rotator at 4°C with: (1) Low-salt buffer (0.1% SDS, 1% Triton-X, 2mM EDTA, 20mM Tris-HCl, 150mM NaCl), (2) LiCl buffer (0.25M LiCl, 1% NP-40, 1% Na-deoxycholate, 1mM EDTA, 1mM Tris-HCl), (3) TE buffer (10mM Tris-HCl and 1mM EDTA). Input samples were similarly incubated overnight without antibody-bound beads and left on ice while beads were washed, and therefore treated similar to immunoprecipitation samples from this step onwards. All samples were treated with RNase A (Sigma-Aldrich) at a final concentration of 3ug/ml at 37°C for 30 minutes. De-crosslinking and Proteinase K digestion were carried out simultaneously in elution buffer (20mM Tris-HCl, pH 7.5, 5mM EDTA, 50mM NaCl, 1% SDS, 20mM sodium-butyrate, 50ug/ml Proteinase K) for 65°C for 3 hours on a Thermomixer heatblock (Eppendorf) at 1300RPM. Immunoprecipitated chromatin was eluted into 500ul of elution buffer, and mixed with 500ul phenol-chloroform-isoamylalcohol, and separated by spinning down at 12,000g for 15minutes at room temperature. The aqueous layer was removed (about 450ul), mixed with an equal amount of isopropanol, 50ul of 3.0M pH 5.2 sodium acetate and 5ul of GlycoBlue coprecipitant (ThermoFisherScientific) and mixed well by vortexing. Samples were incubated at -20°C overnight to precipitate DNA. Tubes were then thawed briefly on the counter, and spun down at maximum speed for 25 minutes at 4°C to pellet DNA. DNA was washed with 70% ethanol twice, and pelleted at maximum speed, 10 minutes, 4°C. The DNA pellet was resuspended in 50ul of TE buffer, and further purified with a MinElute PCR purification kit (Qiagen), and eluted into 16ul of elution buffer. DNA was quantified, and an

equal amount of DNA for both input and immunoprecipitated samples were used for library preparation through the sequential steps of end repair (End-It DNA End-Repair Kit, Epicentre Biotechnologies), A-base addition (New England Biolabs), and adaptor ligation with T4 DNA ligase (Enzymatics, Qiagen). Libraries were purified with AMPure XP Beads (Beckman Coulter), subjected to 5 cycles of amplification to convert Y shaped adapters to DNA, and size-selected for 200bp-500bp fragments using the E-gel Size-Select system (Invitrogen). Size-selected libraries were then amplified for another 5 cycles, purified with AMPure beads to remove adapter dimers, and assessed for purity on the Bioanalyzer. Equal amounts of barcoded libraries were pooled and sequenced on a HiSeq4000.

Short reads (50bp, single end) were aligned to hg19 using Bowtie2 with the following conditions: -p 10 -q -D 15 -R 10 -L 22 -i S,1,1.15, after adapter removal with fastq-mcf. Reads were filtered for mapq \geq 30, and deduplicated, sorted and indexed with samtools. To generate bigwig files, tag density was first calculated by determining the midpoint of tags, and mapping them to within 75 bp of each 20bp genomic bin for both input and immunoprecipitated samples. Blacklist regions were also removed using known regions from the ENCODE consortium using the bedtools –overlap function. Tag counts were normalized to library size, and input counts were subtracted before conversion into the bigwig format for viewing in IGV browser.

3.9 Identification of superenhancers (SEs) and transcriptional enhancers (TE) and comparison of enhancers with DESeq2

To identify H3K27ac peaks, we utilized MACS2 with the callpeak option, specifying the matched input sample as the control, and setting $q < 0.01$. Peaks within 2kb of transcriptional start sites were removed, and peaks subsequently within 12.5kb of each other were stitched using the

ROSE algorithm (79, 80). Cumulative H3K27ac signal was determined for the stitched enhancers and ranked by H3K27ac signal strength in ascending order. When stitched enhancer rank and H3K27ac signal were plotted in a linear scatter plot and both axes scaled from 0 to 1, the point where the tangent of the curve is 1 was used as the cutoff for SEs and TEs. This was carried out for all biological replicates in each sample, and enhancers intersecting in all biological replicates were kept as representative enhancers for each sample type.

In order to carry out principal component analyses and differential analysis, stitched enhancers across each sample type were merged into a masterlist using the `bedops -merge` function. Reads from both H3K27ac ChIPseq and ATACseq were then separately mapped to this masterlist with all stitched enhancers and utilized for DESeq2 analysis (v1.22.2) (118). To identify enhancers with statistically differences in signal intensities both sequencing datasets, data was normalized in DESeq2, before pairwise comparisons between all three populations were carried out. Differentially enriched SEs or TEs with $FDR < 0.05$, \log_2 fold change > 0.5 (fold change > 1.5) were defined as cell-type specific regions and the rest categorized as common shared regions. Associated genes falling 3kb upstream or downstream were assigned to peak regions using the `ChIPseeker` package in R. Principal component analysis was carried out using the `plotPCA` function in DESeq2. Shared T_{reg} -accessible enhancers were identified from pairwise comparisons of adult naïve against adult T_{reg} samples that meet the cut-offs of $FDR < 0.05$, fold change (FC) < -1.5 in both H3K27ac ChIPseq and ATACseq datasets. Shared T_{reg} -inaccessible enhancers were similarly identified with $FC > 1.5$. DESeq2 normalized reads mapping to shared enhancers were then utilized for plotting and statistical analysis.

3.10 Motif analysis for differentially expressed ATAC and H3K27ac peaks

ATAC peaks were identified using MACS2 with the callpeak option and the following parameters: -f BAM --nomodel --shift 100 --extsize 200 -q .05. In order to make peaks comparable across all samples for differential enrichment analysis, peaks were merged across all samples using bedtools –merge function with the following parameters: -o distinct -d 100. Blacklist regions were also removed using known regions from the ENCODE consortium using the bedtools –overlap function. A similar merged peaklist was derived from H3K27ac peaks called by MACS2 as defined above. To identify peaks with statistically differences in signal intensities both sequencing datasets, data was normalized in DESeq2, before pairwise comparisons between all three populations were carried out. Differentially enriched peaks $FDR < 0.05$, \log_2 fold change > 1.5 were defined as cell-type specific peaks and the rest categorized as common shared peaks. Associated genes falling 3kb upstream or downstream were assigned to peak regions using the ChIPseeker package in R. T_{reg} -accessible peaks were identified from pairwise comparisons of adult naïve against adult T_{reg} samples that meet the cutoffs of $FDR < 0.05$, $\log_2 FC > 1.5$ separately for H3K27ac ChIPseq and ATACseq datasets. T_{reg} -accessible peaks shared with fetal naïve T cells were defined as peaks that met the same FDR and FC cutoffs in the same directionality for adult naïve against fetal naïve T cell pairwise comparisons. Given the paucity of shared T_{reg} -accessible peaks within the H3K27ac ChIPseq dataset, motif analysis was carried out on T_{reg} -accessible peaks within the ATACseq dataset. Motif analysis was carried out using HOMER (Hypergeometric Optimization of Motif EnRichment) [cite] using findMotifsGenome.pl with –size 150. *De novo* motifs identified were replotted for publication quality in R using the ggseqlogo package[cite]. FOXP3 binding sites were obtained from a previously published FOXP3 ChIPseq dataset (GSE43119, [cite]). Overlap of FOXP3 binding sites with shared T_{reg} -accessible peaks from both ATAC and H3K27ac

ChIPseq datasets within fetal naïve T cells was determined using bedtools –intersect with an overlap of at least 75%.

3.11 Flow cytometry staining for Helios and activation markers in sorted naïve and T_{reg} cells

Sorted naïve and T_{reg} cells from fetal and adult naïve T cells were incubated in FACS buffer with fluorochrome-conjugated, anti-human surface mAbs. Fixation and permeabilization was performed using the Foxp3/Transcription Factor Staining Buffer set (Tonbo Biosciences) according to manufacturer's instructions. Antibodies used include: CD25 FITC (2A3, BD Biosciences), Helios PE (22F6, Biolegend), FOXP3 PE (PCH101, ThermoFisher Scientific), CD31 PE (WM59, BD Biosciences), IgG1 kappa Isotype Control, PE (MOPC-21, BD Biosciences), CTLA4 PE-CF594 (BNI3, BD Biosciences), CCR4 PE-Cy7 (1G1, BD Biosciences), Ki-67 PE-Cy7 (B56, BD Biosciences), CD69 Alexa Fluor® 700 (FN50, Biolegend), FOXP3 eFluor660 (PCH101, ThermoFisher Scientific), Eos eFluor660 (ESB7C2, ThermoFisher Scientific), IgG2a kappa Isotype Control, eFluor660 (eBR2a, ThermoFisher Scientific) and CD4 APC-H7 (L200, BD Biosciences). All cells were stained with a live/dead marker (GhostDye Violet 510; Tonbo Biosciences) to exclude dead cells from analysis. All data were acquired with an LSRII flow cytometer (BD Biosciences) and analyzed with FlowJo (TreeStar) software. Helios⁺ and Helios⁻ gates were set based on the clearly positive and negative populations seen in adult T_{reg} samples. Using this definition, all adult naïve T cell samples were observed to be fully within the Helios⁻ population, and were subsequently used to define the Helios⁻ gate for subsequent experiments as a biological negative control.

3.12 T_{reg} induction assays

Sorted adult or fetal naïve T cells were differentiated into T_{reg} cells as detailed above with α CD3/ α CD28/ α CD2 tetramers (Stemcell Technologies) in the presence of exogenous IL-2 (10ng/ml, Peprotech) and TGF β (50ng/ml, Peprotech) according to the relevant experimental setup. For T_{reg} induction in the presence of TGF β blocking, 2.5 μ g/ml or 0.5 μ g/ml of neutralizing α TGF β (1D11, R&D Biosystems) antibody was added to the culture medium where specified. Cells were cultured and harvested after 1, 3 and 5 days for analysis by flow cytometry. 100ul media changes were performed every two days starting from the first day of stimulation. Cells were stained, fixed and permeabilized as detailed above in flow cytometry staining. Additional antibodies used in analysis include: GARP PE-Cy7 (7B11, Biolegend), LAP BV421 (TW4-2F8, Biolegend), GITR BV421(108-17, Biolegend). All data were acquired with an LSRII flow cytometer (BD Biosciences) and analyzed with FlowJo (TreeStar) software.

3.13 Methylation analysis of Treg-specific demethylated region (TSDR) in *FOXP3* conserved non-coding sequence 2 (CNS2)

Methylation analysis of the *FOXP3* CNS2 TSDR was carried out for *ex vivo* sorted adult naïve (n=4), fetal naïve (n=5), adult T_{reg} (n=4) and fetal T_{reg} (n=5) cells using the sort strategy defined in Supplementary Figure 1. iT_{reg} populations were differentiated from fetal and adult naïve T cells, where they were harvested at Day 5 of differentiation, stained, fixed and permeabilized for FOXP3 and Helios staining as specified above. iT_{reg} populations were sorted for FOXP3⁻, Helios⁻, FOXP3⁺ and Helios⁺FOXP3⁺ populations where relevant, as defined in Supplementary Figure 11. All donors used for this analysis were confirmed to be male. To maintain parity across the whole analysis, *ex vivo* sorted naïve and T_{reg} cells were also fixed and permeabilized before DNA extraction. DNA extraction for all fixed and permeabilized samples was carried out with a modified phenol-chloroform-isoamylalcohol extraction protocol. Briefly, 0.1x10⁶ sorted cells were

resuspended in 400ul of lysis buffer (0.5% SDS, 50 mM Tris, pH 8, 10 mM EDTA), with the additional of 16ul 5M NaCl, and de-crosslinked overnight at 66°C in a heatblock. Elution was carried out the presence of RNaseA (10mg/ml, Sigma Aldrich) at 37°C for 1hr, before the addition of Proteinase K (20mg/ml, Sigma Aldrich) and further incubation at 45°C for another hour. Samples were then transferred into Phase Lock Gel tubes (Quanta Bio), and an equal amount of phenol-chloroform-isoamylalcohol was added. Tubes were inverted vigorously to mix, and centrifuged at maximum speed for 5 minutes. The aqueous layer was removed, mixed with an equal amount of isopropanol, 50ul of 3.0M pH 5.2 sodium acetate and 5ul of GlycoBlue coprecipitant (ThermoFisherScientific) and mixed well by vortexing. Samples were incubated at -80°C for 30 minutes, and then spun down at maximum speed for 30 minutes to precipitate DNA. The DNA pellet was carefully washed with 75% freshly prepared ethanol, and dried before resuspension in nuclease-free water for analysis. Methylation analysis was conducted by EpigenDx for human *FOXP3* (ADS783-FS2).

3.14 CRISPR-Cas9 editing reagents

Single guide RNAs (gRNAs) were designed against exons in the Helios locus (*IKZF2*, NM_01620 transcript) using the online CHOPCHOPv2 webtool (119). Two independent gRNAs were selected – *GGAGGAATCCGGCTTCCGAA* (gRNA1, targets exon 4), *GATACTACCAAGGCTCCTAA* (gRNA2, targets exon 8). crRNAs for each sequence and associated tracrRNA were chemically synthesized (Dharmacon), and were resuspended in 150 mM KCl, 10 mM Tris pH 7.4 to generate 160uM stocks. A scrambled guide, *GGTTCTTGACTACCGTAATT* (NT) was also synthesized. A HDR template (HDRT) was also utilized to increase nucleofection efficiency (120). Synthesized HDRT (Dharmacon) was resuspended in 150 mM KCl, 10 mM Tris pH 7.4 to a concentration of 100uM. Purified Cas9-

NLS at a concentration of 40uM, and stored in 20mM HEPES-KOH pH 7.5, 150mM KCl, 10% glycerol, 1mM DTT was obtained from Berkeley QB3 Macrolabs.

3.15 CRISPR-Cas9 editing of the *Helios* locus

CRISPR-Cas9 editing was carried out as previously detailed (121, 122). Cas9 gRNA ribonucleoproteins (RNPs) were assembled before experiments by assembling the gRNAs through incubating 160uM of crRNA with 160uM of tracrRNA (Dharmacon) at a 1:1 ratio for 30 minutes at 37°C to a final concentration of 80uM. Assembled gRNAs are then subsequently incubated with 40uM of Cas9-NLS at a 1:1 ratio for 15 minutes at 37°C for a final concentration of 20uM RNPs. Nucleofection was performed using the Amaxa P3 Primary Cell 96-well Nucleofector kit and 4D-Nucleofector (Lonza). 1×10^5 sorted fetal naïve T cells per well were stimulated overnight in 96-well plates pre-coated with anti-CD3 antibodies (1ug/mL, HIT3a, BD Biosciences), and supplemented with soluble anti-CD28 antibodies (2ug/mL, CD28.2, BD Biosciences) and IL-2 (10ng/ml, Peprotech). Stimulated fetal naïve T cells were washed with PBS, and resuspended in 20ul of P3 solution. 5ul of the final 20uM RNP solution was added, along with 1ul of 100uM HDRT solution. Cells were gently mixed, and transferred to the 96-well shuttle device. Cells were electroporated using program EH-115 on the Amaxa 4D-Nucleofector (Lonza). 80ul of prewarmed culture media was added immediately post-nucleofection, and cells were allowed to recover for 15 minutes at 37°C. Nucleofected cells were then transferred into a 96-well U-bottom plate, and additional culture media added to a final volume of 200ul. After 5 hours, cells were spun down and 150ul of the culture media changed to increase cell viability and left to incubate overnight.

Cells were stimulated the next day for T_{reg} induction assays as detailed above, and harvested at Day 6 for analysis. Cells were fixed, permeabilized and stained with the following antibodies:

CD25 FITC (2A3, BD Biosciences), Helios PE (22F6, Biolegend), CTLA-4 (BNI3, BD Pharmingen), FOXP3 eFluor660 (PCH101, ThermoFisher Scientific) and CD4 APC-H7/BV650 (L200, BD Biosciences). All cells were stained with a live/dead marker (GhostDye Violet 510; Tonbo Biosciences) to exclude dead cells from analysis. All data were acquired with an LSRII flow cytometer (BD Biosciences) and analyzed with FlowJo (TreeStar) software.

Cells treated with NT and gRNA1/2 were reserved from some samples for DNA isolation to confirm editing at the Helios locus with Helios gRNAs. Up to 1×10^4 cells were resuspended in 30ul of DNA QuickExtract solution. PCR primers spanning the predicted edited region were designed for each guide: 1) gRNA1_Forward: TCTCTTGCCCTGTTTCAGAAGCA, 2) gRNA1_Reverse: ACCACTGCCACCCCTGAATAAA, 3) gRNA2_Forward: TGCCTGGATTCCACTGACTCAG, 4) gRNA2_Reverse: AAGGCCTAGTGGAAATGTGTGCT. PCR was carried out using the Kapa HiFi PCR kit (Roche) according to manufacturer's instructions. PCR amplicons were purified with MinElue PCR Purification kit (Qiagen) and Sanger sequencing carried out by MCLAB. Tracking of Indels by Decomposition (TIDE) online webtool (<https://tide.deskgen.com>) was utilized to align and compare sequences from the non-edited sample against gRNA1/2-edited samples. Sequences were also visually checked using the ApE editor to assess for sequence aberrations occurring immediately after the predicted cut site.

3.16 RNA sequencing for Helios^{KO} and Helios^{WT} T_{reg} populations

CRISPR-Cas9 mediated Helios knockout in 6 biological replicates of fetal naïve T cells was performed as described above using Helios gRNA1 or the NT control guide for (all samples were all paired across nucleofection conditions). Cells were stimulated the next day for T_{reg} induction assays as detailed above, and harvested at Day 6 for RNA extraction and analysis.

RNA was extracted from 2.5×10^4 iT_{reg} cells and purified with the Nucleospin XS RNA kit (Machery-Nagel) and assessed for quality by RNA Pico (Agilent Technologies). Ribosomal RNA was removed using the NEBNext[®] Poly(A) mRNA Magnetic Isolation Module (New England Biolabs), and library preparation was carried out using the NEBNext[®] Ultra™ II Directional RNA Library Prep Kit for Illumina[®]. Sequencing on a HiSeq4000 was carried out by the Center for Advanced core at University of California, San Francisco. 50bp single-end reads were aligned to hg19 using Bowtie2, and read counts per gene were obtained using RSEM. The EdgeR package for Bioconductor (113, 114) was utilized to perform TMM normalization and differential expression analysis of samples. Due to the multifactorial experimental design, a generalized linear model (gLM) design was specified:

~Donor+Stimulation+Genotype+Stimulation:Genotype

A blocking factor, Donor was added to adjust for differences between biological replicates taking into account the paired design. The design allowed for the assessment of the effect of stimulation condition (Stimulation: IL-2, IL-2 + TGFβ), whether Helios knockout was carried out (Genotype: Knockout, KO or wildtype, WT) and any possible interaction between the two factors. Negative binomial dispersion was estimated using the design specified, and genewise gLM was fit before likelihood ratio tests (LRTs) were utilized to determine differentially expressed genes. Given the low signal to noise ratio, we utilized a less stringent cut off to define differentially expressed genes as false discovery rate <0.05 and fold change>1.1 (FC). PCA analysis was carried out as detailed above. Three dimensional PCA plotting was carried out using the plotly package (v4.8.0).

3.17 T cell restimulation and intracellular cytokine staining

To assess IL-2 secretion after differentiation, fetal iT_{reg} were re-stimulated with 1 μg/ml Phorbol 12-Myristate 13-Acetate (PMA, Santa Cruz Biotechnology), 1 μg/ml ionomycin (EMD Millipore),

and 10ug/ml Brefeldin A (Sigma Aldrich) for 5 hours. Fetal iT_{reg} were assessed at day 5 post stimulation; for cells which had previously undergone CRISPR-mediated editing, cells were analysed at D6. Unstimulated cells were used for gating controls. For analysis by flow cytometry, cells were washed, and then stained, fixed and permeabilized as described above. Antibodies used for staining were: CD25 FITC (2A3, BD Biosciences), Helios PE (22F6, Biolegend), IL-2 PE/Dazzle™594 (MQ1-17H12, Biolegend), FOXP3 eFluor660 (PCH101, ThermoFisher Scientific), CD4 APC-H7 (L200, BD Biosciences). All cells were stained with a live/dead marker (GhostDye Violet 510; Tonbo Biosciences).

3.18 Cytokine bead assays

100ul of culture supernatant were collected at D3 and D5 of T_{reg} differentiation with IL-2 only or in the presence of added TGFβ. Supernatants collected at D5 of T_{reg} differentiation after CRISPR-Cas9 mediated Helios knockout were also analyzed. Supernatants were harvested and stored at -80°C prior to analysis. IL-10 (#558274) and IFNγ (#558269) concentrations were measured using the Cytokine Bead Assay (CBA) Flex kits (BD Biosciences) according to manufacturer's instructions.

3.19 Statistical analyses

All statistical analyses were performed using R (cran.r-project.org, v3.5.2) and Bioconductor (www.bioconductor.org). Tests were specified with each experiment, p<0.05 level of confidence was accepted for statistical significance. Kruskal-Wallis test and Dunn's post-test with Bonferroni correction was performed using the PMCMRplus (v1.4.1) package. Graphs were made using the ggplot2 (v3.1.0), ggrepel (v0.8.0) and cowplot (v0.9.4) R packages. Heatmaps were generated with the ComplexHeatmap (v1.12.0) R package.

3.20 Sequencing data availability

ATACseq, H3K27ac ChIPseq and RNAseq raw and processed files are deposited in the Gene Expression Omnibus database under a superseries entry with the accession number GSE110472 (<https://www.ncbi.nlm.nih.gov/geo/query/acc.cgi?acc=GSE110472>).

CHAPTER 4 – FUTURE DIRECTIONS

4.1 Evaluating the transition from a pro-tolerance immune system *in utero* towards sterilizing immunity in adulthood

We show here that fetal naïve T cells are poised for T_{reg} differentiation through their permissive T_{reg}-biased transcriptional and epigenetic landscape, which is primed to synergize with TCR and cytokine signaling. This skewing towards immunotolerance generation upon antigen encounter is beneficial *in utero*, since most antigens encountered in the periphery will be self-antigens, non-inherited maternal antigens that have crossed the placenta (40), or possibly rare bacterial commensal antigens. However, this raises the question of how the fetal immune system transitions from favoring tolerance to generating the sterilizing, pro-inflammatory immunity required for life after birth, and whether this process is fully complete at the time of birth.

Assessment of T_{reg} proportions in preterm cord blood (the only current proxy for the human third trimester) in multiple studies indicated that preterm neonates had higher T_{reg} percentages compared to term neonates (123) that was correlated with gestational age (124), and this was not altered regardless of the etiology of preterm labour (125, 126). Additionally, comparisons of T_{reg} percentages within a pediatric cohort (<2 years) and an adult cohort (>25 years) showed that the pediatric samples consistently had increased T_{reg} proportions ranging from 20-40% (127), which, barring different strategies in gating, is reminiscent of the increased T_{reg} frequencies seen in fetal spleen and lymph node CD4⁺ T cell populations. This seems to suggest that the transition towards an “adult-like” immune system is incomplete at birth, and that the predisposition for T_{reg} generation could be sustained through early childhood. This could be readily assessed by carrying out T_{reg} differentiation *in vitro* for fetal, pediatric and adult naïve CD4⁺ T cells to evaluate if pediatric naïve T cells still give rise to higher proportions of iT_{reg} cells than adults in both the absence and presence of TGFβ. Additionally, expression of the partial T_{reg}-signature derived within this work could be used to correlate eventual iT_{reg} differentiation potential with age. Lastly, the retention of increased T_{reg} differentiation potential from birth into

childhood could have important implications for infection and vaccination, given that the differentiation of naïve T cells into pro-inflammatory effector Th cell subsets, rather than the re-activation of memory cells, is presumably the primary T cell immune response generated in this age group. As such, T_{reg} predisposition within pediatric naïve CD4 T cells could give rise to the increase susceptibility to viral and bacterial infections, as well as to ineffectual vaccine recall responses generated to childhood vaccines (51). Identification of the extent of this predisposition would be informative for the formulation of vaccines or approaches that can boost differentiation of naïve T cells towards pro-inflammatory Th subsets in newborn/pediatric patients.

4.2 Identifying upstream environmental stimuli that “imprint” the fetal Treg-biased epigenome/transcriptome

Since a partial T_{reg}-biased epigenome and transcriptome is already present within fetal naïve T cells at steady state, future studies are needed to address the questions of what triggers the acquisition of these signatures *in vivo*, and whether this can be replicated *in vitro*.

Transplantation of fetal hematopoietic stem/progenitor cells (HSPCs) into a SCID-hu Thy/Liv humanized mouse model generated CD4 single positive (SP) thymocytes that retained their capability for increased differentiation into FOXP3^{hi}CD25^{hi} T_{reg} cells *in vitro*, and this was reflected in a larger fraction of FOXP3^{hi}CD25^{hi} cell in the CD4 SP compartment *in vivo*. The same changes were not observed in mice transplanted with adult HSPCs (41), indicating that acquisition of predisposition for fetal T_{reg} differentiation can occur as early as the HSPC stage. Given that epigenetic imprinting in the HSPCs can be inherited in subsequent daughter populations, this raises a tantalizing proposition that differences in the fetal environment can already “imprint” a T_{reg}-biased epigenome and transcriptome within the fetal HSPC population.

Multiple factors within the fetal environment *in utero* present ripe areas for investigation. One relevant observation is that members of the TGF β family are enriched in fetal secondary lymphoid organs, consistent with the importance of TGF β and its family members in the control of stemness, differentiation, proliferation and function of multiple cell types during development (128). Depletion of TGF β family members in mice, particularly that of TGF β 2/3, result in developmental defects present in multiple organs at birth (128). Additionally, although we do not observe increased transcription of TGF β 1 within the secondary lymphoid organs (41), we show that fetal iT_{reg} can potently upregulate GARP and LAP during differentiation, and have the machinery available to mediate the activation of bioactive TGF β 1. Further investigations are needed to clarify whether high concentrations of TGF β family members are present at sites of HSPC development, whether fetal HSPCs already have expression of a transcriptional or epigenetic signature similar to that observed in fetal CD4⁺ naïve T cells, and which family members present could potentially drive “imprinting” of these signatures.

Other candidates for consideration include the effect of the hypoxic environment *in utero*, as well as the presence of uniformly high concentrations of estrogen and progesterone throughout pregnancy. The role of hypoxia in T_{reg} induction is complicated since parallel studies exist that implicate hypoxia and the subsequent upregulation of the HIF1 α to predispose CD4⁺ T cell generation both towards a Th17 effector or T_{reg} cell fate. Genetic deletion of HIF1 α in two individual studies resulted in the failure to generate Th17 responses and a corresponding increase in FOXP3⁺ T_{reg} proportions in mice (129, 130). In contrast, when HIF1 α was stabilized by culture *in vitro* in hypoxic environments or *in vivo* within hypoxia-treated animals, an increase in T_{reg} differentiation ability and abundance was observed, with no apparent effect on Th17 effector differentiation (131, 132). Additionally, ablation of HIF1 α specifically in T_{reg} cells resulted in their failure to suppress effector T cell proliferation *in vitro* and colitis development *in vivo*

(132). As such the dosage, as well as the situation in which HIF1 α is induced, seems to matter for whether T_{reg} or Th17 cells are generated, given that full genetic ablation of HIF1 α in the CD4 compartment has drastic consequences on Th17 induction, while the stabilization of HIF1 α via hypoxia is sufficient to favor T_{reg} over Th17 conversion. Given that the fetus is present in the latter environment, it seem likely that HIF1 α and other mediators activated by hypoxia might play an important role driving T_{reg} differentiation over the Th17 phenotype. This can be clarified in future studies assessing the impact of hypoxia on T_{reg} differentiation ability, as well as the acquisition of T_{reg} transcriptional and epigenetic signatures, in adult and fetal naïve CD4⁺ T cells.

Lastly, the pregnancy hormones progesterone and estrogen have been shown to have pleiotropic effects on effector Th and T_{reg} differentiation and function (133). High levels of circulating progesterone and estrogen within the human fetus have been characterized, with both levels increasing rapidly from the early second trimester towards towards term (134). Both progesterone and estrogen have been shown to favor T_{reg} differentiation in multiple parallel studies in mice (summarized in (133)). Of note, one study evaluating the effect of progesterone on human cord blood naïve T cells showed that progesterone could elicit T_{reg} differentiation in the absence of exogenous TGF β in a dosage-dependent manner, and that adult naïve T cells were resistant to the T_{reg}-inducing effect of progesterone (135). This could point to long term transcriptional or epigenetic programming of fetal naïve T cells by progesterone (and estrogen) to favor T_{reg} generation, and that the loss of progesterone exposure at fetal concentrations in adulthood result in the inability for T_{reg} differentiation in response to progesterone signaling. More work is required to assess the effect of progesterone and estrogen on fetal T_{reg} differentiation, and whether physiological levels found within fetal tissues are sufficient to program HSPCs towards the generation of progenitors that favor T_{reg} differentiation.

4.3 Generating functional and stable Treg cell populations from naïve T cells *in vitro*

Since their identification in the early 2000s, adoptive cellular transfer of T_{reg} cells to initiate immunosuppression in autoimmune and inflammatory disease settings have already reached clinical trials in humans (136). The outsized ability of a small population of T_{reg} cells to mediate immunosuppression in a antigen-specific as well as a non-specific manner through bystander activation make them an attractive target, as well as their ability for potential persistence, which will ensure enduring immunotolerance within the patient. Most of the current trials depend on the expansion of *ex vivo* T_{reg} populations over a period of weeks, since a large infusion of T_{reg} cells is needed for efficacy, and only *ex vivo* T_{reg} cells retain the full demethylation of the *FOXP3* TSDR and by proxy, their stable immunosuppressive phenotype (136, 137). As such, the generation of iT_{reg} cells from naïve T cell precursors, which are more abundant and easier to manipulate than *ex vivo* T_{reg} cells, would be a strong alternative to T_{reg} expansion *in vitro*.

However, the use of iT_{reg} cells in clinical settings have proven to be problematic since most iT_{reg} cells have partial or absent demethylation at the *FOXP3* TSDR, which results in instability upon re-transfer *in vivo* in preclinical mouse studies (38, 93). Furthermore, even though it has not been evaluated, it is likely that human adult iT_{reg} cells do not acquire the epigenetic and transcriptional signatures present in *ex vivo* T_{reg} populations that also ensure their phenotypic stability. We show here that human fetal naïve CD4⁺ T cells differentiate into iT_{reg} cells that have phenotypic characteristics that are present in *ex vivo* human T_{reg} cells that are not acquired by human adult iT_{reg} cells, such as the repression of IL-2 and IFN γ secretion, and the ability to secrete IL-10 and produce and sequester latent TGF β 1. In the presence of TGF β , almost all human fetal naïve T cells convert into FOXP3^{hi}CD25^{hi} iT_{reg} cells, and they acquire a transcriptional signature only expressed by both fetal and adult *ex vivo* populations. Given that T_{reg} differentiation ability might persist past time of birth, future studies into whether human cord

blood naïve T cells can recapitulate this effect *in vitro* will be important in bringing this closer to potential clinical application, since cord blood banks could serve as potential reserves for donor-matched iT_{reg} generation.

In this study, we reveal that human fetal iT_{reg} populations do not acquire demethylation at the *FOXP3* TSDR regardless of whether Helios was expressed. We propose that this is due to the inability of TCR and TGFβ signaling *in vitro* to capture the complexity of T_{reg} differentiation *in vivo*, since the input from multiple feed-forward loops likely contribute to full lineage commitment. DNA demethylation at the *FOXP3* locus is governed by ten-eleven-translocation (TET) enzymes which mediate the oxidation of 5-methylcytosine during the process of demethylation (138, 139). Deletion of TET2/3 in mice then result in decreased T_{reg} proportions in the periphery (138, 139), due to decreased stability of the T_{reg} population as observed for *FOXP3*^{ΔCNS2-GFP} mice (29). The use of vitamin C potentiates TET activity, and the addition of vitamin C during iT_{reg} differentiation with TGFβ resulted in the a large drop in of 5-methylcytosine (5-MC) and 5-hydroxymethylcytosine (5-hMC) specifically at the *FOXP3* CNS2 TSDR in mice (138, 139). This resulted in increased retention of FOXP3 in the differentiated vitamin C treated iT_{reg} *in vitro* and *in vivo* (138, 139). Although the extent decrease in 5-MC and 5-hMC was not as apparent, the same effect of vitamin C on the stability of FOXP3 expression was observed in human adult iT_{reg} differentiation (138), indicating that vitamin C could be used a potent co-factor to generate stable iT_{reg} populations. It would be thus interesting to test if the addition of vitamin C to fetal iT_{reg} differentiation would potentiate demethylation at the *FOXP3* TSDR both in the absence or presence of TGFβ. Lastly, given that epigenetic modifications occur at other important T_{reg} gene loci such as *IKZF4*, *IL2RA*, *CTLA4* and *TNFSRF18* (GITR), and precede FOXP3 expression, it will be important to evaluate if global modulation of histone modifications

can boost the acquisition of DNA demethylation patterns at the same underlying genes. Small molecule inhibitors to histone deacetylase complexes (HDACs) are the most well characterized, and the use of HDAC inhibitors in mice have resulted in the increase FOXP3 T_{reg} proportions as well as in their suppressive function (summarized in (140)). However, since the FOXP3 protein itself is stabilized itself by direct acetylation, it is difficult to ascertain if this effect is truly from modulation of the epigenome itself. Targeted histone modification via CRISPR activation (CRISPRa) could possibly be utilized to provide a more specific approach; it would be therefore interesting to assess if we could target fused dCas9 constructs with epigenetic modulators such as p300 to pre-identified enhancer regions to activate the T_{reg} epigenome on a global scale. SE and TE regions identified within our work on the T_{reg} epigenome identified here would be an important resource to inform guide RNA design and specificity in order to achieve appropriate activation only of T_{reg} associated genes.

REFERENCES

1. M. S. Anderson, E. S. Venanzi, L. Klein, Z. Chen, S. P. Berzins, S. J. Turley, H. von Boehmer, R. Bronson, A. Dierich, C. Benoist, D. Mathis, Projection of an immunological self shadow within the thymus by the aire protein, *Science* **298**, 1395–1401 (2002).
2. M. S. Anderson, E. S. Venanzi, Z. Chen, S. P. Berzins, C. Benoist, D. Mathis, The cellular mechanism of Aire control of T cell tolerance, *Immunity* **23**, 227–239 (2005).
3. J. S. A. Perry, C.-W. J. Lio, A. L. Kau, K. Nutsch, Z. Yang, J. I. Gordon, K. M. Murphy, C.-S. Hsieh, Distinct contributions of Aire and antigen-presenting-cell subsets to the generation of self-tolerance in the thymus, *Immunity* **41**, 414–426 (2014).
4. R. Bonasio, M. L. Scimone, P. Schaerli, N. Grabie, A. H. Lichtman, U. H. von Andrian, Clonal deletion of thymocytes by circulating dendritic cells homing to the thymus, *Nat Immunol* **7**, 1092–1100 (2006).
5. R. D. Owen, IMMUNOGENETIC CONSEQUENCES OF VASCULAR ANASTOMOSES BETWEEN BOVINE TWINS, *Science* **102**, 400–401 (1945).
6. R. E. Billingham, G. H. Lampkin, P. B. Medawar, H. L. Williams, Tolerance to homografts, twin diagnosis, and the freemartin condition in cattle, *Heredity* **1952 6:2 6**, 201–212 (1952).
7. R. E. Billingham, L. Brent, P. B. Medawar, Actively acquired tolerance of foreign cells, *Nature* **172**, 603–606 (1953).
8. S. Sakaguchi, N. Sakaguchi, M. Asano, M. Itoh, M. Toda, Immunologic self-tolerance maintained by activated T cells expressing IL-2 receptor alpha-chains (CD25). Breakdown of a single mechanism of self-tolerance causes various autoimmune diseases, *J. Immunol.* **155**, 1151–1164 (1995).
9. R. Khattri, T. Cox, S.-A. Yasayko, F. Ramsdell, An essential role for Scurfin in CD4+CD25+ T regulatory cells, *Nat Immunol* **4**, 337–342 (2003).
10. S. Hori, Control of Regulatory T Cell Development by the Transcription Factor Foxp3, *Science* **299**, 1057–1061 (2003).

11. J. D. Fontenot, M. A. Gavin, A. Y. Rudensky, Foxp3 programs the development and function of CD4+CD25+ regulatory T cells, *Nat Immunol* **4**, 330–336 (2003).
12. Y. Nishizuka, T. Sakakura, Thymus and reproduction: sex-linked dysgenesis of the gonad after neonatal thymectomy in mice, *Science* **166**, 753–755 (1969).
13. Sakaguchi, T. Yamaguchi, T. Nomura, M. Ono, Regulatory T Cells and Immune Tolerance, *Cell* **133**, 775–787 (2008).
14. R. S. Wildin, F. Ramsdell, J. Peake, F. Faravelli, J. L. Casanova, N. Buist, E. Levy-Lahad, M. Mazzella, O. Goulet, L. Perroni, F. D. Bricarelli, G. Byrne, M. McEuen, S. Proll, M. Appleby, M. E. Brunkow, X-linked neonatal diabetes mellitus, enteropathy and endocrinopathy syndrome is the human equivalent of mouse scurfy, *Nat. Genet.* **27**, 18–20 (2001).
15. C. L. Bennett, J. Christie, F. Ramsdell, M. E. Brunkow, P. J. Ferguson, L. Whitesell, T. E. Kelly, F. T. Saulsbury, P. F. Chance, H. D. Ochs, The immune dysregulation, polyendocrinopathy, enteropathy, X-linked syndrome (IPEX) is caused by mutations of FOXP3, *Nat. Genet.* **27**, 20–21 (2001).
16. M. M. Xavier-da-Silva, C. A. Moreira-Filho, E. Suzuki, F. Patricio, A. Coutinho, M. Carneiro-Sampaio, Fetal-onset IPEX: report of two families and review of literature, *Clin. Immunol.* **156**, 131–140 (2015).
17. A. Vasiljevic, B. Poreau, R. Bouvier, A. Lachaux, C. Arnoult, J. Fauré, M. P. Cordier, P. F. Ray, Immune dysregulation, polyendocrinopathy, enteropathy, X-linked syndrome and recurrent intrauterine fetal death, *Lancet* **385**, 2120 (2015).
18. W. Rae, Y. Gao, D. Bunyan, S. Holden, K. Gilmour, S. Patel, D. Wellesley, A. Williams, A novel FOXP3 mutation causing fetal akinesia and recurrent male miscarriages, *Clin. Immunol.* **161**, 284–285 (2015).
19. S. L. Reichert, E. M. McKay, J. S. Moldenhauer, Identification of a novel nonsense mutation

- in the FOXP3 gene in a fetus with hydrops--Expanding the phenotype of IPEX syndrome, *Am. J. Med. Genet. A* **170A**, 226–232 (2016).
20. O. Shehab, D. J. Tester, N. C. Ackerman, F. S. Cowchock, M. J. Ackerman, Whole genome sequencing identifies etiology of recurrent male intrauterine fetal death, *Prenat. Diagn.* **37**, 1040–1045 (2017).
21. W. Lee, G. R. Lee, Transcriptional regulation and development of regulatory T cells, *Exp. Mol. Med.* **50**, e456 (2018).
22. C. M. Sun, J. A. Hall, R. B. Blank, N. Bouladoux, M. Oukka, J. R. Mora, Y. Belkaid, Small intestine lamina propria dendritic cells promote de novo generation of Foxp3 T reg cells via retinoic acid, *J. Exp. Med.* **204**, 1775–1785 (2007).
23. M. J. Benson, K. Pino-Lagos, M. Roseblatt, R. J. Noelle, All-trans retinoic acid mediates enhanced T reg cell growth, differentiation, and gut homing in the face of high levels of co-stimulation, *J. Exp. Med.* **204**, 1765–1774 (2007).
24. J. L. Coombes, K. R. R. Siddiqui, C. V. Arancibia-Cárcamo, J. Hall, C. M. Sun, Y. Belkaid, F. Powrie, A functionally specialized population of mucosal CD103+ DCs induces Foxp3+ regulatory T cells via a TGF-beta and retinoic acid-dependent mechanism, *J. Exp. Med.* **204**, 1757–1764 (2007).
25. J. C. Marie, J. J. Letterio, M. Gavin, A. Y. Rudensky, TGF-beta1 maintains suppressor function and Foxp3 expression in CD4+CD25+ regulatory T cells, *J. Exp. Med.* **201**, 1061–1067 (2005).
26. J. C. Marie, D. Liggitt, A. Y. Rudensky, Cellular mechanisms of fatal early-onset autoimmunity in mice with the T cell-specific targeting of transforming growth factor-beta receptor, *Immunity* **25**, 441–454 (2006).
27. M. O. Li, S. Sanjabi, R. A. Flavell, Transforming growth factor-beta controls development, homeostasis, and tolerance of T cells by regulatory T cell-dependent and -independent

- mechanisms, *Immunity* **25**, 455–471 (2006).
28. N. Ohkura, M. Hamaguchi, H. Morikawa, K. Sugimura, A. Tanaka, Y. Ito, M. Osaki, Y. Tanaka, R. Yamashita, N. Nakano, J. Huehn, H. J. Fehling, T. Sparwasser, K. Nakai, S. Sakaguchi, T Cell Receptor Stimulation-Induced Epigenetic Changes and Foxp3 Expression Are Independent and Complementary Events Required for Treg Cell Development, *Immunity* **37**, 785–799 (2012).
29. Y. Zheng, S. Josefowicz, A. Chaudhry, X. P. Peng, K. Forbush, A. Y. Rudensky, Role of conserved non-coding DNA elements in the Foxp3 gene in regulatory T-cell fate, *Nature* **463**, 808–812 (2010).
30. Y. Kitagawa, N. Ohkura, Y. Kidani, A. Vandenbon, K. Hirota, R. Kawakami, K. Yasuda, D. Motooka, S. Nakamura, M. Kondo, I. Taniuchi, T. Kohwi-Shigematsu, S. Sakaguchi, Guidance of regulatory T cell development by Satb1-dependent super-enhancer establishment, *Nat Immunol* **18**, 173–183 (2017).
31. Y. Zheng, S. Z. Josefowicz, A. Kas, T.-T. Chu, M. A. Gavin, A. Y. Rudensky, Genome-wide analysis of Foxp3 target genes in developing and mature regulatory T cells, *Nature* **445**, 936–940 (2007).
32. S. Sakaguchi, T. Yamaguchi, T. Nomura, M. Ono, Regulatory T cells and immune tolerance, *Cell* **133**, 775–787 (2008).
33. E. M. Shevach, Mechanisms of foxp3+ T regulatory cell-mediated suppression, *Immunity* **30**, 636–645 (2009).
34. S. Sakaguchi, M. Miyara, C. M. Costantino, D. A. Hafler, FOXP3+ regulatory T cells in the human immune system, *Nature Publishing Group* **10**, 490–500 (2010).
35. W. Chen, W. Jin, N. Hardegen, K.-J. Lei, L. Li, N. Marinos, G. McGrady, S. M. Wahl, Conversion of peripheral CD4+CD25- naive T cells to CD4+CD25+ regulatory T cells by TGF-beta induction of transcription factor Foxp3, *J. Exp. Med.* **198**, 1875–1886 (2003).

36. M. C. Fantini, C. Becker, G. Monteleone, F. Pallone, P. R. Galle, M. F. Neurath, Cutting edge: TGF-beta induces a regulatory phenotype in CD4+CD25- T cells through Foxp3 induction and down-regulation of Smad7, *J. Immunol.* **172**, 5149–5153 (2004).
37. D. Q. Tran, H. Ramsey, E. M. Shevach, Induction of FOXP3 expression in naive human CD4+FOXP3 T cells by T-cell receptor stimulation is transforming growth factor-beta dependent but does not confer a regulatory phenotype, *Blood* **110**, 2983–2990 (2007).
38. C. Koenecke, N. Czeloth, A. Bubke, S. Schmitz, A. Kissenpfennig, B. Malissen, J. Huehn, A. Ganser, R. Förster, I. Prinz, Alloantigen-specific de novo-induced Foxp3+ Treg revert in vivo and do not protect from experimental GVHD, *Eur. J. Immunol.* **39**, 3091–3096 (2009).
39. J. Michaelsson, J. E. Mold, J. M. McCune, D. F. Nixon, Regulation of T Cell Responses in the Developing Human Fetus, *J. Immunol.* **176**, 5741–5748 (2006).
40. J. E. Mold, J. Michaelsson, T. D. Burt, M. O. Muench, K. P. Beckerman, M. P. Busch, T. H. Lee, D. F. Nixon, J. M. McCune, Maternal Alloantigens Promote the Development of Tolerogenic Fetal Regulatory T Cells in Utero, *Science* **322**, 1562–1565 (2008).
41. J. E. Mold, S. Venkatasubrahmanyam, T. D. Burt, J. Michaelsson, J. M. Rivera, S. A. Galkina, K. Weinberg, C. A. Stoddart, J. M. McCune, Fetal and Adult Hematopoietic Stem Cells Give Rise to Distinct T Cell Lineages in Humans, *Science* **330**, 1695–1699 (2010).
42. Y. Bronevetsky, T. D. Burt, J. M. McCune, Lin28b Regulates Fetal Regulatory T Cell Differentiation through Modulation of TGF- β Signaling, *The Journal of Immunology* **197**, 4344–4350 (2016).
43. D. Mucida, N. Kutchukhidze, A. Erazo, M. Russo, J. J. Lafaille, M. A. Curotto de Lafaille, Oral tolerance in the absence of naturally occurring Tregs, *J. Clin. Invest.* **115**, 1923–1933 (2005).
44. D. Haribhai, J. B. Williams, S. Jia, D. Nickerson, E. G. Schmitt, B. Edwards, J. Ziegelbauer, M. Yassai, S.-H. Li, L. M. Relland, P. M. Wise, A. Chen, Y.-Q. Zheng, P. M. Simpson, J.

- Gorski, N. H. Salzman, M. J. Hessner, T. A. Chatila, C. B. Williams, A requisite role for induced regulatory T cells in tolerance based on expanding antigen receptor diversity, *Immunity* **35**, 109–122 (2011).
45. J. Zhu, W. E. Paul, CD4 T cells: fates, functions, and faults, *Blood* **112**, 1557–1569 (2008).
46. J. Zhu, H. Yamane, W. E. Paul, Differentiation of effector CD4 T cell populations (*), *Annu. Rev. Immunol.* **28**, 445–489 (2010).
47. M. S. Sundrud, M. A. Nolan, Synergistic and combinatorial control of T cell activation and differentiation by transcription factors, *Curr. Opin. Immunol.* **22**, 286–292 (2010).
48. Y. Chen, J. K. Kim, A. J. Hirning, K. Josi, M. R. Bennett, Emergent genetic oscillations in a synthetic microbial consortium, *Science* **349**, 986–989 (2015).
49. M. E. Brunkow, E. W. Jeffery, K. A. Hjerrild, B. Paepfer, L. B. Clark, S. A. Yasayko, J. E. Wilkinson, D. Galas, S. F. Ziegler, F. Ramsdell, Disruption of a new forkhead/winged-helix protein, scurf, results in the fatal lymphoproliferative disorder of the scurfy mouse, *Nat. Genet.* **27**, 68–73 (2001).
50. S. Sakaguchi, Naturally arising Foxp3-expressing CD25+ CD4+ regulatory T cells in immunological tolerance to self and non-self, *Nat Immunol* (2005).
51. T. D. Burt, Fetal Regulatory T Cells and Peripheral Immune Tolerance In Utero: Implications for Development and Disease, *Am J Reprod Immunol* **69**, 346–358 (2013).
52. R. Bacchetta, F. Barzaghi, M. G. Roncarolo, N. R. Rose, Ed. From IPEX syndrome to FOXP3 mutation: a lesson on immune dysregulation, *Annals of the New York Academy of Sciences* **1417**, 5–22 (2018).
53. S. K. Tripathi, R. Lahesmaa, Transcriptional and epigenetic regulation of T-helper lineage specification, *Immunological Reviews* **261**, 62–83 (2014).
54. M. L. T. Nguyen, S. A. Jones, J. E. Prier, B. E. Russ, Transcriptional Enhancers in the Regulation of T Cell Differentiation, *Front Immunol* **6**, 462 (2015).

55. A. Arvey, J. van der Veecken, G. Plitas, S. S. Rich, P. Concannon, A. Y. Rudensky, Genetic and epigenetic variation in the lineage specification of regulatory T cells, *Elife* **4**, e07571 (2015).
56. J. A. Hill, M. Feuerer, K. Tash, S. Haxhinasto, J. Perez, R. Melamed, D. Mathis, C. Benoist, Foxp3 Transcription-Factor-Dependent and -Independent Regulation of the Regulatory T Cell Transcriptional Signature, *Immunity* **27**, 786–800 (2007).
57. W. Fu, A. Ergun, T. Lu, J. A. Hill, S. Haxhinasto, M. S. Fassett, R. Gazit, S. Adoro, L. Glimcher, S. Chan, P. Kastner, D. Rossi, J. J. Collins, D. Mathis, C. Benoist, A multiply redundant genetic switch “locks in” the transcriptional signature of regulatory T cells, *Nat Immunol* **13**, 972–980 (2012).
58. T. J. Curiel, G. Coukos, L. Zou, X. Alvarez, P. Cheng, P. Mottram, M. Evdemon-Hogan, J. R. Conejo-Garcia, L. Zhang, M. Burow, Y. Zhu, S. Wei, I. Kryczek, B. Daniel, A. Gordon, L. Myers, A. Lackner, M. L. Disis, K. L. Knutson, L. Chen, W. Zou, Specific recruitment of regulatory T cells in ovarian carcinoma fosters immune privilege and predicts reduced survival, *Nature Medicine* **10**, 942–949 (2004).
59. M. Miyara, S. Sakaguchi, Natural regulatory T cells: mechanisms of suppression, *Trends Mol Med* **13**, 108–116 (2007).
60. Z. Cao, A. K. Wara, B. Icli, X. Sun, R. R. S. Packard, F. Esen, C. J. Stapleton, M. Subramaniam, K. Kretschmer, I. Apostolou, H. von Boehmer, G. K. Hansson, T. C. Spelsberg, P. Libby, M. W. Feinberg, Kruppel-like Factor KLF10 Targets Transforming Growth Factor-1 to Regulate CD4⁺CD25⁻ T Cells and T Regulatory Cells, *Journal of Biological Chemistry* **284**, 24914–24924 (2009).
61. Y. Xiong, S. Khanna, A. L. Grzenda, O. F. Sarmiento, P. A. Svingen, G. A. Lomber, R. A. Urrutia, W. A. Faubion, Polycomb Antagonizes p300/CREB-binding Protein-associated Factor to Silence FOXP3 in a Kruppel-like Factor-dependent Manner, *Journal of Biological*

- Chemistry* **287**, 34372–34385 (2012).
62. Y. Xiong, P. A. Svingen, O. O. Sarmento, T. C. Smyrk, M. Dave, S. Khanna, G. A. Lomberk, R. A. Urrutia, W. A. Faubion, Differential coupling of KLF10 to Sin3-HDAC and PCAF regulates the inducibility of the FOXP3 gene, *AJP: Regulatory, Integrative and Comparative Physiology* **307**, R608–R620 (2014).
63. A. M. Thornton, P. E. Korty, D. Q. Tran, E. A. Wohlfert, P. E. Murray, Y. Belkaid, E. M. Shevach, Expression of Helios, an Ikaros Transcription Factor Family Member, Differentiates Thymic-Derived from Peripherally Induced Foxp3+ T Regulatory Cells, *The Journal of Immunology* **184**, 3433–3441 (2010).
64. H.-J. Kim, R. A. Barnitz, T. Kreslavsky, F. D. Brown, H. Moffett, M. E. Lemieux, Y. Kaygusuz, T. Meissner, T. A. W. Holderried, S. Chan, P. Kastner, W. N. Haining, H. Cantor, Stable inhibitory activity of regulatory T cells requires the transcription factor Helios, *Science* **350**, 334–339 (2015).
65. M. Sebastian, M. Lopez-Ocasio, A. Metidji, S. A. Rieder, E. M. Shevach, A. M. Thornton, Helios Controls a Limited Subset of Regulatory T Cell Functions, *The Journal of Immunology* **196**, 144–155 (2016).
66. F. Pan, H. Yu, E. V. Dang, J. Barbi, X. Pan, J. F. Grosso, D. Jinasena, S. M. Sharma, E. M. McCadden, D. Getnet, C. G. Drake, J. O. Liu, M. C. Ostrowski, D. M. Pardoll, Eos mediates Foxp3-dependent gene silencing in CD4+ regulatory T cells, *Science* **325**, 1142–1146 (2009).
67. H. Morikawa, N. Ohkura, A. Vandenbon, M. Itoh, S. Nagao-Sato, H. Kawaji, T. Lassmann, P. Carninci, Y. Hayashizaki, A. R. R. Forrest, D. M. Standley, H. Date, S. Sakaguchi, FANTOM Consortium, M. Itoh, S. Sakaguchi, Differential roles of epigenetic changes and Foxp3 expression in regulatory T cell-specific transcriptional regulation, *Proc. Natl. Acad. Sci. U.S.A.* **111**, 5289–5294 (2014).

68. A. Yu, L. Zhu, N. H. Altman, T. R. Malek, A low interleukin-2 receptor signaling threshold supports the development and homeostasis of T regulatory cells, *Immunity* **30**, 204–217 (2009).
69. N. Joller, E. Lozano, P. R. Burkett, B. Patel, S. Xiao, C. Zhu, J. Xia, T. G. Tan, E. Sefik, V. Yajnik, A. H. Sharpe, F. J. Quintana, D. Mathis, C. Benoist, D. A. Hafler, V. K. Kuchroo, Treg cells expressing the coinhibitory molecule TIGIT selectively inhibit proinflammatory Th1 and Th17 cell responses, *Immunity* **40**, 569–581 (2014).
70. S. N. Furlan, B. Watkins, V. Tkachev, S. Cooley, A. Panoskaltsis-Mortari, K. Betz, M. Brown, D. J. Hunt, J. B. Schell, K. Zeleski, A. Yu, C. R. Giver, E. K. Waller, J. S. Miller, B. R. Blazar, L. S. Kean, Systems analysis uncovers inflammatory Th/Tc17-driven modules during acute GVHD in monkey and human T cells, *Blood* **128**, 2568–2579 (2016).
71. T. Takimoto, Y. Wakabayashi, T. Sekiya, N. Inoue, R. Morita, K. Ichiyama, R. Takahashi, M. Asakawa, G. Muto, T. Mori, E. Hasegawa, S. Saika, S. Shizuya, T. Hara, M. Nomura, A. Yoshimura, Smad2 and Smad3 are redundantly essential for the TGF-beta-mediated regulation of regulatory T plasticity and Th1 development, *The Journal of Immunology* **185**, 842–855 (2010).
72. G. M. Delgoffe, S.-R. Woo, M. E. Turnis, D. M. Gravano, C. Guy, A. E. Overacre, M. L. Bettini, P. Vogel, D. Finkelstein, J. Bonnevier, C. J. Workman, D. A. A. Vignali, Stability and function of regulatory T cells is maintained by a neuropilin-1-semaphorin-4a axis, *Nature* **501**, 252–256 (2013).
73. M. A. Travis, D. Sheppard, TGF- β activation and function in immunity, *Annu. Rev. Immunol.* **32**, 51–82 (2014).
74. F. Ocklenburg, D. Moharreggh-Khiabani, R. Geffers, V. Janke, S. Pfoertner, H. Garritsen, L. Groebe, J. Klempnauer, K. E. J. Dittmar, S. Weiss, J. Buer, M. Probst-Kepper, UBD, a downstream element of FOXP3, allows the identification of LGALS3, a new marker of

- human regulatory T cells, *Lab. Invest.* **86**, 724–737 (2006).
75. M. Probst-Kepper, R. Geffers, A. Kröger, N. Viegas, C. Erck, H.-J. Hecht, H. Lünsdorf, R. Roubin, D. Moharreggh-Khiabani, K. Wagner, F. Ocklenburg, A. Jeron, H. Garritsen, T. P. Arstila, E. Kekäläinen, R. Balling, H. Hauser, J. Buer, S. Weiss, GARP: a key receptor controlling FOXP3 in human regulatory T cells, *J. Cell. Mol. Med.* **13**, 3343–3357 (2009).
76. A. M. Pesenacker, A. Y. Wang, A. Singh, J. Gillies, Y. Kim, C. A. Piccirillo, D. Nguyen, W. N. Haining, S. J. Tebbutt, C. Panagiotopoulos, M. K. Levings, A Regulatory T-Cell Gene Signature Is a Specific and Sensitive Biomarker to Identify Children With New-Onset Type 1 Diabetes, *Diabetes* **65**, 1031–1039 (2016).
77. J. P. Edwards, A. M. Thornton, E. M. Shevach, Release of active TGF- β 1 from the latent TGF- β 1/GARP complex on T regulatory cells is mediated by integrin β 8, *The Journal of Immunology* **193**, 2843–2849 (2014).
78. R. Wang, L. Kozhaya, F. Mercer, A. Khaitan, H. Fujii, D. Unutmaz, Expression of GARP selectively identifies activated human FOXP3+ regulatory T cells, *Proc. Natl. Acad. Sci. U.S.A.* **106**, 13439–13444 (2009).
79. W. A. Whyte, D. A. Orlando, D. Hnisz, B. J. Abraham, C. Y. Lin, M. H. Kagey, P. B. Rahl, T. I. Lee, R. A. Young, Master Transcription Factors and Mediator Establish Super-Enhancers at Key Cell Identity Genes, *Cell* **153**, 307–319 (2013).
80. J. Lovén, H. A. Hoke, C. Y. Lin, A. Lau, D. A. Orlando, C. R. Vakoc, J. E. Bradner, T. I. Lee, R. A. Young, Selective inhibition of tumor oncogenes by disruption of super-enhancers, *Cell* **153**, 320–334 (2013).
81. D. Shlyueva, G. Stampfel, A. Stark, Transcriptional enhancers: from properties to genome-wide predictions, *Nature Publishing Group* **15**, 272–286 (2014).
82. R. M. Samstein, A. Arvey, S. Z. Josefowicz, X. Peng, A. Reynolds, R. Sandstrom, S. Neph, P. Sabo, J. M. Kim, W. Liao, M. O. Li, C. Leslie, J. A. Stamatoyannopoulos, A. Y. Rudensky,

Foxp3 Exploits a Pre-Existent Enhancer Landscape for Regulatory T Cell Lineage Specification, *Cell* **151**, 153–166 (2012).

83. R. C. Adam, H. Yang, S. Rockowitz, S. B. Larsen, M. Nikolova, D. S. Oristian, L. Polak, M. Kadaja, A. Asare, D. Zheng, E. Fuchs, Pioneer factors govern super-enhancer dynamics in stem cell plasticity and lineage choice, *Nature* **521**, 366–370 (2015).
84. Y. Wakabayashi, H. Watanabe, J. Inoue, N. Takeda, J. Sakata, Y. Mishima, J. Hitomi, T. Yamamoto, M. Utsuyama, O. Niwa, S. Aizawa, R. Kominami, Bcl11b is required for differentiation and survival of alphabeta T lymphocytes, *Nat Immunol* **4**, 533–539 (2003).
85. N. Muthusamy, K. Barton, J. M. Leiden, Defective activation and survival of T cells lacking the Ets-1 transcription factor, *Nature* **377**, 639–642 (1995).
86. N. Sugimoto, T. Oida, K. Hirota, K. Nakamura, T. Nomura, T. Uchiyama, S. Sakaguchi, Foxp3-dependent and -independent molecules specific for CD25+CD4+ natural regulatory T cells revealed by DNA microarray analysis, *International Immunology* **18**, 1197–1209 (2006).
87. R. A. Gottschalk, E. Corse, J. P. Allison, Expression of Helios in peripherally induced Foxp3+ regulatory T cells, *The Journal of Immunology* **188**, 976–980 (2012).
88. D. Getnet, J. F. Grosso, M. V. Goldberg, T. J. Harris, H.-R. Yen, T. C. Bruno, N. M. Durham, E. L. Hipkiss, K. J. Pyle, S. Wada, F. Pan, D. M. Pardoll, C. G. Drake, A role for the transcription factor Helios in human CD4(+)CD25(+) regulatory T cells, *Molecular Immunology* **47**, 1595–1600 (2010).
89. R. S. Paiva, A. C. Lino, M.-L. Bergman, I. Caramalho, A. E. Sousa, S. Zelenay, J. Demengeot, Recent thymic emigrants are the preferential precursors of regulatory T cells differentiated in the periphery, *Proc. Natl. Acad. Sci. U.S.A.* **110**, 6494–6499 (2013).
90. S. Kimmig, G. K. Przybylski, C. A. Schmidt, K. Laurisch, B. Möwes, A. Radbruch, A. Thiel, Two subsets of naive T helper cells with distinct T cell receptor excision circle content in human adult peripheral blood, *J. Exp. Med.* **195**, 789–794 (2002).

91. T. Akimova, U. H. Beier, L. Wang, M. H. Levine, W. W. Hancock, C. Molina-Paris, Ed. Helios expression is a marker of T cell activation and proliferation, *PLoS ONE* **6**, e24226 (2011).
92. S. Floess, J. Freyer, C. Siewert, U. Baron, S. Olek, J. Polansky, K. Schlawe, H.-D. Chang, T. Bopp, E. Schmitt, S. Klein-Hessling, E. Serfling, A. Hamann, J. Huehn, P. Marrack, Ed. Epigenetic control of the *foxp3* locus in regulatory T cells, *PLoS Biol.* **5**, e38 (2007).
93. A. Beres, R. Komorowski, M. Mihara, W. R. Drobyski, Instability of Foxp3 Expression Limits the Ability of Induced Regulatory T Cells to Mitigate Graft versus Host Disease, *Clinical Cancer Research* **17**, 3969–3983 (2011).
94. H. Jonuleit, E. Schmitt, M. Stassen, A. Tuettenberg, J. Knop, A. H. Enk, Identification and functional characterization of human CD4(+)CD25(+) T cells with regulatory properties isolated from peripheral blood, *J. Exp. Med.* **193**, 1285–1294 (2001).
95. I. Baine, S. Basu, R. Ames, R. S. Sellers, F. Macian, Helios Induces Epigenetic Silencing of IL2 Gene Expression in Regulatory T Cells, *J. Immunol.* **190**, 1008–1016 (2013).
96. G. Gasteiger, W. Kastenmuller, Foxp3+ Regulatory T-cells and IL-2: The Moirai of T-cell Fates? *Front Immunol* **3**, 179 (2012).
97. H. Takatori, H. Kawashima, A. Matsuki, K. Meguro, S. Tanaka, T. Iwamoto, Y. Sanayama, N. Nishikawa, T. Tamachi, K. Ikeda, A. Suto, K. Suzuki, S.-I. Kagami, K. Hirose, M. Kubo, S. Hori, H. Nakajima, Helios Enhances Treg Cell Function in Cooperation With FoxP3, *Arthritis Rheumatol* **67**, 1491–1502 (2015).
98. S.-H. Fu, L.-T. Yeh, C.-C. Chu, B. L.-J. Yen, H.-K. Sytwu, New insights into Blimp-1 in T lymphocytes: a divergent regulator of cell destiny and effector function, *J. Biomed. Sci.* **24**, 49 (2017).
99. A. Onodera, K. Kokubo, T. Nakayama, Epigenetic and Transcriptional Regulation in the Induction, Maintenance, Heterogeneity, and Recall-Response of Effector and Memory Th2 Cells, *Front Immunol* **9**, 2929 (2018).

100. M. R. Quirion, G. D. Gregory, S. E. Umetsu, S. Winandy, M. A. Brown, Cutting edge: Ikaros is a regulator of Th2 cell differentiation, *The Journal of Immunology* **182**, 741–745 (2009).
101. L. Y. Wong, J. K. Hatfield, M. A. Brown, Ikaros sets the potential for Th17 lineage gene expression through effects on chromatin state in early T cell development, *J. Biol. Chem.* **288**, 35170–35179 (2013).
102. J. D. Wheaton, C.-H. Yeh, M. Ciofani, Cutting Edge: c-Maf Is Required for Regulatory T Cells To Adopt ROR γ t+ and Follicular Phenotypes, *The Journal of Immunology* **199**, 3931–3936 (2017).
103. J.-M. Choi, A. L. M. Bothwell, The nuclear receptor PPARs as important regulators of T-cell functions and autoimmune diseases, *Mol. Cells* **33**, 217–222 (2012).
104. O. Kaminuma, N. Kitamura, Y. Nishito, S. Nemoto, H. Tatsumi, A. Mori, T. Hiroi, Downregulation of NFAT3 Due to Lack of T-Box Transcription Factor TBX5 Is Crucial for Cytokine Expression in T Cells, *The Journal of Immunology* **200**, 92–100 (2018).
105. Q. Li, J. Zou, M. Wang, X. Ding, I. Chepelev, X. Zhou, W. Zhao, G. Wei, J. Cui, K. Zhao, H. Y. Wang, R.-F. Wang, Critical role of histone demethylase Jmjd3 in the regulation of CD4+ T-cell differentiation, *Nat Commun* **5**, 5780 (2014).
106. R. Sridharan, S. T. Smale, Predominant interaction of both Ikaros and Helios with the NuRD complex in immature thymocytes, *Journal of Biological Chemistry* **282**, 30227–30238 (2007).
107. S. Zhao, W. Liu, Y. Li, P. Liu, S. Li, D. Dou, Y. Wang, R. Yang, R. Xiang, F. Liu, C. Song, Ed. Alternative Splice Variants Modulates Dominant-Negative Function of Helios in T-Cell Leukemia, *PLoS ONE* **11**, e0163328 (2016).
108. Q. Cai, A. Dierich, M. Oulad-Abdelghani, S. Chan, P. Kastner, Helios deficiency has minimal impact on T cell development and function, *The Journal of Immunology* **183**, 2303–

2311 (2009).

109. S. Yang, N. Fujikado, D. Kolodin, C. Benoist, D. Mathis, Regulatory T cells generated early in life play a distinct role in maintaining self-tolerance, *Science*, 1–9 (2015).
110. H. Smith, I. M. Chen, R. Kubo, K. S. Tung, Neonatal thymectomy results in a repertoire enriched in T cells deleted in adult thymus, *Science* **245**, 749–752 (1989).
111. Y. C. Kim, R. Bhairavabhotla, J. Yoon, A. Golding, A. M. Thornton, D. Q. Tran, E. M. Shevach, Oligodeoxynucleotides stabilize Helios-expressing Foxp3+ human T regulatory cells during in vitro expansion, *Blood* **119**, 2810–2818 (2012).
112. A. M. Thornton, J. Lu, P. E. Korty, Y. C. Kim, C. Martens, P. D. Sun, E. M. Shevach, Helios+ and Helios- Treg subpopulations are phenotypically and functionally distinct and express dissimilar TCR repertoires, *Eur. J. Immunol.* **112**, 137 (2019).
113. M. D. Robinson, D. J. McCarthy, G. K. Smyth, edgeR: a Bioconductor package for differential expression analysis of digital gene expression data, *Bioinformatics* **26**, 139–140 (2010).
114. D. J. McCarthy, Y. Chen, G. K. Smyth, Differential expression analysis of multifactor RNA-Seq experiments with respect to biological variation, *Nucleic Acids Research* **40**, 4288–4297 (2012).
115. J. D. Buenrostro, P. G. Giresi, L. C. Zaba, H. Y. Chang, W. J. Greenleaf, Transposition of native chromatin for fast and sensitive epigenomic profiling of open chromatin, DNA-binding proteins and nucleosome position, *Nat Meth* **10**, 1213–1218 (2013).
116. J. D. Buenrostro, B. Wu, H. Y. Chang, W. J. Greenleaf, ATAC-seq: A Method for Assaying Chromatin Accessibility Genome-Wide, *Curr Protoc Mol Biol* **109**, 21.29.1–9 (2015).
117. P. Collas, A chromatin immunoprecipitation protocol for small cell numbers, *Methods Mol. Biol.* **791**, 179–193 (2011).
118. M. I. Love, W. Huber, S. Anders, Moderated estimation of fold change and dispersion for

- RNA-seq data with DESeq2, *Genome Biol.* **15**, 550 (2014).
119. K. Labun, T. G. Montague, J. A. Gagnon, S. B. Thyme, E. Valen, CHOPCHOP v2: a web tool for the next generation of CRISPR genome engineering, *Nucleic Acids Research* **44**, W272–6 (2016).
120. C. D. Richardson, G. J. Ray, N. L. Bray, J. E. Corn, Non-homologous DNA increases gene disruption efficiency by altering DNA repair outcomes, *Nat Commun* **7**, 12463 (2016).
121. K. Schumann, S. Lin, E. Boyer, D. R. Simeonov, M. Subramaniam, R. E. Gate, G. E. Haliburton, C. J. Ye, J. A. Bluestone, J. A. Doudna, A. Marson, Generation of knock-in primary human T cells using Cas9 ribonucleoproteins, *Proc. Natl. Acad. Sci. U.S.A.* **112**, 10437–10442 (2015).
122. J. F. Hultquist, K. Schumann, J. M. Woo, L. Manganaro, M. J. McGregor, J. Doudna, V. Simon, N. J. Krogan, A. Marson, A Cas9 Ribonucleoprotein Platform for Functional Genetic Studies of HIV-Host Interactions in Primary Human T Cells, *Cell Rep* **17**, 1438–1452 (2016).
123. C. Rennó, M. I. V. Nadaf, C. A. Zago, M. Carneiro-Sampaio, P. Palmeira, Healthy Preterm Newborns Show an Increased Frequency of CD4(+) CD25(high) CD127(low) FOXP3(+) Regulatory T Cells with a Naive Phenotype and High Expression of Gut-Homing Receptors, *Scand. J. Immunol.* **83**, 445–455 (2016).
124. A. A. Luciano, I. M. Arbona-Ramirez, R. Ruiz, B. J. Llorens-Bonilla, D. G. Martinez-Lopez, N. Funderburg, M. J. Dorsey, R. E. Morty, Ed. Alterations in regulatory T cell subpopulations seen in preterm infants, *PLoS ONE* **9**, e95867 (2014).
125. J. Pagel, A. Hartz, J. Figge, C. Gille, S. Eschweiler, K. Petersen, L. Schreiter, J. Hammer, C. M. Karsten, D. Friedrich, E. Herting, W. Göpel, J. Rupp, C. Härtel, Regulatory T cell frequencies are increased in preterm infants with clinical early-onset sepsis, *Clin. Exp. Immunol.* **185**, 219–227 (2016).
126. C. M. Rueda, C. B. Wells, T. Gisslen, A. H. Jobe, S. G. Kallapur, C. A. Chougnet, Effect of

- chorioamnionitis on regulatory T cells in moderate/late preterm neonates, *Hum. Immunol.* **76**, 65–73 (2015).
127. J. J. C. Thome, K. L. Bickham, Y. Ohmura, M. Kubota, N. Matsuoka, C. Gordon, T. Granot, A. Griesemer, H. Lerner, T. Kato, D. L. Farber, Early-life compartmentalization of human T cell differentiation and regulatory function in mucosal and lymphoid tissues, *Nature Medicine* **22**, 72–77 (2016).
128. M. Morikawa, R. Derynck, K. Miyazono, TGF- β and the TGF- β Family: Context-Dependent Roles in Cell and Tissue Physiology, *Cold Spring Harbor Perspectives in Biology* **8**, a021873 (2016).
129. E. V. Dang, J. Barbi, H.-Y. Yang, D. Jinasena, H. Yu, Y. Zheng, Z. Bordman, J. Fu, Y. Kim, H.-R. Yen, W. Luo, K. Zeller, L. Shimoda, S. L. Topalian, G. L. Semenza, C. V. Dang, D. M. Pardoll, F. Pan, Control of T(H)17/T(reg) balance by hypoxia-inducible factor 1, *Cell* **146**, 772–784 (2011).
130. L. Z. Shi, R. Wang, G. Huang, P. Vogel, G. Neale, D. R. Green, H. Chi, HIF1 α -dependent glycolytic pathway orchestrates a metabolic checkpoint for the differentiation of TH17 and Treg cells, *Journal of Experimental Medicine* **208**, 1367–1376 (2011).
131. J. Ben-Shoshan, S. Maysel-Auslender, A. Mor, G. Keren, J. George, Hypoxia controls CD4+CD25+ regulatory T-cell homeostasis via hypoxia-inducible factor-1 α , *Eur. J. Immunol.* **38**, 2412–2418 (2008).
132. E. T. Clambey, E. N. McNamee, J. A. Westrich, L. E. Glover, E. L. Campbell, P. Jedlicka, E. F. de Zoeten, J. C. Cambier, K. R. Stenmark, S. P. Colgan, H. K. Eltzschig, Hypoxia-inducible factor-1 α -dependent induction of FoxP3 drives regulatory T-cell abundance and function during inflammatory hypoxia of the mucosa, *Proc. Natl. Acad. Sci. U.S.A.* **109**, E2784–93 (2012).
133. B. Polese, V. Gridelet, E. Araklioti, H. Martens, S. Perrier d'Hauterive, V. Geenen, The

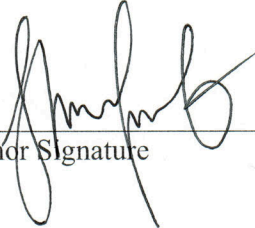
- Endocrine Milieu and CD4 T-Lymphocyte Polarization during Pregnancy, *Front Endocrinol (Lausanne)* **5**, 106 (2014).
134. M. Hill, A. Pašková, R. Kančeva, M. Velíková, J. Kubátová, L. Kancheva, K. Adamcová, M. Mikešová, Z. Žižka, M. Koucký, H. Šarapatková, V. Kačer, P. Matucha, M. Meloun, A. Pařízek, Steroid profiling in pregnancy: a focus on the human fetus, *J. Steroid Biochem. Mol. Biol.* **139**, 201–222 (2014).
135. J. H. Lee, B. Ulrich, J. Cho, J. Park, C. H. Kim, Progesterone promotes differentiation of human cord blood fetal T cells into T regulatory cells but suppresses their differentiation into Th17 cells, *The Journal of Immunology* **187**, 1778–1787 (2011).
136. J. H. Esensten, Y. D. Muller, J. A. Bluestone, Q. Tang, Regulatory T-cell therapy for autoimmune and autoinflammatory diseases: The next frontier, *J. Allergy Clin. Immunol.* **142**, 1710–1718 (2018).
137. B. D. Singer, L. S. King, F. R. D'Alessio, Regulatory T cells as immunotherapy, *Front Immunol* **5**, 46 (2014).
138. X. Yue, S. Trifari, T. Åijö, A. Tsagaratou, W. A. Pastor, J. A. Zepeda-Martínez, C.-W. J. Lio, X. Li, Y. Huang, P. Vijayanand, H. Lähdesmäki, A. Rao, Control of Foxp3 stability through modulation of TET activity, *Journal of Experimental Medicine* **213**, 377–397 (2016).
139. V. S. Nair, M. H. Song, M. Ko, K. I. Oh, DNA Demethylation of the Foxp3 Enhancer Is Maintained through Modulation of Ten-Eleven-Translocation and DNA Methyltransferases, *Mol. Cells* **39**, 888–897 (2016).
140. J. Lopez-Pastrana, Y. Shao, V. Chernaya, H. Wang, X.-F. Yang, Epigenetic enzymes are the therapeutic targets for CD4+CD25+/highFoxp3+ regulatory T cells, *Translational Research* **165**, 221–240 (2015).

Publishing Agreement

It is the policy of the University to encourage the distribution of all theses, dissertations, and manuscripts. Copies of all UCSF theses, dissertations, and manuscripts will be routed to the library via the Graduate Division. The library will make all theses, dissertations, and manuscripts accessible to the public and will preserve these to the best of their abilities, in perpetuity.

Please sign the following statement:

I hereby grant permission to the Graduate Division of the University of California, San Francisco to release copies of my thesis, dissertation, or manuscript to the Campus Library to provide access and preservation, in whole or in part, in perpetuity.



Author Signature

05/30/2019
Date